Dynamical Climatology

Handbook of the Meteorological Office
11— layer atmospheric general circulation model.

Volume 1: Model description.

Edited by

A.Slingo

DCTN 29

September 1985

Meteorological Office (Met. O. 20)
London Road
Bracknell
Berkshire RG12 2SZ

DYNAMICAL CLIMATOLOGY TECHNICAL NOTE NO. 29

HANDBOOK OF THE METEOROLOGICAL OFFICE 11-LAYER ATMOSPHERIC GENERAL CIRCULATION MODEL

Volume 1 : Model Description

Edited by

A SLINGO

Met O 20 (Dynamical
Climatology Branch)
Meteorological Office
London Road
Bracknell
Berkshire RG12 2SZ

September 1985

Note: This paper has not been published. Permission to quote from it should be obtained from the Assistant Director of the above Meteorological Office Branch.

PREFACE

This is the first comprehensive handbook of the Meteorological Office 11-Layer Atmospheric General Circulation Model, as integrated on the Cyber 205 computer. In this volume, a detailed description of the model is given, including notes on the scientific subroutines. Volume 2 gives more information on the model's data organisation, method of running and additional subroutines concerned with non-meteorological tasks such as re-starting and dumping.

In constructing this handbook I have had considerable support from several scientists and others. Contributions were specially commissioned from J F Dyson, R N B Smith and R C Wilderspin. A Dickinson provided drafts of chapters from the handbook of the operational numerical weather prediction model which have been incorporated with only minor alterations (Climatological Radiation, Large-Scale Precipitation and Convection). Existing material by C C Heasman, T S Hills, M K Hinds, P R Rowntree, J M Slingo and J M Walker (sic) have also been used. R N B Smith helped edit the material on the boundary layer and convection subroutines.

This handbook is intended to be a useful source of reference which is both accurate and up-to-date. The entire volume (except Appendix 2 of Chapter 2 and the figures, obviously) has therefore been word-processed for ease of amendment and kept (I hope) on indefinite retention on diskette by the typing pool, who are also thanked for their excellent work. Users of the model are invited to correct errors and to provide constructive criticism and new material to ensure that the handbook remains authoritative.

A Slingo
Met O 20
September 1985

CONTENTS

1. Introduction and brief description of the model.

2. Dynamical formulation.

3. Physical processes: Climatological radiation scheme.

4. " " Interactive radiation scheme.

5. " " Surface and boundary layer.

6. " " Large-scale precipitation

7. " " Convection.

8. References

1. INTRODUCTION AND BRIEF DESCRIPTION OF THE MODEL

Numerical modelling of the atmospheric general circulation in the Dynamical Climatology Branch began with the development of the 5-Layer Atmospheric General Circulation Model (AGCM) (Corby et al. 1972, 1977) which was integrated on the Science Research Council's "Atlas" computer and subsequently on the Meteorological Office IBM 360/195 computer (Hinds 1981). This model has been used in several studies, notably of the atmospheric response to sea surface temperature anomalies (Rowntree 1976), of the effect of soil moisture anomalies on the summer circulation (Rowntree and Bolton 1983), of the factors which control the earth's radiation budget (J M Slingo 1982) and of the effect of increases in carbon dioxide concentrations on climate (Mitchell 1983). In many respects the 11-Layer Model is very similar, with the obvious difference of enhanced vertical resolution (Figure 1.1). The model is a global primitive-equation finite-difference AGCM with sigma (pressure divided by its surface value) as the vertical coordinate and 11 unevenly-spaced layers, to provide enhanced resolution near the surface and in the upper troposphere (Rowntree 1971). The horizontal grid in the original version (Saker 1975) was 2 degrees in latitude, with the number of points in each row progressively reduced towards the poles, thus maintaining a roughly uniform resolution of about 220 km. A limited-area version was used in the GATE experiment (Lyne et al. 1976, Rowntree and Cattle 1983) and for experiments with a cloud parametrization scheme (J M Slingo 1980). Global integrations on the IBM 360/195 were mostly of 50 days duration with fixed external forcing conditions for either January or July. The climatology of the IBM global model is discussed by Wilson and Slingo (1983) and Wilson (1984a). Studies with the model include those of Carson (1982a), Cunnington (1983a) and Cunnington and Rowntree (1985).

The first integration of the 11-Layer Model through a complete annual cycle was carried out on the CRAY-1 computer at the European Centre for Medium Range Weather Forecasts (ECMWF), using some of the time allocated to the United Kingdom as a member state (Cunnington 1983b, Slingo 1984/1985). The integration was run for just over 500 model days, starting from an analysis for 25 July 1979 produced by the assimilation version of the model during the FGGE experiment (Lyne et al 1982). The sea surface temperatures, sea-ice limits and cloud amounts were prescribed and updated in the same way as for the annual-cycle integrations of the 5-Layer Model (J M Slingo 1982). The zonally-averaged cloud amounts were taken from surface-based climatologies as described by Bolton (1981).

When the Meteorological Office installed the first production Cyber 205 computer in 1982, the model was re-programmed and is now integrated on a regular latitude-longitude grid. The first version used a resolution of 2 x 3 degrees (90 x 120 points; Figure 1.2) as this approximates the resolution of the IBM and CRAY-1 versions. This is still used for forecast integrations (e.g. Kershaw 1984), but most work is now carried out with a 2.5 x 3.75 degree grid (72 x 96 points; Figure 1.3) and a 5 x 7.5 degree grid (36 x 48 points; Figure 1.4), with a 10 minute timestep as standard. The land-sea mask for the 2.5 x 3.75 degree version was chosen to enable the model to be coupled to dynamical ocean and sea-ice models which are also being developed (Gordon and Bottomley 1984). The land surface elevations in each grid box (Figures 1.5 — 1.7) were taken as the mean of the values from a 1° x 1° dataset (Gates and Nelson 1973). Multipoint filtering in the E-W direction of the increments for the rows near each pole maintains computational stability at high latitudes (Hills 1982). Non-linear diffusion (to control grid-point noise) is applied to a linear

combination of temperature and potential temperature, designed to have a small variation in each sigma surface for a horizontally homogeneous atmosphere, rather than to potential temperature as in the IBM and CRAY versions. This produces a better formulation near steep topography and removes a part of the global-mean cooling of the model when integrated from real data. The dynamical routines now use virtual temperatures in order to include the effect of the moisture content on the air density.

Physical processes are modelled in four subroutines, which deal with radiative processes, boundary layer and surface exchanges, large scale precipitation and finally convection. A simple "climatological" radiation scheme was developed, based on the one used in the 5-Layer Model (see Chapter 3), which was incorporated into the new operational numerical weather prediction model (Gilchrist and White 1982, Dickinson and Temperton 1984). For most applications, however, the interactive radiation scheme is required (J. M. Walker 1977). This is similar to that in the 5-Layer Model (J. M. Slingo 1982) but has been modified by Slingo and Wilderspin (1984a,b). The so-called "Clarke" boundary layer scheme is based on Method 1 of Clarke (1970). The boundary layer is assumed to occupy the lowest three model layers in all conditions and transfers of heat, moisture and momentum between the layers are modelled by an eddy diffusivity approach (Carson 1982a,b). A more general scheme in which the number of model layers within the boundary layer is allowed to vary was developed by Richards (1980a,b) and was included in the new operational model. A further scheme in which the boundary layer depth is modelled explicitly using a mixed layer approach was produced (Richards 1980b, Heasman 1983) but is not available in the Cyber version. All three boundary layer schemes have the same treatment of the surface, with interactive soil

moisture and snow depth, similar to that used in the 5-Layer Model (J M Slingo 1982). Evaporation is limited for soil moisture less than 5 cm of water and runoff occurs to prevent the soil moisture from exceeding 15 cm. Large-scale precipitation, in the form of rain or snow, is formed whenever the relative humidity exceeds 100%. The convection scheme treats both unsaturated and saturated convection as it penetrates the vertical grid of the model (Lyne and Rowntree 1976, Rowntree 1984) and this has also been incorporated into the operational model.

One novel feature of the Cyber model is the use of a 360-day year, made up of twelve months each of 30 days, which leads to a considerable simplification of the logic required to run the model and produce diagnostics. The small error thus introduced into the incoming solar radiation is minimised by a slight adjustment to the date of perihelion (Slingo 1982). The diagnostics are passed through a high-speed link to the front-end IBM computers for off-line processing.

Results from the first 8-year annual cycle integration on the Cyber 205 are briefly shown in S.D.C.B. (1984) and other aspects of the model's climatology by Rowntree and Mitchell (1982), Rowntree (1983a), Wilson (1984b), Mitchell et al (1984), Dyson (1984), Slingo and Wilson (1984), Cattle (1985) and Slingo and Wilderspin (1985). The model is being used to continue research on the impact of increasing carbon dioxide concentrations (Mitchell 1984) and of sea surface temperature anomalies (Palmer and Mansfield 1984) on climate and, among many other projects, on the onset of the Asian summer monsoon (Kershaw 1984).

The model is continually being developed, particularly in the area of the representation of clouds, which has involved changes to the radiation, convection and boundary layer subroutines (Slingo and Wilderspin 1985). A

version is also being developed with an explicit representation of the cloud liquid water content (Smith 1985). The problem of the excessive westerly flow in the northern mid-latitudes in winter has been attacked by a project (Slingo and Pearson 1985) to compare simulations using an envelope orography (Wallace et al. 1983) and the parametrization of momentum transport by breaking gravity waves (Palmer and Shutts 1984).

2. DYNAMICAL FORMULATION

By

J. F. Dyson and T. S. Hills

2.1 Basic structure

In atmospheric GCMs, the three dimensional time-dependent equations (the primitive equations) for the rate of change of surface pressure (p_*), horizontal wind components (u,v), temperature (T) and moisture content (q) are solved, taking account of sources and sinks of heat, moisture and momentum. These equations are usually expressed either in finite difference form for a three dimensional array of points (as in the 11-Layer Model), or more recently in spectral form in each layer of the model (e.g. Bourke et al. 1977). Whichever form is used, the source and sink terms, represented by the 'physical parametrizations' are calculated at grid points. The basic atmospheric variables of the 11-Layer Model are thus p_* and 11 values of (u,v,T,q). In addition, three prognostic surface variables are held: surface temperature, soil moisture content and snowdepth. The Richards boundary layer scheme (see section 3) also uses a variable for the depth of the boundary layer.

The 11-Layer Model is designed for long period integrations and in such a model it is desirable to have a finite difference scheme which conserves certain important properties, for example mass and energy. In this section the basic model equations are presented and the finite difference formulations described which go some way towards satisfying these requirements. Finally, the relationship between the finite difference formulation and the actual computer code on the Cyber 205 is discussed.

2.2 The primitive equations in sigma co-ordinates

One of the problems encountered when using the conventional isobaric co-ordinate system is the form of the lower boundary conditions resulting from the inclusion of surface topography. Also, since some of the model

grid points on the lower levels will be underground some of the time, there is the difficulty of deciding what values the variables should take here. The way many GCMs (including the 11-Layer Model and the current operational forecast model) avoid this problem is to transform the equations to a different co-ordinate system (x,y,σ), where $\sigma = p/p_*$. This ensures that the lower boundary is specified as σ = constant (i.e. 1). The basic equations in these sigma (σ) co-ordinates are:

Momentum equation: $$\frac{D\underline{v}}{Dt} + f\,\underline{k} \times \underline{v} + \underline{\nabla}_\sigma \Phi + \frac{RT}{p_*}\underline{\nabla}_\sigma p_* + \underline{D}_{\underline{v}}^{H} + \underline{D}_{\underline{v}}^{v} = 0 \qquad (2.1)$$

Hydrostatic equation: $$\frac{RT}{\sigma} + \frac{\partial \Phi}{\partial \sigma} = 0 \qquad (2.2)$$

Thermodynamic equation: $$C_p \frac{DT}{Dt} - \alpha \frac{Dp}{Dt} - \dot{Q} + D_T^H = 0 \qquad (2.3)$$

Mass conservation: $$\frac{\partial p_*}{\partial t} + \underline{\nabla}_\sigma . (p_* \underline{V}) + p_* \frac{\partial \dot{\sigma}}{\partial \sigma} = 0 \qquad (2.4)$$

These result from substitution in the general s coordinate system. (Appendix 1 to this chapter).

In addition, we carry humidity mixing ratio q as a variable and therefore have a sixth equation, conservation of water vapour:

$$\frac{\partial}{\partial t}(p_* q) + \underline{\nabla}_\sigma . (p_* q \underline{v}) + p_* \frac{\partial}{\partial \sigma}(q \dot{\sigma}) = S + D_q^H \qquad (2.5)$$

The upper and lower boundary conditions now become

$$\dot{\sigma} = 0 \quad \text{at } \sigma = 0 \quad \text{(top of atmosphere)} \qquad (2.6)$$

$$\dot{\sigma} = 0 \quad \text{at } \sigma = 1 \quad \text{(surface)} \qquad (2.7)$$

It should be noted that although we now have a simple lower boundary condition, we have two pressure gradient terms in the momentum equations which, as we shall see later, causes some difficulty.

In the momentum equation, there are source terms due to horizontal and vertical sub-gridscale turbulent mixing ($\underline{D}^H_v$ and $\underline{D}^V_v$). The former is represented by horizontal diffusion (discussed in more detail below) and the latter is due to stress arising from surface friction, which is applied in the boundary layer scheme. The source term in the thermodynamic equation, $\dot{Q}$, represents the heat sources from radiation, latent heat release and vertical turbulent mixing; D^H_T represents the source (or sink) due to horizontal turbulent mixing. In the water vapour conservation equation the source term S is due to turbulent mixing and condensation. In the original version of the model the latter is synonymous with precipitation as there is no representation of cloud liquid water and condensed moisture is assumed to fall immediately as precipitation. Such a representation has been included recently in the convection scheme (see Chapter 7) and has also been formulated for non-convective cloudiness (Smith 1985).

2.3 Finite Difference grid

The positioning of the grid points in the Cyber 205 version of the model uses the so-called regular latitude-longitude grid. As the name implies, this has points regularly placed along parallels and meridians so that we may think of it as being built up of rows of points equally spaced along lines of latitudes with the same number of points in each row. The grid used is the Arakawa A grid in which p_*, u,v,T and q are all stored at the same points. The regular latitude-longitude grid is particularly suitable for efficient vectorization of the code on the Cyber 205. Because of the convergence of the meridians towards the poles, the east-west grid length (in terms of distance rather than angle of longitude) decreases towards the poles. The Courant-Friedrichs-Lewy (CFL) stability criterion,

for the numerical scheme used, then requires a very short timestep, which leads to unacceptably long computation times. This problem is overcome by the use of a stability filter applied to a number of rows nearest each pole. This filter is described in section 2.8. The vertical distribution of levels and variables is shown in Figure 1.1.

The choice of the layer boundaries, the fundamental vertical co-ordinate, is discussed in Rowntree (1971). They are chosen to give enhanced resolution in the boundary layer and near the tropopause. The proof of the energy conservation properties of the spatial part of the finite difference equations (Saker 1975; attached as Appendix 2 to this chapter) is dependent upon the relationship between the layer boundaries defined by $\sigma_{k+1/2}$ and the levels σ_k. The necessary relationship is:

$$\sigma_k = \Delta\sigma_k \; / \; \Delta(\log\sigma)_k \qquad (2.8)$$

where $\Delta(\;)_k = (\;)_{k+1/2} - (\;)_{k-1/2}$.

At the top level $\Delta(\log\sigma)_1$ is not well defined (the levels are counted from the top downwards). Either σ_1 or $\Delta(\log\sigma)_1$ can be given any reasonable value. The value chosen for σ_1 is $e^{-1}\,\sigma_{1.5}$ (see Rowntree (1971) for motivation). The value for $\Delta(\log\sigma)_1$ follows from the relation:

$$\sum_{k=1}^{11} \Delta\sigma_k = \sum_{k=1}^{11} \sigma_k \, \Delta(\log\sigma)_k = 1 \qquad (2.9)$$

2.4 Flux-form of equations

The equations of motion as they stand are not in fact used in finite difference form in the model. The model integrates the flux-form of the equations, which may be obtained by further manipulation. We consider that each grid point lies in the approximate centre of a 'box', the boundaries of which are the lines of latitude and longitude mid-way between the

central point and the adjacent points. The values of variables at the central point are then considered to be representative of the values throughout the box. Changes to these values are then computed by, for example, evaluating the flux of the quantity in question across the boundaries, and calculating the pressure difference across the box and so on. One of the consequences of the manipulation of the equations is that the advective terms become divergences.

We form the momentum flux equations by evaluating:

$$p^* \times (\text{equation 2.1}) + \underline{v} \times (\text{equation 2.4}) \quad ;$$

$$p^* \frac{\partial \underline{v}}{\partial t} + p^* \underline{v} . \underline{\nabla}_\sigma \underline{v} + p^* \dot{\sigma} \frac{\partial \underline{v}}{\partial \sigma} + p^* f \underline{k} \times \underline{v} + p^* \underline{\nabla}_\sigma \Phi + RT \underline{\nabla}_\sigma p^*$$

$$+ \underline{v} \frac{\partial p^*}{\partial t} + \underline{v}\, \underline{\nabla}_\sigma . (p^* \underline{v}) + v p^* \frac{\partial \dot{\sigma}}{\partial \sigma} = 0 \qquad (2.10)$$

which becomes

$$\frac{\partial}{\partial t}(p^* \underline{v}) + \begin{bmatrix} \nabla_\sigma . [p^* \underline{v}\, u] \\ \underline{\nabla}_\sigma . [p^* \underline{v}\, v] \end{bmatrix} + \frac{\partial}{\partial \sigma}(p^* \dot{\sigma} \underline{v})$$

$$+ f p^* \underline{k} \times \underline{v} + p^* \underline{\nabla}_\sigma \Phi + RT \underline{\nabla}_\sigma p^* = 0 \qquad (2.11)$$

Where $\underline{v}$ may be written in component form $\begin{bmatrix} u \\ v \end{bmatrix}$

The hydrostatic equation goes over unchanged. The thermodynamic equation transforms in the same way as the momentum equations to give;

$$\frac{\partial}{\partial t}(p^* T) + \underline{\nabla}_\sigma . (p^* \underline{v} T) + \frac{\partial}{\partial \sigma}(p^* \dot{\sigma} T) - \frac{p^* \alpha \omega}{c_p} = \frac{Q p^*}{c_p} \qquad (2.12)$$

Note that α (the specific volume) may be written $\frac{RT}{p}$ and so the last term on the left-hand-side becomes $p^* \frac{RT\omega}{\rho c_p} = \frac{\kappa T \omega}{\sigma}$ where $\kappa = \frac{R}{c_p}$

The equations of conservation of mass and of water vapour are already in flux-form and so are unaltered. The horizontal and vertical sub gridscale turbulent terms have been omitted for brevity.

From these flux form equations we may derive certain diagnostic relations and a prognostic equation for surface pressure.

(i) Φ, the geopotential height of a sigma level, may be obtained from the hydrostatic equation (2.2) by integrating from σ to the surface at $\sigma=1$.

$$\Phi = \Phi_* + \int_\sigma^1 RTd(\ln \sigma) \qquad (2.13)$$

(ii) To obtain a prognostic equation for p_*, we integrate (2.4) from $\sigma=0$ to $\sigma=1$, thereby eliminating $\dot{\sigma}$ by using $\dot{\sigma}=0$ at $\sigma=0,1$.

$$\frac{\partial p_*}{\partial t} = - \int_0^1 \underline{\nabla}_\sigma . (p_* \underline{v}) d\sigma \qquad (2.14)$$

(iii) We may obtain $\dot{\sigma}$ by again integrating (2.4), this time stopping at level σ:

$$p_* \dot{\sigma} = -\sigma \frac{\partial p_*}{\partial t} - \int_0^\sigma \underline{\nabla}_\sigma . (p_* \underline{v}) d\sigma \qquad (2.15)$$

$$= \sigma \int_0^1 \underline{\nabla}_\sigma . (p_* \underline{v}) d\sigma - \int_0^\sigma \underline{\nabla}_\sigma . (p_* \underline{v}) d\sigma \qquad (2.16)$$

(iv) We need an expression for the term in (2.12) containing $\omega \equiv \left[\frac{Dp}{Dt}\right]$

$$\frac{-\kappa T \omega}{\sigma} = \frac{-\kappa T}{\sigma} \frac{D}{Dt} (\sigma p_*) \qquad (2.17)$$

$$= \frac{-\kappa T}{\sigma} \left[p_* \frac{D\sigma}{Dt} + \sigma \frac{Dp_*}{Dt} \right] \qquad (2.18)$$

$$= \frac{-\kappa T}{\sigma} \left(p_* \dot{\sigma} + \sigma \frac{\partial p_*}{\partial t} + \sigma \underline{v} . \underline{\nabla} p_* + \dot{\sigma} . \frac{\partial p_*}{\partial \sigma} \right) \qquad (2.19)$$

But note that the last term here is zero. Thus using the result in (iii) we obtain;

$$\frac{-\kappa T\omega}{\sigma} = \frac{\kappa T}{\sigma} \int_0^\sigma \underline{\nabla}.(p_*\underline{v})d\sigma - \sigma\underline{v}.\nabla p_* \qquad (2.20)$$

2.5 Spherical polar coordinates

Since we need to solve the equations on a sphere, we express them in spherical polar coordinates. We use λ for longitude increasing eastwards and θ for latitude increasing northwards. Since the atmosphere is regarded as thin in comparison with the radius of the earth, the distance of a point from the centre of the earth is replaced by the radius a.

The full equations with diabatic and dissipative terms included are then:

$$\frac{\partial}{\partial t}(p_*u) + \frac{1}{a\cos\theta}\left[\frac{\partial}{\partial\lambda}(p_*uu) + \frac{\partial}{\partial\theta}(p_*v\,u\cos\theta)\right] + \frac{\partial}{\partial\sigma}(p_*\dot{\sigma}u)$$

$$- p_*v\left(f + \frac{u\tan\theta}{a}\right) + \frac{1}{a\cos\theta}\left[p_*\frac{\partial\Phi}{\partial\lambda} + RT\frac{\partial p_*}{\partial\lambda}\right] = F_\lambda \qquad (2.21)$$

$$\frac{\partial}{\partial t}(p_*v) + \frac{1}{a\cos\theta}\left[\frac{\partial}{\partial\lambda}(p_*uv) + \frac{\partial}{\partial\theta}(p_*vu\cos\theta)\right] + \frac{\partial}{\partial\sigma}(p_*\dot{\sigma}v)$$

$$+ p_*u\left(f + \frac{u\tan\theta}{a}\right) + \frac{1}{a}\left[p_*\frac{\partial\Phi}{\partial\theta} + RT\frac{\partial p_*}{\partial\theta}\right] = F_\theta \qquad (2.22)$$

$$\frac{\partial\Phi}{\partial\sigma} + \frac{RT}{\sigma} = 0 \qquad (2.23)$$

$$\frac{\partial p_*}{\partial t} + \frac{1}{a\cos\theta}\left[\frac{\partial}{\partial\lambda}(p_*u) + \frac{\partial}{\partial\theta}(p_*v\cos\theta)\right] + \frac{\partial}{\partial\sigma}(p_*\dot{\sigma}) = 0 \qquad (2.24)$$

$$\frac{\partial}{\partial t}(p_*T) + \frac{1}{a\cos\theta}\left[\frac{\partial}{\partial\lambda}(p_*u\,T) + \frac{\partial}{\partial\theta}(p_*vT\cos\theta)\right]$$

$$+ \frac{\partial}{\partial\sigma}(p_*\dot{\sigma}T) - \frac{\kappa T\omega}{\sigma} = \frac{p_*}{C_p}\dot{Q} + D_T^H \qquad (2.25)$$

$$\frac{\partial}{\partial t}(p_*q) + \frac{1}{a\cos\theta}\left[\frac{\partial}{\partial\lambda}(p_*uq) + \frac{\partial}{\partial\theta}(p_*vq\cos\theta)\right] + \frac{\partial}{\partial\sigma}(p_*\dot{\sigma}q) = D_q^H + S \qquad (2.26)$$

Here F_λ, F_θ, $\dot{Q}$, D^H_T, D^H_q and S are the various source and sink terms mentioned above.

2.6 Finite-difference scheme

i) Bryan (1966) showed how to form finite differences of equations in flux form so that scalar quantities such as mass and quadratic quantities such as energy are conserved in the space differencing. In flux form we need to estimate the value of quantities on the 'grid-box' boundaries so that we can calculate the flux across the boundaries (Figure 2.1). Bryan showed that the conservation properties mentioned above apply if the mean value of the quantity of the points either side of the boundary is taken as the value at the boundary. We denote the east-west mean $\frac{1}{2}(\alpha_{\lambda+\Delta\lambda/2} + \alpha_{\lambda-\Delta\lambda/2})$ by $\overline{\alpha}^{\lambda}$ and the north-south mean $\frac{1}{2}(\alpha_{\theta+\Delta\theta/2} + \alpha_{\theta-\Delta\theta/2})$ by $\overline{\alpha}^{\theta}$. Differences are denoted in a similar manner,

$$\delta_\lambda\alpha = \frac{1}{\Delta\lambda}(\alpha_{\lambda+\Delta\lambda/2} - \alpha_{\lambda-\Delta\lambda/2}) \qquad (2.27)$$

With this notation we may write the finite difference form of the advective term in (2.22) as

$$\frac{1}{a\cos\theta}\left[\delta_\lambda(\overline{\overline{p_*u}^{\lambda}}\ \overline{u}^{\lambda}) + \delta_\theta(\overline{\overline{p_*v}^{\theta}}\ \overline{u}^{\theta}\cos\theta)\right] \qquad (2.28)$$

Similar forms exist for (2.24) and (2.26). That for the thermodynamic equation (2.25) will be considered later.

ii) For vertical differencing consider Figure 1.1.

$\frac{\partial}{\partial\sigma}(p_*\dot{\sigma}\alpha)$ is approximated by $\delta_\sigma(p_*\dot{\sigma}\,\overline{\alpha}^{\sigma})$

where α may be u,v,T or q; σ does not appear meaned because it is held at intermediate levels. Care is needed in defining $\bar{\alpha}^{\sigma}$ because of the uneven σ levels;

$$\bar{\alpha}^{\sigma}_{k+1/2} = \alpha_k \, w_{k+1/2} + (1 - w_{k+1/2}) \, \alpha_{k+1} \qquad (2.29)$$

For $\bar{u}^{\sigma}$ and $\bar{v}^{\sigma}$ it is necessary to choose the $w_{k+1/2}$ to be $1/2$ (see also Appendix 2). The choice of the $w_{k+1/2}$ for T and q is discussed by Rowntree (1971). The values used are shown in Table 2.1.

TABLE 2.1 - WEIGHTS FOR T AND Q

Level	Weights for T	Weights for q
$1\,1/2$	0.378	0.8580
$2\,1/2$	0.464	0.7251
$3\,1/2$	0.482	0.6053
$4\,1/2$	0.542	0.6947
$5\,1/2$	0.551	0.7048
$6\,1/2$	0.469	0.6124
$7\,1/2$	0.476	0.5888
$8\,1/2$	0.422	0.5059
$9\,1/2$	0.394	0.4475
$10\,1/2$	0.246	0.2664

(iii) The form of the hydrostatic relation and the diagnostic equation for $Dp/Dt = \omega$ are shown in the Appendix. Note how more care is needed in representing these than in the 5-Layer Model with its evenly-spaced σ levels. The reason for the exact form of these is discussed in Rowntree (1971).

(iv) As noted earlier, we now have two pressure gradient terms in the momentum equations, and this produces a problem. These terms are $p_* \underline{\nabla}_\sigma \Phi + RT \underline{\nabla}_\sigma p_*$ (equation 2.11). Each of these terms separately can be much larger than their sum, especially near high topography where large gradients of p_* exist (Figure 2.2).

Across the Andes, for example, adjacent grid points may have surface pressures differing by as much as 300 mb, with a corresponding large difference in Φ, the geopotential height of a sigma level. Care must therefore be taken to estimate the two terms consistently. The form used is,

$$\frac{1}{a\cos\theta} \; p_* \left(\delta_\lambda \overline{\Phi}^{\lambda} + R \overline{T}^{\lambda} \delta_\lambda \log p_* \right) \qquad (2.30)$$

for the east-west gradient and a similar expression for the north-south gradient. Gilchrist (1975) justifies this form as follows. Consider the case of an atmosphere without horizontal gradients when the two parts of the pressure gradient term should cancel exactly. Thus with a mountain (assumed to replace a part of the atmosphere without otherwise altering the situation) we have the configuration illustrated in Figure 2.2, where x indicates the intersection of pressure surfaces p_1 and p_2 by a sigma surface. We clearly need only treat

$$\delta_x \Phi + \overline{RT}^{x} \delta_x \log p_* \qquad (2.31)$$

and thus replacing gradients along sigma surfaces by values in the vertical this estimate of the pressure gradient is

$$\Delta\phi - \bar{R}\bar{T} \log (p_2/p_1) \qquad (2.32)$$

where $\bar{T}$ is now the mean of the temperature at the top and bottom of the layer. For a model in which the hydrostatic relation has been integrated in the above form, this finite difference estimate of the pressure gradient is "ideal". Considering an example with no horizontal variation does not justify preferring

$$\frac{}{\bar{R}\bar{T}^{x}\ \delta_x \log p_*}^{x} \quad \text{to} \quad \bar{R}\bar{T}^{2x}\ \delta_{2x} \log p_*$$

but the former follows if we accept that if we wish to minimise truncation error, estimates should be based on the smallest grid length possible. As discussed in the previous section, in order to ensure energy conservation with unequal σ layer intervals the form of the hydrostatic relation used is

$$\Delta\phi = RT_2 \log (p_2/p_s) + RT_1 \log (p_s/p_1) \qquad (2.33)$$

p_s being the pressure at the sigma level boundary between p_1 and p_2. This gives the 'ideal' answer if

$$p_s = (p_1p_2)^{1/2} \qquad \text{i.e. } \sigma_s = (\sigma_1\sigma_2)^{1/2} \qquad (2.34)$$

and the error is

$$\bar{R}\bar{T} \log \frac{(\sigma_1\sigma_2)^{1/2}}{\sigma_s} \qquad (2.35)$$

The difference in the thicknesses can be estimated from Table 2.2, in which the layer boundaries are compared with $(\sigma_1\sigma_2)^{1/2}$ for the model

TABLE 2.2

Level no.	σ Levels in model	σ Layer boundaries in model	σ Layer boundaries from $(\sigma_k\sigma_{k+1})^{1/2}$
1	0.02207	0.06	0.044
2	0.08856	0.125	0.118
3	0.15741	0.195	0.190
4	0.23047	0.27	0.270
5	0.31738	0.37	0.372
6	0.43626	0.51	0.502
7	0.57717	0.65	0.644
8	0.71772	0.79	0.778
9	0.84320	0.900	0.889
10	0.93701	0.975	0.962
11	0.98744	1.000	1.000

The difference between the two thickness estimates is not large in an absolute sense. There does seem to be a danger that over high mountains, for instance, a gradient could be badly estimated, but there does not seem to be any evidence of this in practice.

(v) We now come to the finite sum equivalents of the expressions for $\partial p_*/\partial t$ and $\dot{\sigma}$. As with the momentum advective term, the divergence is approximated thus

$$\underline{\nabla}_\sigma.(p_*\underline{v}) \rightarrow \delta_\lambda(\overline{p_*u}^{\lambda}) + \delta_\theta(\overline{p_*v}^{\theta}\cos\theta) \qquad (2.36)$$

Hence, in a similar manner to the above;

$$(p^*\dot{\sigma})_{k+1/2} = -\sigma_{k+1/2}\left[\frac{\partial p^*}{\partial t}\right] - \frac{1}{a\cos\theta}\sum_{s=1}^{k}\left[\delta_\lambda\overline{(p^*u)_s}^{\lambda} + \delta_\theta(\overline{p^*v_s\cos\theta}^{\theta})\right]\Delta\sigma_s \qquad (2.37)$$

Where $\left[\frac{\partial p^*}{\partial t}\right]$ represents the finite difference representation of $\frac{\partial p^*}{\partial t}$ (yet to be chosen).

Putting k=n we sum over all the levels and obtain an expression for $\left[\frac{\partial p^*}{\partial t}\right]$;

$$\left[\frac{\partial p^*}{\partial t}\right] = -\frac{1}{a\cos\theta}\sum_{s=1}^{n}\left[\delta_\lambda(\overline{(p^*u)_s}^{\lambda} + \delta_\theta(\overline{p^*v_s}^{\theta}\cos\theta)\right]\Delta\sigma_s \qquad (2.38)$$

We can then use this to evaluate $\dot{\sigma}$ in (2.37).

(vi) It was mentioned in sub-section (i) that the advective term in the thermodynamic equation is treated differently to those in the momentum equations. This is because a problem arises which is similar to that concerning the pressure gradient terms in the momentum equations. It is again due to the near cancelling of large terms in the presence of steep topography. To see this, suppose we have a horizontally homogeneous atmosphere with a dry adiabatic lapse rate. Air moving along sigma surfaces and rising over topography gives rise to no change in temperature higher up due to advection of warmer air from upstream on the sigma surface cancelling an adiabatic cooling of this air. Having chosen, therefore, our finite difference form of the adiabatic term

$\left[\frac{-\kappa T\omega}{\sigma}\right]$, we choose the form of the advective term which cancels with the adiabatic term in these circumstances.

Assuming $\underline{\nabla}_p T$, $\partial p^*/\partial t$ and $\dot{\sigma}$ are negligible, so that sigma surfaces are stream surfaces, and using a result like that in appendix I we obtain

$$\underline{\nabla}_\sigma T = \kappa T \underline{\nabla}_\sigma \ln p^* \tag{2.39}$$

Now the advective term in the thermodynamic equation (2.25) is

$$\frac{1}{a\cos\theta}\left[\frac{\partial}{\partial\lambda}(p^*uT) + \frac{\partial}{\partial\theta}(p^*vT\cos\theta)\right] \tag{2.40}$$

Taking for simplicity only the zonal part $\frac{1}{a\cos\theta}\frac{\partial}{\partial\lambda}(p^*uT)$ this can be written

$$\frac{1}{a\cos\theta}\left[T\frac{\partial}{\partial\lambda}(p^*u) + p^*u\frac{\partial T}{\partial\lambda}\right] \tag{2.41}$$

Under our assumptions the second term is, from (2.39),

$$\frac{1}{a\cos\theta}p^*u\frac{\partial T}{\partial\lambda} = \frac{1}{a\cos\theta}p^*u\kappa T\frac{\partial}{\partial\lambda}\ln p^* \tag{2.42}$$

The corresponding term $-\kappa T\, p^*u\frac{\partial}{\partial\lambda}\ln p^*$ in the adiabatic term was

approximated by $-\kappa p^*u\,\overline{T}^{\lambda}\,\delta_\lambda \ln p^*$

and so we must use $\frac{p^*u}{a\cos\theta}\overline{\delta_\lambda T}^{\lambda} = \frac{p^*u}{a\cos\theta}\delta_\lambda \overline{T}^{\lambda}$ in (2.42) (2.43)

The first term of (2.41), $\frac{1}{a\cos\theta}T\frac{\partial}{\partial\lambda}(p^*u)$ is approximated by

$$\frac{1}{a\cos\theta}T\,\delta_\lambda\,\overline{p^*u}^{\lambda} \tag{2.44}$$

in view of our choice of approximation for the similar term in the mass conservation equation (2.24).

Hence we represent $\frac{1}{a\cos\theta}\frac{\partial}{\partial\lambda}(p^*uT)$ by

$$\frac{1}{a\cos\theta}T\,\delta_\lambda\,\overline{p^*u}^{\lambda} + p^*u\delta_\lambda\overline{T}^{\lambda}$$

$$= \frac{1}{a\cos\theta}\,\delta_\lambda\,\widetilde{p^*u.T}^{\lambda} \tag{2.45}$$

Where the notation $\widetilde{AB}^{x}$ means

$$\frac{1}{2}\left[A_{x+\Delta x/2}\,B_{x-\Delta x/2} + A_{x-\Delta x/2}\,B_{x+\Delta x/2}\right] \tag{2.46}$$

For completeness, the entire set of finite difference equations is included as Appendix 2. This is reproduced from Saker (1975). Also included is a proof of the energy conservation properties of the model. It is important to note that when time stepping and spatial smoothing (needed to suppress the so-called non-linear instability) are taken into account, energy conservation no longer holds. It is easy to see from (2.37) that, by considering

$$\sum_{\substack{\text{all grid} \\ \text{points}}} \left[\frac{\partial p^*}{\partial t} \right] \cos\theta$$

which is proportional to the rate of change of total mass, that the total mass is conserved by the finite difference scheme. This is not affected by the time stepping and, since the mass field is not smoothed, mass is exactly conserved in the model (ignoring rounding error).

2.7 Time-Stepping Scheme

A centred or leap-frog time step is used;

$$\left[\frac{\partial \phi}{\partial t} \right] = \frac{1}{2\Delta t} (\phi_{t+\Delta t} - \phi_{t-\Delta t}) = \delta_t \bar{\phi}^t \qquad (2.47)$$

This has the virtue of not damping the motions, and any damping that is required (see below) can be applied explicitly by terms whose magnitude can be controlled.

A problem which arises from the use of this scheme is that solutions tend to split; that is the solutions at odd time levels deviate more and more as time goes on from the solutions at even time levels. This is overcome by the use of a time filter (Asselin 1972). When a provisional value of a variable at time level $(t+\Delta t)$ has been computed, its value at level t is adjusted thus,

$$\phi^{t} = (\phi^{t})' + {}^{1}/_{2}\,\alpha\,((\phi^{t+\Delta t})' - 2(\phi^{t})' + \phi^{t-\Delta t}) \qquad (2.48)$$

where a prime indicates a provisional value. This has the effect of keeping the solutions at adjacent time levels 'tied together'. In the original version of the model, α takes the value 0.005 over all the grid; recent evidence suggests that this should be increased to 0.01 to prevent spurious oscillations near the poles (Dyson 1985) and this value is now used. Currently the odd timestep solution is not used at the start of each model day because a forward timestep is done then; this helps to supress the time splitting.

2.8 Stability Filtering (Linear)

As mentioned in section 2.3, the choice of a regular latitude-longitude grid causes problems near the pole. Since the meridians of the globe converge towards the poles, the grid has a very short zonal distance between adjacent grid points at high latitudes. For example, in one of the grids commonly used for the model, which has a 3.75° grid interval east-west and 2.5° north-south, the grid length is about 8.5 km at 88.75°N and °S.

The Courant-Friedrichs-Lewy (CFL) stability criterion therefore implies that for the model to remain stable at high latitudes a very short timestep would be required. The fastest propagation speed to be considered is of order 360 ms^{-1} (external gravity wave phase speed plus the maximum expected wind speed). So for a speed of 360 ms^{-1} and a grid length of 8.5 km we require a timestep of less than 25 seconds. This would make the model outrageously expensive to integrate.

When a detailed stability analysis is done for a given gridlength and unstable timestep (Hills 1982), it is seen that only certain wavelengths are unstable. This is manifested in an amplification rate greater than unity. Furthermore, it is only those waves shorter than a critical length that are unstable. We are therefore led to a solution of our problem: keep a long timestep, but remove short wavelengths along the row (Williamson 1976). The amplification rate mentioned above may be defined as the factor by which the amplitude of a wave increases in one timestep. So instead of removing unstable waves completely, we might try to damp them at each timestep by an appropriate factor related to the amplification factor. This can be done explicitly by Fourier-analysing the field along a row and rather than setting the Fourier coefficients of the unstable waves to zero (Fourier chopping), we reduce them in size (Fourier damping). Alternatively, it is possible to damp the unstable waves by using a local numerical filter in which averaging is carried out in the east-west direction. Vanderman (1972) describes experiments with such a scheme in which the filter weighting is triangular, centred on the point at which filtering is applied. He found that a global barotropic model ran to 60 days with this filter. Umscheid and Sankar-Rao (1971) used a three-point filter on the zonal momentum flux and the east-west pressure gradient terms in a divergence-formulation model of the shallow-water equations.

In the 11-Layer Model we therefore damp the unstable waves by designing a local numerical filter which has the transfer characteristics we require.

One of the model equations in which filtering is required is that which predicts surface pressure, p_*. We could clearly filter the p_* field itself to maintain stability, but then we would find that the resulting

field is inconsistent with the orography. This is prescribed in the model in terms of the surface geopotential height ϕ_*. Alternatively, as mentioned before, we may filter the increments to p_* at each timestep, and this is what is done. Similarly, increments to all the other variables are filtered along each row at each timestep. Increments due to diffusion and physical parametrizations are left unfiltered.

2.9 Stability filtering (non-linear)

Since the dynamical equations are non-linear there is in the continuous system a transfer of properties (e.g. momentum, energy etc) between different scales of motion. Because of the energy conserving properties of the model, the system of finite difference equations, as it stands, cannot represent the transfer of properties from resolvable to unresolvable scales. This results in a build-up of energy at small scales and necessitates the introduction of dissipative terms. There are thus two main reasons for introducing such a term. One is pragmatic; without any dissipation term the model would become unstable (by non-linear instability, which occurs however short the timestep). The other reason is to try to simulate the transfer of properties (energy at small scales, enstrophy at large scales) from large to small scales which occurs in the real atmosphere.

In its simplest form, such a term is merely a linear viscosity. Problems arise from this kind of term, however, since it is not sufficiently scale-selective. As well as damping the very short waves considerably, linear viscosity also damps the longer meteorological waves, resulting in an unrealistically high ratio of zonal kinetic energy to eddy kinetic energy and an exaggerated north-south temperature contrast.

Such a linear viscosity (often referred to as a diffusion term) for the u equation would be,

$$D_u = K_u [\underline{\nabla} . (p*\underline{\nabla}u)] \qquad (2.49)$$

With K_u constant. To alleviate this problem and make the diffusion more scale selective, we take K_u as being proportional to the quantity in square brackets so that

$$D_u = K \mid \underline{\nabla}.(p*\underline{\nabla}u)\mid(\underline{\nabla}.(p*\underline{\nabla}u)) \qquad (2.50)$$

This allows a smaller average value of K to be sufficient to maintain stability.

A computational stability problem arises when using this form of 'non-linear diffusion' on a regular latitude-longitude grid, because of the small longitudinal gridlength. To overcome this, instead of

$$\underline{\nabla}.(p*\underline{\nabla}u) = \frac{1}{a^2\cos^2\theta}\frac{\partial}{\partial\lambda}\left(p*\frac{\partial u}{\partial\lambda}\right) + \frac{1}{a^2\cos\theta}\frac{\partial}{\partial\theta}\left(p*\frac{\partial D}{\partial\theta}\cos\theta\right) \qquad (2.51)$$

the modified operator

$$\frac{r^2}{a^2\cos^2\theta}\frac{\partial}{\partial\lambda}\left(p*\frac{\partial D}{\partial\lambda}\right) + \frac{1}{a^2\cos\theta}\frac{\partial}{\partial\theta}\left(p*\frac{\partial D}{\partial\theta}\cos\theta\right) \qquad (2.52)$$

is used, where $r = \Delta\lambda\cos\theta/\Delta\theta$ is the ratio of the grid lengths. For a more detailed discussion of this and related problems see Gadd (1983).

2.10 PROGRAMME DETAILS

The subroutine DYNEQS which performs the calculations described here is extremely well commented. Thus it is only necessary to outline briefly the organisation of the code. The Cyber 205 is a vector computer which means that more than one grid point may be processed at once; in fact because of the particular architecture of this machine the more grid points that are processed together (ie the longer the vector length) the more the speed of the machine is optimised. Consider two possible ways of arranging the data (vectors are, by definition, contiguous in store);

1. (East-West, North-South, Up-Down) (field form)

2. (East-West, Up-Down, North-South)

The first permits longer vector lengths because many calculations involve vector lengths of N_{EW} x N_{NS} (N_{EW} being the number of grid points around a latitude circle; N_{NS} being the number of latitude circles in the grid; N_{UD} the number of model levels). The longest vector length possible if arrangement (2) is used is N_{EW} x N_{UD} which is generally a lot less than N_{EW} x $N_{N\,S}$ (on the 2.5° x 3.75° grid N_{EW} x N_{NS} = 6984 whilst N_{EW} x N_{UD} = 1067). On grounds of computation time arrangement (1) is thus preferable and this is the one used in the current operational model. However, there are other reasons why arrangement (2) may be preferable, for instance there are many terms which involve multiplication by latitude constants eg

$$p*v2\Omega \sin\theta, \qquad \frac{p*}{a\cos\theta} \qquad \delta_\lambda \overrightarrow{\Phi}^{\lambda}$$

When using data structure (1), field-length vectors of latitude constants need to be constructed; this is time-consuming and an expensive use of memory. The 11-Layer Model uses arrangement (2). The variables updated in DYNEQS (and also the variables needed to compute the updates) are p*,u,v,T and q. These variables are stored in the A stores (ie an array with name A) as 32-bit numbers. Considered as a 32 bit array, A is dimensioned

A(no. of points in row +1, 1+4 (no of levels), no of rows, 2)

The value of each variable at the beginning of each row is repeated at the end of the row to facilitate east-west differencing and averaging. The order of storage is; a rows-worth of p*'s followed by a rows-worth of the lowest level u's then the next level of u's etc. This is followed by v,T and q in the same manner. The 2 in the dimension statement reflects the fact that two time levels are needed because of the leap-frog timestep.

The code loops through the rows, starting at the north pole and scanning southward (this loop is labelled 100). Before computing any differences a subroutine FIFNP is called. This computes certain functions of p_* and ϕ which are used frequently throughout the routine. (namely ϕ, $p_*^{-\kappa}$, $\ln p_*$, $p_*^{\kappa+1}$, p_*, $p_*/2a\cos\theta$. There are N_{UD} copies of these to facilitate vectorization of a whole row).

East-west fluxes are computed next. Note the use of offset in instructions to do East-West differencing and meaning; a typical instruction to compute $\bar{u}^{\lambda}$ is;

```
DATA    M1/-1/
CALL    Q8ADDNV(X'80',M1,UCCD,,UCCD,,TEMP2D)
```

The convention for naming descriptors is explained in the code. Similar expressions occur for $\delta_{\lambda}\bar{u}^{\lambda}$. Note that in computing the East-West differences, the storage area allocated to the North-South fluxes is used as temporary work space.

A rather neat trick is employed to compute the North-South fluxes. The fluxes from the row to the north of the one currently being processed are kept from the previous scan through the 100 loop. The fluxes to the row to the south are then computed and kept for the next row I. (Note that descriptors for work areas point to different areas of storage for alternate rows). Their contribution to the increment is obtained by taking the difference between the fluxes from the row to the north and those to the row to the south (i.e. the flux divergence). For the polar-most rows the flux over the pole is set to zero; this may be viewed as a boundary condition but really reflects the fact that $\cos\theta$ vanishes at the pole.

There is no a priori guarantee that the numerical scheme will not produce negative values of q, even though the initial q field is everywhere positive. To prevent q from becoming too negative if it does become negative at some grid point, at the next time step if any flux into the grid box in question is such as to make the q there more negative than this flux is set to zero. This procedure ensures that the global moisture content is still conserved, but is upset by the linear stability filter.

After the North-South fluxes are computed comes the vertical differencing. It should be noted that the vector lengths here are of one rows length only; in the rest of the code they are this value times the number of levels.

The multipoint filter is then performed, by subroutine FILTER. Note that the polar-most rows are filtered differently, using the subroutine POLAR which keeps wave zero and half of wave one in the increments. Also note that the penultimate row is filtered twice. The reason for this is purely pragmatic; if it is not done the integration often goes unstable.

In the final section the time meaning and incrementing of the A stores is performed.

APPENDIX 1

The equations of motion with a general vertical coordinate, s

Lemma 1

We have

$$\left.\frac{\partial \phi}{\partial x}\right]_z = \left.\frac{\partial \phi}{\partial x}\right]_s + \left.\frac{\partial \phi}{\partial s}\right]_x \left.\frac{\partial s}{\partial x}\right]_z$$ where, for example, $\left.\frac{\partial \phi}{\partial x}\right]_z$ denotes differentiation of some arbitrary function ϕ with respect to x at constant z (and holding constant variables not explicitly mentioned, ie y, t). Hence

$$\underline{\nabla_z \phi = \nabla_s \phi + \frac{\partial \phi}{\partial s} \nabla_z s} \qquad \text{and} \qquad \underline{\left.\frac{\partial \phi}{\partial t}\right]_z = \left.\frac{\partial \phi}{\partial t}\right]_s + \left.\frac{\partial \phi}{\partial s}\right]_t \left.\frac{\partial s}{\partial t}\right]_z}$$

Also we have

$$\underline{\frac{\partial \phi}{\partial z} = \frac{\partial \phi}{\partial s} \frac{\partial s}{\partial z}}$$

Lemma 2

In z-coordinates, $\frac{D\phi}{Dt} = \left.\frac{\partial \phi}{\partial t}\right]_z + \underline{v}.\nabla_z \phi + w \frac{\partial \phi}{\partial z}$

and so, applying Lemma 1,

$$\frac{D\phi}{Dt} = \left.\frac{\partial \phi}{\partial t}\right]_s + \left.\frac{\partial \phi}{\partial s}\right]_t \left.\frac{\partial s}{\partial t}\right]_z + \underline{v}.\nabla_s \phi + \frac{\partial \phi}{\partial s} \underline{v}.\nabla_z s + w \frac{\partial \phi}{\partial s} \frac{\partial s}{\partial z}$$

$$= \left.\frac{\partial \phi}{\partial t}\right]_s + \underline{v}.\nabla_s \phi + \frac{\partial \phi}{\partial s} \left\{ \left.\frac{\partial s}{\partial t}\right]_z + \underline{v}.\nabla_z s + w \frac{\partial s}{\partial z} \right\}$$

$$= \left.\frac{\partial \phi}{\partial t}\right]_s + \underline{v}.\nabla_s \phi + \frac{\partial \phi}{\partial s} \frac{Ds}{Dt}$$

or writing $\dot{s} = \frac{Ds}{Dt}$;

$$\underline{\frac{D\phi}{Dt} = \left.\frac{\partial \phi}{\partial t}\right]_s + \underline{v}.\nabla_s \phi + s \frac{\partial \phi}{\partial s}}$$

In deriving the equations of motion, one may either work from first principles, as in the derivation of the usual Navier-Stokes equations, or transform the Navier-Stokes equations themselves.

The form of the momentum equations and hydrostatic equation will here be derived by transformation.

Momentum equations [Inviscid]

$$\frac{Dv}{Dt} + f\underline{k}\underline{x}\underline{v} + \frac{1}{\rho} \nabla_z p = 0$$

$\frac{Dv}{Dt}$ transforms as in Lemma 2.

Using Lemma 1, $\nabla_z p = \nabla_s p + \frac{\partial p}{\partial s} \nabla_z s$

Using the equation of state for a perfect gas:

$$\frac{1}{\rho}\,\underline{\nabla}_z p \;=\; \frac{RT}{p}\,\underline{\nabla}_s p \;+\; \frac{1}{\rho}\,\frac{\partial p}{\partial s}\left[-\,\underline{\nabla}_s z\;\;\frac{\partial s}{\partial z}\right] \qquad (1)$$

where use has been made of the equality

$$\left.\frac{\partial s}{\partial x}\right]_z \;\; \left.\frac{\partial x}{\partial z}\right]_s \;\; \left.\frac{\partial z}{\partial s}\right]_x = -1$$

which implies

$$\left.\frac{\partial s}{\partial x}\right]_z = \left.\frac{-\partial z}{\partial x}\right]_s \;\; \left.\frac{\partial s}{\partial z}\right]_x \qquad \text{Hence} \qquad \underline{\nabla}_z s = -\,\frac{\partial s}{\partial z}\;\underline{\nabla}_s z$$

(1) may then be written

$$\frac{1}{\rho}\,\underline{\nabla}_z p \;=\; \frac{RT}{p}\,\underline{\nabla}_s p + \frac{1}{\rho}\,(-\,\underline{\nabla}_s z)(-\rho g) \quad \text{using} \quad \frac{\partial p}{\partial z} = -\rho g$$

Hence $\frac{1}{f}\,\underline{\nabla}_z p = \frac{RT}{p}\,\underline{\nabla}_s p + \nabla_s \Phi$ where Φ is geopotential.

We therefore have the momentum equations

$$\underline{\frac{Dv}{Dt} + f\underline{k}\underline{x}\underline{v} + \frac{RT}{p}\,\underline{\nabla}_s p + \underline{\nabla}_s \Phi = 0}$$

Hydrostatic equation

As in Lemma 1,

$$\frac{\partial p}{\partial z} \;=\; \frac{\partial p}{\partial s}\;\frac{\partial s}{\partial z} \;=\; -\rho g \;=\; \frac{-pg}{RT}$$

Hence $$\underline{\frac{RT}{p}\;\frac{\partial p}{\partial s} + \frac{\partial \Phi}{\partial s} = 0}$$

Thermodynamic equation

This may be written, as usual, as

$$\dot{Q} \;=\; C_p\,\frac{DT}{Dt} - \alpha\;\frac{Dp}{Dt} \;=\; C_p\,\frac{DT}{Dt} - \alpha\omega$$

assuming we use the appropriate form of $\frac{D}{Dt}$ as in Lemma 2.

Mass conservation

This is most simply derived from first principles. Consider a closed surface S fixed relative to the coordinate system, enclosing a volume V entirely occupied by fluid.

The mass within V is $\int_v \rho dV = \int_v -\frac{1}{g}\frac{\partial p}{\partial s} dV'$

where $dV = dxdydz$, $dV' = dxdyds$ and using $dz = -\frac{1}{\rho g}\frac{\partial p}{\partial s} ds$

Similarly the flow out across S is $\int_s \rho \underline{u}.\underline{n} ds = \int_s -\frac{1}{g}\frac{\partial p}{\partial s}\underline{u}.\underline{n} dS'$

where dS' is an element of area of S in s-coordinates.

Hence, to conserve mass,

$$\frac{d}{dt}\int_v \frac{\partial p}{\partial s} dV' + \int_s \frac{\partial p}{\partial s}\underline{u}.\underline{n} dS' = 0$$

Hence $$\int_v \left\{ \frac{\partial}{\partial t}\left[\frac{\partial p}{\partial s}\right] + \underline{\nabla}_s.\left[\underline{u}\frac{\partial p}{\partial s}\right] + \frac{\partial}{\partial s}\left[\dot{s}\frac{\partial p}{\partial s}\right] \right\} dV' = 0$$

using the divergence theorem. Since this is true for arbitrary V;

$$\underline{\frac{\partial}{\partial t}\left[\frac{\partial p}{\partial s}\right] + \underline{\nabla}_s.\left[\underline{u}\frac{\partial p}{\partial s}\right] + \frac{\partial}{\partial s}\left[s\frac{\partial p}{\partial s}\right] = 0}$$

As an alternative derivation consider the mass of an element of fluid;

$$\delta M = \rho \delta x \delta y \delta z = -\frac{\delta x \delta y}{g}\frac{\partial p}{\partial s}\delta s$$

Since $\frac{D}{Dt}\delta M = 0$ we have $\frac{1}{\delta x \delta y \delta s}\frac{D}{Dt}\left[\delta x \delta y \delta s \frac{\partial p}{\partial s}\right] = 0$

Hence $$\frac{\partial p}{\partial s}\left.\frac{\partial u}{\partial x}\right]_s + \frac{\partial p}{\partial s}\left.\frac{\partial v}{\partial y}\right]_s + \frac{\partial p}{\partial s}\frac{\partial \dot{s}}{\partial s} + \frac{D}{Dt}\frac{\partial p}{\partial s} = 0$$

Thus $$\underline{\frac{\partial}{\partial t}\left[\frac{\partial p}{\partial s}\right] + \underline{\nabla}_s.\left[\underline{v}\frac{\partial p}{\partial s}\right] + \frac{\partial}{\partial s}\left[\dot{s}\frac{\partial p}{\partial s}\right] = 0}$$

Note that upon substitution of s=z or s=p we recover the familiar equations.

APPENDIX 2: Finite difference equations

This is reproduced from Saker (1975) with minor changes. Note that

$U = p_* u$, $V = p_* v$ and so on.

Definitions:

$$\bar{A}^{x} = \tfrac{1}{2}\left[A\left(x+\tfrac{1}{2}\Delta x\right) + A\left(x-\tfrac{1}{2}\Delta x\right)\right]$$

$$\delta_x A = \frac{1}{\Delta x}\left[A\left(x+\tfrac{1}{2}\Delta x\right) - A\left(x-\tfrac{1}{2}\Delta x\right)\right]$$

$$\widetilde{AB}^{x} = \tfrac{1}{2}\left[A\left(x+\tfrac{1}{2}\Delta x\right)B\left(x-\tfrac{1}{2}\Delta x\right) + A\left(x-\tfrac{1}{2}\Delta x\right)B\left(x+\tfrac{1}{2}\Delta x\right)\right]$$

Ignoring the right hand sides, equations 2.21-2.26 in finite difference form are:

$$\delta_t \bar{U}^t + \frac{1}{a\cos\theta}\left[\delta_\lambda \bar{U}^\lambda \bar{u}^\lambda + \delta_\theta\left(\bar{V}^\theta \bar{u}^\theta \cos\theta\right)\right] + \delta_\sigma\left(\dot{\sigma}\bar{u}^\sigma\right) - V\left(f + \frac{u\tan\theta}{a}\right) + \frac{p_*}{a\cos\theta}\left[\delta_\lambda \overline{\Phi}^\lambda + R\,\overline{\bar{T}^\lambda \delta_\lambda \log p_*}^{\lambda}\right] = 0 \quad (11)$$

$$\delta_t \bar{V}^t + \frac{1}{a\cos\theta}\left[\delta_\lambda \bar{U}^\lambda \bar{v}^\lambda + \delta_\theta\left(\bar{V}^\theta \bar{v}^\theta \cos\theta\right)\right] + \delta_\sigma\left(\dot{\sigma}\bar{v}^\sigma\right) + U\left(f + \frac{u\tan\theta}{a}\right) + \frac{p_*}{a\cos\theta}\left[\cos\theta\,\overline{\delta_\theta \Phi}^{\theta} + R\cos\theta\,\overline{\bar{T}^\theta \delta_\theta \log p_*}^{\theta}\right] = 0 \quad (12)$$

$$\delta_t \bar{p}_*^t + \frac{1}{a\cos\theta}\sum_{k=1}^{n}\left[\left(\delta_\lambda \bar{U}_k^\lambda + \delta_\theta\left(\bar{V}^\theta \cos\theta\right)_k\right)\Delta\sigma_k\right] = 0 \quad (13)$$

$$\Phi_k = \Phi_* + \sum_{s=k+1}^{n}\left[R T_s \log\left(\frac{\sigma_{s+1/2}}{\sigma_{s-1/2}}\right)\right] + \lambda_k R T_k \log\left(\frac{\sigma_{k+1/2}}{\sigma_{k-1/2}}\right) \quad (14)$$

$$\delta_t\left(\overline{p_* T}\right)^t + \frac{1}{a\cos\theta}\left[\delta_\lambda\left(\widetilde{UT}\right)^\lambda + \delta_\theta\left(\widetilde{VT}^\theta \cos\theta\right)\right] + \delta_\sigma\left(p_*\dot{\sigma}\bar{T}^\sigma\right) - \frac{\kappa T\omega}{\sigma} = 0 \quad (15)$$

$$\delta_t\left(\overline{p_* q}\right)^t + \frac{1}{a\cos\theta}\left[\delta_\lambda\left(\bar{U}^\lambda \bar{q}^\lambda\right) + \delta_\theta\left(\bar{V}^\theta \bar{q}^\theta \cos\theta\right)\right] + \delta_\sigma\left(p_*\dot{\sigma}\bar{q}^\sigma\right) = 0 \quad (16)$$

To obtain $(P^*\dot{\sigma})_{k+1/2}$, we integrate 2.24 from the top of the atmosphere:

$$\left(p_*\dot{\sigma}\right)_{k+1/2} = -\sigma_{k+1/2}\,\delta_t \bar{p}_*^t - \frac{1}{a\cos\theta}\sum_{s=1}^{k}\left[\delta_\lambda \bar{U}_s^\lambda + \delta_\theta\left(\bar{V}^\theta \cos\theta\right)_s\right]\Delta\sigma_s \quad (17)$$

For the adiabatic term, $\frac{\kappa T\omega}{\sigma}$ we use $\frac{\kappa T\omega}{\sigma} = \frac{\kappa T}{\sigma}\left(p_*\dot{\sigma} + \sigma\frac{\partial p_*}{\partial t} + \sigma \underline{V}\cdot\nabla p_*\right)$

to obtain:

$$\left(-\frac{\kappa T\omega}{\sigma}\right)_k = \frac{\kappa}{a\cos\theta}\left[U\,\overline{\bar{T}^\lambda \delta_\lambda \log p_*}^{\lambda} + V\cos\theta\,\overline{\bar{T}^\theta \delta_\theta \log p_*}^{\theta}\right]_k$$

$$-\frac{\kappa T_k}{\sigma_k}\sum_{s=1}^{k+1}\left(\nabla\cdot V_s\right)\sigma_s \log\frac{\sigma_{s+1/2}}{\sigma_{s-1/2}} + \lambda_k\left(\nabla\cdot V_k\right)\sigma_k \log\frac{\sigma_{k+1/2}}{\sigma_{k-1/2}} \quad (18)$$

where $\nabla\cdot V_s = \frac{1}{a\cos\theta}\left(\delta_\lambda \bar{U}_s^\lambda + \delta_\theta \bar{V}_s^\theta \cos\theta\right)$

The choice of λ_k, which appears in (14) and (18) is arbitrary. Various possibilities are discussed by Rowntree (1971).

We have chosen $$\lambda_k = \left(\log\left(\frac{\sigma_{k+1/2}}{\sigma_k}\right)\right) \Big/ \log\left(\frac{\sigma_{k+1/2}}{\sigma_{k-1/2}}\right) \quad (19)$$

The vertical means $\bar{T}^\sigma, \bar{q}^\sigma, \bar{u}^\sigma, \bar{v}^\sigma$ are defined:

$$\bar{T}^\sigma = W_{k+1/2}\,T_k + \left(1 - W_{k+1/2}\right)T_{k+1} \quad (20)$$

and similarly for $\bar{q}^\sigma, \bar{u}^\sigma, \bar{v}^\sigma$.

Energy conservation in the 11 layer model's finite difference scheme

To prove formal energy conservation in the space difference scheme we operate on equations 2.21 to 2.25 to form the following integral, I:

$$I = \frac{1}{g}\iiint \left[u\times(2.21) + v\times(2.22) + \frac{1}{2}(u^2+v^2)\times(2.24) + c_p\times(2.25)\right] 2\pi a^2\cos\theta\, d\theta\, d\lambda\, d\sigma\, d\log\sigma = 0$$

$$\text{then } I = \frac{1}{g}\left\{\frac{\partial}{\partial t}\iiint\left[\frac{1}{2}p_*(u^2+v^2) + c_p p_* T\right].2\pi a^2\cos\theta\, d\theta\, d\lambda\, d\sigma\, d\log\sigma\right.$$

$$\left. + \iiint\left[A+B+C+D\right]\,.\,2\pi a^2\cos\theta\, d\theta\, d\lambda\, d\sigma\, d\log\sigma\right\} \qquad (1)$$

We add $\pm\frac{1}{g}\phi_* p_*$ to each of the integrals, and then let E be the total kinetic and internal + potential energy. Equation (1) becomes:

$$I = \frac{\partial}{\partial t}\iiint_v E\, dV + \frac{1}{g}\iiint_v \left[A+B+C+D+E\right] dV = 0 \qquad (2)$$

where: A = the horixontal advection terms
B = the vertical advection terms
C = the terms containing $(f + \frac{u\tan\theta}{a})$
D = the pressure gradient and w terms
E = $-\phi_* p_*$

and all diffusion and external energy source and sink terms are ignored.

We require to prove that $\frac{\partial}{\partial t}\iiint_v E\, dV = 0$. This is equivalent to proving that the finite difference representation of the 2nd terms in (2) is zero.

The finite difference representation of A is:

$$A = \sum_{\Delta\theta}\sum_{\Delta\lambda}\sum_{\Delta\sigma}\frac{1}{a\cos\theta}\left\{u\left[\delta_\lambda(\bar{u}^\lambda\bar{u}^\lambda) + \delta_\theta(\bar{v}^\theta\bar{u}^\theta\cos\theta)\right] + v\left[\delta_\lambda(\bar{u}^\lambda\bar{v}^\lambda) + \delta_\theta(\bar{v}^\theta\bar{v}^\theta\cos\theta)\right]\right.$$

$$\left. -\frac{1}{2}(u^2+v^2)\left[\delta_\lambda\bar{u}^\lambda + \delta_\theta(\bar{v}^\theta\cos\theta)\right] + c_p\left[\delta_\lambda(\widetilde{uT}^\lambda) + \delta_\theta(\widetilde{vT}^\theta\cos\theta)\right]\right\} \qquad (3)$$

Consider $u\,\delta_\lambda(\bar{u}^\lambda\bar{u}^\lambda) - \frac{1}{2}u^2\delta_\lambda\bar{u}^\lambda$

This can be shown to be equivalent to $\frac{1}{2}\delta_\lambda u\widetilde{(uu)}^\lambda$, and this vanishes when summed in the 'λ' direction. The other terms in u,v vanish similarly when summed in the horizontal. The final term in T vanishes immediately upon horizontal summation.

The finite difference representation of B is:

$$B = u\,\delta_\sigma(p_*\dot{\sigma}\bar{u}^\sigma) + v\,\delta_\sigma(p_*\dot{\sigma}\bar{v}^\sigma) - \frac{1}{2}(u^2+v^2)\frac{\partial}{\partial\sigma}(p_*\dot{\sigma})$$

$$+ c_p\,\delta_\sigma(p_*\dot{\sigma}\bar{T}^\sigma) \qquad (4)$$

The terms $\left[u\delta_\sigma(p_*\dot\sigma\bar u^\sigma)-\frac{1}{2}u^2\delta_\sigma(p_*\dot\sigma)\right]$ and $\left[v\delta_\sigma(p_*\dot\sigma\bar v^\sigma)-\frac{1}{2}v^2\delta_\sigma(p_*\dot\sigma)\right]$ vanish when summed in the vertical using the boundary conditions $\dot\sigma=0$ at $\sigma=0,1$.

Note that it is essential that the weights for u and v in (2.29) are each $1/2$.

The $\delta_\sigma(p_*\dot\sigma\bar T^\sigma)$ term vanishes when summed in the vertical, regardless of the definition of $\bar T^\sigma$.

The term C is $-\bar v u(f+\frac{u\tan\theta}{a})+\bar u v(f+\frac{u\tan\theta}{a})$ which is identically zero.

The finite difference representation of $\iiint_V (D+E)\,dV$ is:

$$\sum_{\Delta\theta}\sum_{\Delta\lambda}\sum_{k=1}^{n}\left[p_*\mathbf{V}\cdot\nabla\phi+p_*RT\mathbf{V}\cdot\nabla\log p_*-\frac{RT\omega}{\sigma}-\phi_*\frac{\partial p_*}{\partial t}\right]_k\sigma_k\Delta\log\sigma_k\cos\theta\Delta\theta\Delta\lambda \qquad (5)$$

where $\mathbf{V}=(u,v)$ and $\nabla=\left(\frac{\partial}{\partial\lambda},\frac{1}{\cos\theta}\frac{\partial}{\partial\theta}\right)$

Substitute (13), (14) and (15) into (5) and consider the sum over the σ - levels:

$$\begin{aligned}\sum_{k=1}^{n}\Bigg\{&(p_*\mathbf{V})_k\cdot\nabla\Big(\phi_*+\sum_{s=k+1}^{n}RT_s\log\frac{\sigma_{s+1/2}}{\sigma_{s-1/2}}+\lambda_kRT_k\log\frac{\sigma_{k+1/2}}{\sigma_{k-1/2}}\Big)\\
&+\frac{R}{a\cos\theta}\Big[(p_*u)_k\overline{\bar T_k^{\lambda}\delta_\lambda(\log p_*)_k}^{\lambda}+(p_*v)_k\cos\theta\,\overline{\bar T_k^{\theta}\delta_\theta(\log p_*)_k}^{\theta}\Big]\\
&+\frac{RT_k}{\sigma_k}\Big[\sum_{s=1}^{k-1}\Big(\overline{\nabla\cdot(p_*\mathbf{V}_s)\sigma_s\log\Big(\frac{\sigma_{s+1/2}}{\sigma_{s-1/2}}\Big)}^{\lambda}+\lambda_k\overline{\nabla\cdot(p_*\mathbf{V})_k\sigma_k\log\Big(\frac{\sigma_{s+1/2}}{\sigma_{k-1/2}}\Big)}^{\lambda}\Big]\\
&-\frac{R}{a\cos\theta}\Big[(p_*u)_k\overline{\bar T_k^{\lambda}\delta_\lambda\log p_*}^{\lambda}+(p_*v)_k\cos\theta\,\overline{\bar T_k^{\theta}\delta_\theta\log p_*}^{\theta}\Big]\\
&+\phi_*\sum_{s=1}^{n}\left[\nabla\cdot(p_*\mathbf{V})_s\Delta\sigma_s\right]\Bigg\}\sigma_k\Delta\log\sigma_k \qquad (6)\end{aligned}$$

We use the identity defined in (2.8): $\sigma_k\cdot\Delta\log\sigma_k=\Delta\sigma_k$

Then the two terms in ϕ_* in (6) combine to give:

$$\sum_{\Delta\theta}\sum_{\Delta\lambda}\left\{\sum_{k=1}^{n}\nabla\cdot(\phi_*p_*\mathbf{V})_k\cdot\Delta\sigma_k\right\}$$

and this vanishes when summed over $\Delta\theta,\Delta\lambda$

The terms in $\delta_\lambda\log p_*$ and $\delta_\theta\log p_*$ vanish identically at each point.

This leaves:

$$\begin{aligned}\sum_{k=1}^{n}\Bigg\{&(p_*\mathbf{V})_k\cdot\nabla\Big(\sum_{s=k+1}^{n}RT_s\log\Big(\frac{\sigma_{s+1/2}}{\sigma_{s-1/2}}\Big)+\lambda_kRT_k\log\frac{\sigma_{k+1/2}}{\sigma_{k-1/2}}\Big)\\
&+\frac{RT_k}{\sigma_k}\Big[\sum_{s=1}^{k-1}\Big(\nabla\cdot(p_*\mathbf{V})_s\sigma_s\log\Big(\frac{\sigma_{s+1/2}}{\sigma_{s-1/2}}\Big)\Big)\\
&+\lambda_k\nabla\cdot(p_*\mathbf{V})_k\sigma_k\log\Big(\frac{\sigma_{k+1/2}}{\sigma_{k-1/2}}\Big)\Big]\Bigg\}\sigma_k\Delta\log\sigma_k \qquad (7)\end{aligned}$$

We use the identity: $$\sum_{k=1}^{n} a_k \sum_{s=1}^{k-1} b_s \equiv \sum_{k=1}^{n} b_k \sum_{s=k+1}^{n} a_s$$

to transform (7) into:

$$\sum_{k=1}^{n} \left\{ \sum_{s=1}^{k-1} \left[(P_* V)_s \nabla \cdot (RT_k) \Delta \log \sigma_k \cdot \sigma_s \Delta \log \sigma_s + \frac{RT_k}{\sigma_k} \nabla \cdot (P_* V)_s \sigma_s \Delta \log \sigma_s \Delta \log \sigma_k \right] \right.$$
$$\left. + R\lambda_k \left[(P_* V)_k \nabla (T_k \Delta \log \sigma_k) + T_k \Delta \log \sigma_k \nabla \cdot (P_* V)_k \right] \right\}$$

Both the double sum, and the single sum terms combine to form divergences which vanish where summed over $\Delta\theta, \Delta\lambda$.

Hence we have proved that $\iiint [A+B+C+D+E] dV = 0$ and that the finite difference scheme formally conserves energy.

3. CLIMATOLOGICAL RADIATION SCHEME

3.1 Introduction

The radiation scheme used in the original version of the 11-Layer Model was described by O'Neill (1974). It was adapted from the one used in the COMESA thirteen-level model (see Mattingly 1975), which was based on the formulation described by Manabe and Möller (1961). The scheme was separated into a part due to solar radiation and a part due to longwave effects. Model temperatures and humidities were used in their calculation. It also contained the radiative effect of a single layer of cloud at a fixed height; layer 9 in the model i.e. $\sigma = p/p* = 0.84380$. The cloud amount was calculated using a formula due to Ricketts (1973) and used the model relative humidity at this level. The radiative cooling was implemented at the level above, i.e. $\sigma = 0.71772$. Because of this use of model variables to determine the radiative effects, the scheme was termed interactive.

Rowntree and Walker (1977) pointed out defects in this scheme, the most serious being the fixed layer of cloud. Because of these faults it was decided to change to a climatologically based scheme until a better interactive formulation could be developed. The climatological scheme (Richards 1977) was based on that employed in the 5-Layer Model (Rowntree 1975). Rowntree's functions tabulated in that scheme were at 10° latitude intervals and for 200 mb slabs. These are used directly in the 11-Layer Model with simple linear interpolation or extrapolation between latitude bands and pressure levels. The scheme has been used widely in integrations where detailed radiation calculations are not required as it is much faster than the interactive scheme described in the next chapter. It was also incorporated into the new 15-level operational numerical weather prediction model (Dickinson and Temperton 1984).

It is possible to divide the scheme into four sections: longwave cooling in the atmosphere and at the surface and solar heating of the atmosphere and of the surface.

3.2 Long-wave cooling in the atmosphere

The long-wave radiative cooling is calculated using empirical emissivities combined with the cooling to boundaries approximation to give cooling rates in the form

$$\frac{\partial T_k}{\partial t} = -a_k T_k^4 + b_k (T_*^4 - T_k^4) \qquad (3.1)$$

where T_k is the temperature of the kth level and T_* is the surface temperature. The parameters a_k and b_k are functions of latitude, pressure and time of year. Values of a_k are tabulated in Table 3.4.

Since the second term on the right-hand-side of equation (3.1) is generally small, it is neglected above the lowest layer. This term, in effect, represents the radiative exchange with the earth's surface. The coefficient b_k is related to b_*, the coefficient of radiative exchange at the surface, by

$$b_k = \frac{g\, b_*}{c_p\, p_*\, \Delta\sigma_k} \qquad (3.2)$$

The values of b_* used in the model are given in Table 3.3

3.3 Long-wave cooling at the surface

From the parameter a_k, an effective emissivity ϵ_k for cooling to space may be calculated. This is given by

$$\epsilon_k = \frac{a_k\, C_p\, p_*\, \Delta\sigma_k}{C\, g} \qquad (3.3)$$

where c_p is the specific heat of air and C is Stefan's constant. This allows the surface emissivity, ϵ_*, to be calculated from observed values of total column emissivity, ϵ_T, by using the relationship

$$\epsilon_* = \epsilon_T - \sum_{k=1}^{TOP} \epsilon_k \qquad (3.4)$$

ϵ_T is tabulated in Table 3.1.

The rate of long-wave cooling to space from the earth's surface may now be calculated using equation (3.4) and is given by

$$\frac{\partial T_*}{\partial t} = - \frac{C \epsilon_* T_*^4}{H} \qquad (3.5)$$

where H is the thermal capacity of the soil, taken to be equivalent to that of 5 cm of water.

A second term is also required in order to balance the heating of the bottom model layer through the radiative exchange term in equation (3.1). A compensating cooling of the ground is therefore incorporated through

$$\frac{\partial T_*}{\partial t} = - \frac{b_*}{H} (T_*^4 - T_1^4) \qquad (3.6)$$

where b_* is the coefficient of radiative exchange at the surface.

3.4 Solar heating of the atmosphere

The instantaneous solar heating rate, H_k, at level k is computed from the 24-hour mean value, $\bar{H}_k$, by imposing a diurnal variation such that

$$\frac{\partial T}{\partial t}_k = H_k = \beta \bar{H}_k \qquad (3.7)$$

where β depends on latitude, longitude, time of year and time of day. Values of $\bar{H}_k$ are given in Table 3.5.

β is calculated by assuming that the solar radiation, R_k, reaching some point in the atmosphere at time t may be expressed as

$$R_k = F_k S_o \cos \zeta \tag{3.8}$$

where ζ is the solar zenith angle, S_o is the solar constant and F_k is an attenuation function that depends only on latitude, height and time of year.

The zenith angle may be expanded in terms of the model's parameters so that equation (3.8) becomes

$$R_k = F_k S \{\cos\theta \cos\delta \cos(\lambda + \tau) - \sin\theta \sin\delta\} \tag{3.9}$$

where δ is the solar declination and $\tau = \pi\, t/12$ where t is GMT in hours.

It is reasonable to assume that the instantaneous heating is proportional to the incident radiation. Thus

$$H_k = d\, R_k \tag{3.10}$$

where d is a constant of proportionality. Moreover, $\bar{H}_k$ is similarly proportional to R_k integrated over the daylight hours. Therefore

$$\bar{H}_k = \frac{d\, F_k\, S}{2\pi} \int_{-\Omega_S - \lambda}^{\Omega_S - \lambda} [\cos\theta \cos\delta \cos(\lambda + \tau) - \sin\theta \sin\delta]\, d\tau$$

$$= \frac{d\, F_k\, S}{\pi} [\cos\theta \cos\delta \sin\Omega_S - \Omega_S \sin\theta \sin\delta] \tag{3.11}$$

where Ω_S is half the length of daylight in radians, given by

$$\cos \Omega_S = \tan\theta \tan\delta$$

On substituting equations (3.10) and (3.11) into (3.7)

$$\beta = \begin{cases} \pi \dfrac{[\cos\theta \cos\delta \cos(\lambda + \tau) - \sin\theta \sin\delta]}{[\cos\theta \cos\delta \sin\Omega_S - \Omega_S \sin\theta \sin\delta]} & \text{if } |\tau| \leq \Omega_S \\ 0 & \text{if } |\tau| > \Omega_S \end{cases} \tag{3.12}$$

3.5 Solar heating at the surface

The surface solar heating is calculated in essentially the same way as the solar heating of the atmosphere, with allowances being made for the effects of the surface albedo, α. 24-hour mean values of the incident solar flux $S*$, are used to give heating rates of the form

$$H* = \frac{\beta S* (1 - \alpha)}{H} \qquad (3.13)$$

where β is given by equation (3.12) and H is the thermal capacity of the soil. Values of $S*$ are given in Table 3.2. The albedos used are 0.2 for snow-free land, 0.5 for snow-covered land and 0.8 for land ice and sea ice.

3.6 Radiation constants

This section tabulates the constants used by the climatological radiation scheme. These are specified for each solstice and equinox at 10° latitude intervals and in the case of atmospheric functions at 200 mb intervals. The scheme assumes that there are 365 days in the year, that the northern winter solstice is on December 22nd (ITD=1) and that the equinoxes are 105 and 290 days after this. Values for the southern hemisphere are the same as those for the northern hemisphere in the opposite season.

Simple linear interpolation between latitude bands and between pressure levels is used in the model to derive the value of a function at any spatial position. Interpolation is also carried out in time. This ensures that the correct solar heating and long wave cooling rates are specified for the given time of year. The sinusoidal variation in the

values of the mean solar heating and long wave cooling rates is modelled by using the solstice values for the 30 days before and after the solstice. At other times linear interpolation between adjacent solstice and equinox values is used.

TABLE 3.1 TOTAL COLUMN EMISSIVITIES

Latitude (°)	0	10	20	30	40	50	60	70	80	90
Winter solstice	0.910	0.918	0.928	0.937	0.942	0.946	0.949	0.950	0.952	0.952
Spring equinox	0.911	0.915	0.923	0.931	0.937	0.942	0.946	0.949	0.951	0.952
Summer solstice	0.910	0.910	0.918	0.927	0.935	0.940	0.944	0.947	0.949	0.950
Autumnal equinox	0.911	0.914	0.920	0.928	0.933	0.937	0.941	0.943	0.947	0.947

TABLE 3.2 SURFACE SOLAR FLUX IN Wm^{-2} DAY^{-1}

Latitude (°)	0	10	20	30	40	50	60	70	80	90
Winter solstice	227.	222.	199.	148.	93.6	52.3	21.3	0.	0.	0.
Spring equinox	235.	264.	284.	263.	223.	193.	171.	180.	160.	140.
Summer solstice	227.	249.	273.	295.	277.	237.	218.	230.	230.	230.
Autumnal equinox	235.	224.	221.	194.	144.	94.5	56.	27.2	2.9	0.

TABLE 3.3 SURFACE RADIATIVE EXCHANGE COEFFICIENTS 10^{-9} Wm^{-2} K^{-4}

Latitude (°)	0	10	20	30	40	50	60	70	80	90
Northern Hemisphere	11.43	11.19	10.61	9.793	8.996	8.126	7.437	6.772	6.350	5.810
Southern Hemisphere	11.43	11.95	11.78	11.44	10.75	10.30	9.844	9.161	7.910	6.700

TABLE 3.4 LONG WAVE COOLING COEFFICIENTS IN 10^{-10} K^{-3} DAY^{-1}

Latitude (°)	0	10	20	30	40	50	60	70	80	90
1000 – 800 mb										
Winter solstice	2.69	2.76	2.86	3.1	3.29	3.48	3.5	3.34	3.17	3.12
Spring equinox	2.71	2.76	2.9	3.07	3.29	3.53	3.65	3.6	3.17	3.17
Summer solstice	2.69	2.71	2.86	3.0	3.22	3.46	3.70	3.65	3.34	3.36
Autumnal equinox	2.71	2.71	2.76	2.93	3.10	3.34	3.38	3.36	3.31	3.24
800 – 600 mb										
Winter solstice	3.65	3.77	3.94	4.22	4.44	4.68	4.70	4.56	4.39	4.34
Spring equinox	3.67	3.74	3.96	4.15	4.44	4.68	4.82	4.80	4.37	4.37
Summer solstice	3.65	3.67	3.86	4.06	4.32	4.61	4.87	4.82	4.54	4.54
Autumnal equinox	3.67	3.72	3.79	4.01	4.20	4.46	4.54	4.54	4.49	4.44
600 – 400 mb										
Winter solstice	4.82	4.61	4.34	4.25	4.27	4.34	4.27	4.06	3.82	3.74
Spring equinox	4.82	4.73	4.54	4.44	4.44	4.51	4.51	4.32	3.84	3.82
Summer solstice	4.82	4.82	4.68	4.63	4.44	4.51	4.63	4.44	4.08	4.06
Autumnal equinox	4.82	4.73	4.54	4.42	4.42	4.49	4.42	4.30	4.15	4.03
400 – 200 mb										
Winter solstice	6.05	5.62	5.04	4.68	4.61	4.54	4.39	4.13	3.82	3.77
Spring equinox	6.02	5.81	5.38	5.06	4.87	4.82	4.68	4.44	3.91	3.86
Summer solstice	6.05	6.05	5.69	5.28	4.97	4.90	4.87	4.61	4.20	4.15
Autumnal equinox	6.02	5.83	5.47	5.14	5.02	4.92	4.78	4.38	4.30	4.20
200 – 0 mb										
Winter solstice	3.17	3.07	3.00	3.05	3.17	3.29	3.24	3.07	2.83	2.81
Spring equinox	3.17	3.14	3.12	3.14	3.24	3.38	3.43	3.31	2.86	2.86
Summer solstice	3.17	3.17	3.17	3.17	3.22	3.63	3.53	3.38	3.10	3.07
Autumnal equinox	3.17	3.12	3.07	3.07	3.14	3.29	3.26	3.19	3.07	3.00

TABLE 3.5 SOLAR HEATING IN K DAY^{-1}

Latitude (°)	0	10	20	30	40	50	60	70	80	90
1000 – 800 mb										
Winter solstice	0.568	0.585	0.501	0.376	0.262	0.240	0.103	0	0	0
Spring equinox	0.706	0.769	0.739	0.628	0.576	0.510	0.658	0.597	0.494	0.391
Summer solstice	0.568	0.623	0.664	0.716	0.693	0.723	1.096	1.199	1.199	1.199
Autumnal equinox	0.706	0.660	0.556	0.468	0.339	0.266	0.255	0.132	0.014	0
800 – 600 mb										
Winter solstice	0.999	0.945	0.780	0.653	0.488	0.273	0.112	0	0	0
Spring equinox	1.023	1.036	1.094	1.035	1.070	0.983	0.708	0.533	0.439	0.325
Summer solstice	0.999	1.067	1.108	1.169	1.257	1.409	1.188	1.279	1.279	1.279
Autumnal equinox	1.023	0.941	0.879	0.752	0.658	0.499	0.305	0.143	0.016	0
600 – 400 mb										
Winter solstice	1.035	0.809	0.653	0.513	0.378	0.219	0.088	0	0	0
Spring equinox	1.059	1.010	0.916	0.893	0.863	0.843	0.669	0.480	0.408	0.336
Summer solstice	1.035	1.103	1.131	1.114	1.140	1.049	0.979	0.970	0.970	0.970
Autumnal equinox	1.059	0.998	0.854	0.704	0.564	0.438	0.270	0.110	0.015	0
400 – 200 mb										
Winter solstice	0.883	0.607	0.477	0.374	0.265	0.147	0.077	0	0	0
Spring equinox	0.783	0.734	0.665	0.657	0.631	0.479	0.468	0.337	0.314	0.291
Summer solstice	0.883	0.936	0.899	0.897	0.829	0.819	0.733	0.688	0.688	0.688
Autumnal equinox	0.783	0.738	0.635	0.542	0.411	0.320	0.172	0.089	0.011	0
200 – 0 mb										
Winter solstice	0.550	0.493	0.439	0.426	0.396	0.316	0.204	0	0	0
Spring equinox	0.626	0.658	0.686	0.706	0.755	0.728	0.799	0.782	0.875	0.968
Summer solstice	0.550	0.589	0.681	0.659	0.721	0.795	0.852	0.961	0.961	1.961
Autumnal equinox	0.626	0.587	0.556	0.520	0.488	0.431	0.363	0.223	0.050	0

4. INTERACTIVE RADIATION SCHEME

By

A. Slingo, A. Darlington, J.M. Slingo and R.C. Wilderspin

4.1 Introduction

Although climatological radiation schemes (such as that described in the previous chapter) are computationally economical, they have several drawbacks. Firstly, they assume the specific humidities and cloud amounts to be fixed in time and are thus unsatisfactory for simulating a climate substantially different from that for which the assumed humidities and clouds are valid. For monthly or seasonal predictions this may not be a serious criticism, although how important time variations are on this scale is still unknown since there may be important feedback mechanisms involving clouds. Secondly, climatological radiation schemes are unsuitable for assessing the effects of environmental changes, whether natural or man-made, since they are unable to respond to such things as changes in humidity and cloud distributions caused by changes in the circulation patterns.

It is thus clear that there is a need for an interactive radiation scheme which is not constrained by parameters based on present day climate. Another important feature of interactive schemes, lacking in climatological schemes, is their ability to interact with humidity and cloud distributions and thus predict the form of the feedback mechanisms involved. Experiments to assess the effects of increasing CO_2, for example, require an accurate radiation scheme to incorporate its effect on the fluxes, quite apart from the effect of radiation on the simulations.

The most important advantage of interactive schemes over climatological schemes is probably their capacity to interact with clouds predicted from model variables. For climatic change studies this feedback mechanism is of the highest importance since any long term increase or decrease in cloud cover, resulting in an enhancement or reduction of global

albedo, can substantially alter the energy balance of the earth-atmosphere system and thereby the climate. Interactive clouds may also play a significant role in forecasting for periods of a few days or weeks since they affect not only the atmospheric heating through reflection, absorption and emission of radiation but also the surface balance through modification of the shortwave and longwave fluxes reaching the surface. Changes in the horizontal and vertical distribution of cloudiness can therefore alter horizontal temperature gradients and atmospheric stability and thus affect circulation patterns.

4.2 Basic features of the scheme

One of the main factors determining the complexity of a radiation scheme is the number of cloud layers. If random overlap of clouds is assumed then the number of possible paths of the solar beam from the top of the atmosphere to the ground is given by 2^n where n is the number of cloud layers. Results from GATE suggested that even to begin to describe a cloud field adequately it would be necessary to divide clouds into four groups -low level, medium level, high level and convective. Bearing in mind that the complexity of the scheme increases rapidly with the number of clouds, a scheme was designed (Walker 1977) which would allow for three layer clouds and a convective tower (Figure 1.1). The layer clouds are assumed to be one sigma layer in thickness, but the convective cloud may occupy more than one sigma layer. The clouds overlap randomly in the vertical, except that where layer and convective clouds are present at the same level then the overlap of the layer clouds occurs only in the clear air, after allowing for the convective cloud. As a first approximation, convective cloud is pictured as a vertical column with no reflection or interaction by the

sides with the surrounding cloud or air. Any shortwave radiation entering the cloud is assumed to pass straight through, after attenuation by the cloud, and emerge at the cloud base.

Three radiatively-active gases (water vapour, ozone and carbon dioxide) are considered in calculating the radiative heating rates. The water vapour mass mixing ratio (q) is of course a basic model variable, but amounts of the other two gases are prescribed. Ozone mixing ratios above 200 mb are obtained by linear interpolation from climatological zonally-meaned values for 40 mb layers (Bolton 1977) and are updated monthly when the model is run in annual-cycle mode. A minimum ozone mass mixing ratio of 10^{-8} g/g is imposed for each of the 11 layers. The mass mixing ratio of carbon dioxide (CO_2) is taken to be 4.9×10^{-4} throughout the model, corresponding to 323 parts per million by volume (ppmv).

The radiation scheme is essentially divided into two parts; short-wave and longwave. It is possible to do this since there is very little overlap in terms of wavelength between the incoming solar radiation and the outgoing terrestrial radiation. In each part, the fluxes are calculated at the layer boundaries (Figure 1.1) and at the end of the subroutine the two contributions are added. The downward flux is subtracted from the upward flux to give the net flux F. The heating rate of layer k is then given by;

$$\frac{\partial T_k}{\partial t} = -\frac{g}{Cp}\frac{\Delta F}{\Delta p} = \frac{g}{Cp}\frac{(F_{k+1/2} - F_{k-1/2})}{p_* (\sigma_{k+1/2} - \sigma_{k-1/2})} \qquad (4.1)$$

and at the surface the heating rate is

$$\frac{\partial T_*}{\partial t} = \frac{F_*}{H} \qquad (4.2)$$

where H is the thermal capacity of the surface (as in equation 3.5).

4.3 Treatment of Shortwave Radiation

4.3.1 Incoming radiation

The solar constant (the energy received from the sun on unit area exposed normally to the sun's rays in the absence of the earth's atmosphere at the mean sun-earth distance $\bar{r}$) is taken to be 1373 Wm^{-2} (Neckel and Labs 1981). For computational efficiency, the model uses a 360-day year, in which each month is 30 days in length (Slingo 1982). The earth's orbit is illustrated in Figure 4.1, where various quantities are defined. Let time ITD be measured in days from the beginning of the year (which is 0000 GMT on 1 January). Perihelion occurs when ITD = τ. The Mean anomaly M is given by;

$$M = \frac{2\pi}{T} (ITD - \tau) \qquad (4.3)$$

where T is the number of days in the year, here taken to be 360. The True Anomaly v is given by the Equation of the Centre;

$$v = M + (2e - \frac{e^3}{4}) \sin M + \frac{5}{4} e^2 \sin 2M + \frac{13}{12} e^3 \sin 3M + ... \qquad (4.4)$$

where e is the eccentricity of the earth's orbit. The incoming solar radiation at the top of the atmosphere on day ITD is then approximated by;

$$S(ITD) = S_o \left[\frac{1 + e(\cos v)}{(1 - e^2)} \right]^2 \qquad (4.5)$$

To determine the incoming radiation at any given location the solar zenith angle must be found. Firstly, the solar declination δ is calculated;

$$\sin \delta = -\sin \epsilon \sin (v + w) \qquad (4.6)$$

where ϵ is the obliquity of the ecliptic, which is the angle between the earth's spin axis and the axis of its orbit around the sun. In the above equations the orbital constants have the values τ = 3.2 days, e = 0.0167, ϵ = 23.44° and w = 102.5°. The solar zenith angle ζ at latitude θ, longitude λ (increasing eastwards) and at model time t (measured in hours from 0000 GMT) is given by;

$$\cos\zeta = \cos\theta\cos\delta\cos\Omega - \sin\theta\sin\delta \qquad (4.7)$$

where $\Omega = \lambda + \pi\frac{(t-12)}{12}$ is the hour angle of the sun (e.g. Paltridge and Platt 1976). This formulation assumes that on the Greenwich meridian the sun is due south each day at 1200 GMT (i.e. the equation of time is always zero, which is a reasonable approximation).

Since the radiation scheme is called only every few hours rather than every timestep, a mean value of cos ζ is required in order to obtain an accurate estimate of the incoming solar radiation over these hours. The hour angles for sunrise and sunset are needed for this calculation since cos ζ cannot take negative values. The hour angle for sunset (Ω_s) is given by:

$$\Omega_s = \cos^{-1}(\tan\theta\tan\delta) \qquad (4.8)$$

and the mean cosine of the zenith angle between hour angles Ω_1 and Ω_2 by:

$$\overline{\cos\zeta} = \int_{\Omega_1}^{\Omega_2} \frac{(\cos\theta\cos\delta\cos\Omega - \sin\theta\sin\delta)d\Omega}{\Omega_2 - \Omega_1}$$

$$= \frac{\cos\theta\cos\delta(\sin\Omega_2 - \sin\Omega_1) - \sin\theta\sin\delta(\Omega_2 - \Omega_1)}{\Omega_2 - \Omega_1} \qquad (4.9)$$

provided that cos ζ is always positive. If the time period in question spans the hour of sunset, for example, then $\overline{\cos\zeta}$ is given by:

$$\overline{\cos\zeta} = \int_{\Omega_1}^{\Omega_s} \frac{(\cos\theta\cos\delta\cos\Omega - \sin\theta\sin\delta)d\Omega}{\Omega_2 - \Omega_1} \qquad (4.10)$$

Similar integral limits are required to deal with sunrise.

The incoming radiation used by the scheme at any location is thus S(ITD) times $\overline{\cos\zeta}$. In the program these are named OC and COSZ, respectively.

Rayleigh scattering from the air molecules is parametrized very simply by reducing the incoming radiation by 3%. It is important to note that as a consequence this contributes about 10% to the globally-averaged flux reflected back to space by the model.

4.3.2 Gaseous absorption

The absorption by the radiatively-active gases and the absorption and reflection by clouds and the surface are treated in a single spectral band. The absorptivity curves for water vapour, ozone and carbon dioxide were taken from Manabe and Möller (1961) and are illustrated in Figure 4.2. In reality, the absorptions take place in different spectral regions, so the total absorption in such a scheme is simply the sum of that from each gas. The absorption of the incoming radiation down to layer boundary $j+1/2$, say, is calculated as a function of the total effective amount of absorber $u_s(o,j+1/2)$ from the top of the atmosphere to that level;

$$u_s(o,j+1/2) = \int_o^{u_{j+1/2}} \left[\frac{p}{p_o}\right]^{\alpha} du \approx \sum_{k=1}^{j} u'_k \qquad (4.11)$$

where $du = \rho_{gas}\, dz = m\rho_{air}\, dz = m\, dp/g$ and m is the mass mixing ratio of the gas. The term in brackets is the pressure scaling factor which takes account of the dependence of the absorption on pressure (e.g. Houghton

1977, page 140), p_o is standard pressure (1013.25 mb). The scaling is only applied for water vapour, for which $\alpha = 0.9$. No temperature dependence is included.

$$u'_k = \frac{m_k}{g} \int_{p_{k-1/2}}^{p_{k+1/2}} \left[\frac{p}{p_o} \right]^{\alpha} dp = \frac{m_k}{g} p_* \left[\frac{p_*}{p_o} \right]^{\alpha} \int_{\sigma_{k-1/2}}^{\sigma_{k+1/2}} \sigma^{\alpha} \, d\sigma \qquad (4.12)$$

$$= m_k \; p_* \left[\frac{p_*}{p_o} \right]^{\alpha} \frac{10}{g} \frac{1}{(1+\alpha)} \left[\sigma_{k+1/2}^{(1+\alpha)} - \sigma_{k-1/2}^{(1+\alpha)} \right] \qquad (4.13)$$

Where u'_k is in gcm^{-2}. Note that the mass mixing ratio m_k is taken to be constant within layer k. The term $(p_*/p_o)^{\alpha}$ is approximated as 1.01325, but this is clearly incorrect over high topography. This will be corrected in future versions of the scheme.

For the direct beam, the scaled pathlength u_s is multiplied by a magnification factor M, to allow for the greater amount of atmosphere traversed when the zenith angle ζ increases. Houghton (1963) has expressed M in the following way;

$$M = \left[1 + \frac{h}{a} \right] \left[\frac{2h}{a} + \cos^2 \zeta \right]^{-1/2} \qquad (4.14)$$

where a is the radius of the earth and h is a height which is representative for ozone absorption (taken to be 25 km). This formula takes account of the curvature of the atmosphere; for a plane-parallel atmosphere M would simply be sec ζ.

For diffuse radiation, defined as any radiation reflected by the surface and clouds or transmitted through clouds, the scaled pathlength is multiplied by a diffusivity factor (taken to be 1.67, see Liou 1980). This

allows the absorption of isotropic radiation to be calculated to a good approximation without the need for an explicit integration over zenith angle.

4.3.3 Clouds

The effect of clouds on the solar beam is shown in Figure 4.3 for a typical cloud configuration. During its passage through the atmosphere the beam is progressively split into five components; the direct beam (D) through the clear air and the four diffuse beams (B1, B2, B3 and B4), one from each cloud. The calculation of the contributions to the flux at any level is somewhat involved as it is necessary to consider all possible configurations of the convective tower with respect to the layer clouds. The basic building block is simple, however, and may be understood by considering the following example. The downward flux of solar radiation at level $k+1/2$, below a single cloud layer occupying layer j is given by;

$$S_{k+1/2} = (1-c_j)\left[S(ITD) - A^{clear}_{k+1/2} \right] \cos\zeta + c_j T_j \left[S(ITD) - A^{cloudy}_{k+1/2} \right] \cos\zeta \quad (4.15)$$

where c_j is the cloud amount and T_j the cloud transmissivity. The absorption of the clear (i.e. direct) beam and of the cloudy (i.e. diffuse after encountering cloud top) beam are;

$$A^{clear}_{k+1/2} = S(ITD).\ a\ \{ M.\ u_s\ (o,\ k+1/2)\} \quad (4.16)$$

$$A^{cloudy}_{k+1/2} = S(ITD).\ a\ \{ M.u_s\ (o,\ j-1/2) + 1.67\ u_s\ (j-1/2,\ k+1/2)\ \} \quad (4.17)$$

where a represents the combined absorption from the radiatively-active gases.

The treatment of reflection at the earth's surface is also simple with the assumption that reflected radiation is isotropically scattered. The increased absorption at the surface as a result of multiple reflections between clouds and the surface has also been included. The mean reflectivity $\bar{R}$ of the clouds as seen from the surface is calculated by weighting each cloud reflectivity R_i by the amount of solar flux S_i reaching the surface from that cloud. Figure 4.4 shows how the terms build up as the number of reflections increases. The infinite series obtained can be expressed in the following way;

$$\alpha_{eff} = \alpha \, (1 - \bar{c} \, \bar{R}) \, / \, (1 - \alpha \, \bar{c} \, \bar{R}) \qquad (4.18)$$

where α_{eff} is the effective surface albedo, α the value for clear skies and $\bar{c}$ and $\bar{R}$ are given by;

$$\bar{c} = 1 - \prod_{i=1}^{4} (1 - c_i) \qquad \bar{R} = \sum_{i=1}^{4} R_i S_i / \sum_{i=1}^{4} S_i \qquad (4.19)$$

where c_i is the amount of cloud type i.

This decrease in surface albedo can be important in cases with large amounts of low cloud which has a high reflectivity. For example, consider the extreme case of a full cover of stratus with reflectivity of 70% over snow-covered ground with an albedo of 80%. Consideration of multiple reflections decreases the albedo to an effective value of 55%. No allowance has been made for the additional absorption occurring in the atmosphere and the cloud due to multiple reflections nor for multiple reflections between two cloud layers.

The scheme includes the additional atmospheric absorption of the beams reflected from cloud and the earth's surface. As a first approximation, the reflected beams are assumed to pass to space with no further interactions with other clouds. Even with this assumption the treatment of

the reflected beam is fairly complex. Since absorption is a cumulative process and dependent on the amount of energy already extracted from that part of the spectrum, it is necessary to know the total pathlength travelled by the beam before and after reflection at the cloud or surface. This requires knowledge of what fraction of the beam, incident on the reflecting surface, has come from clouds above, i.e. at what stage in its passage through the atmosphere the beam had become diffuse.

The shortwave radiative properties of clouds are dependent on a large number of cloud parameters such as thickness and shape, liquid water content and drop size distribution, as well as on external parameters such as the wavelength of the incident radiation and the solar zenith angle (e.g. Welch et al. 1980). It is theoretically possible to determine the gross parameters of total reflectivity, transmissivity and absorptivity by using results from Mie theory and multiple-scattering calculations. However, it is difficult enough to predict the cloud amount from the model variables without additionally trying to model the above cloud parameters. The simplest approach was therefore followed when the radiation scheme was developed, in which the radiative properties are pre-set for each cloud type using typical observed values, as listed in Table 4.1.

TABLE 4.1 CLOUD SHORTWAVE PROPERTIES ASSUMED IN THE SCHEME

CLOUD TYPE	REFLECTIVITY	TRANSMISSIVITY	ABSORPTIVITY
HIGH	0.2	0.75	0.05
MEDIUM	0.6	0.3	0.1
LOW	0.6	0.3	0.1
CONVECTIVE	0.6	0.3	0.1

Given the importance of cloud-radiation interaction in modelling studies, the use of fixed cloud radiative properties is probably too crude an approximation (e.g. see Somerville and Remer (1984) and references therein). Three important effects should be considered. Firstly, the cloud radiative properties are strong functions of the total liquid water path (for a given cloud thickness and shape). The liquid water path could be parametrized from the temperature and humidity fields or held as an additional model variable (see chapter 1). Secondly, the properties depend on the solar zenith angle with, for example, the reflectivity increasing as the zenith angle increases (Liou 1976). Thirdly, the properties depend strongly on the incident wavelength, as do the surface properties (e.g. see Figure 1b of Shine et al (1984)). It is probably impractical to include the spectral detail in schemes such as that of Slingo and Schrecker (1982), but it should be possible to use, say, up to four sub-intervals (Stephens 1984). Further development of the present scheme along the above lines is not planned, however, as the intention is to replace it with a version of the scheme used in the ECMWF model (Louis 1984), which lends itself more easily to these and other improvements.

4.3.4 Surface albedos

In the original version of the scheme, the shortwave surface albedos for clear skies were 0.06 (sea), 0.2 (land), 0.5 (snow-covered land) and 0.8 (sea-ice and land-ice. Antarctica and Greenland are in the latter category). With the exception of sea and land-ice, these have been changed to incorporate more realistic values.

Firstly, the global dataset of land cover and soils data compiled by M. F. Wilson and Henderson-Sellers (1985) was used to create a geographical distribution of the snow-free land albedo α_L. This dataset has formed the

basis of a series of experiments to determine the sensitivity of the model to the land surface albedo (M. F. Wilson 1984). Secondly, the albedo of snow-covered land α_S is now a function of the snow-depth, through a formulation similar to that employed in the 5-layer model (J. M. Slingo 1982);

$$\alpha_S = \alpha_L + 0.38\ (\text{Snowdepth})^{1/2} \qquad (4.20)$$

where the snowdepth is measured in mm of the equivalent depth of water and α_S is limited to a maximum value of 0.6. This is designed to take account of the fact that as the mean snow-depth increases, not only does the snow more completely cover any surface irregularities but also the area of the grid box which is snow-free is likely to decrease. Finally, the sea-ice albedo is now a function of the ice temperature, such that above 268K the albedo drops linearly from 0.8 to a value of 0.5 at 273K. This crudely represents the tendency for leads to open through the ice and for melt ponds to form on the surface as the temperature increases.

Figures 4.5 and 4.6 show maps of the resulting surface albedo distributions used for the 2.5 x 3.75 and 5 x 7.5 degree grids, respectively.

4.4 Treatment of Longwave Radiation

Longwave radiation is absorbed and emitted by atmospheric gases, clouds and the earth's surface. The absorption by water drops is so strong that most clouds in the lower troposphere absorb essentially all the incident flux and emit a flux which is similar to that for a black-body at the cloud boundary temperature. Cloud radiative properties in the longwave region are thus independent of wavelength for practical purposes. In contrast, the wavelength-dependence of the absorption and emission by the radiatively-active gases is enormously complex. This is because they have

many vibrational and rotational energy transitions which may be excited by longwave radiation. As a result, there are tens of thousands of spectral lines, grouped into a much smaller number of bands. The design of a longwave radiation scheme thus requires a judicious division of the spectrum, such that these bands and the main regions of overlap between the contributions from the various gases are represented as accurately as possible, whilst keeping the computational expense to a minimum. The original version of the scheme used in the 11-Layer Model was described by Walker (1977) and the new (i.e. the present) version by Slingo and Wilderspin (1984b).

4.4.1 Spectral intervals

Seven spectral divisions are used to represent the complex wavelength dependence of atmospheric absorption and emission. These divisions are grouped into six distinct intervals (or bands), as shown by the circled numbers 1-6 on the bottom frame of Figure 4.7. The first interval treats the far-infrared rotation band of water vapour (0-400 cm^{-1}) and the second deals with the overlap between the weaker line absorption around the 20μm window and absorption by the water vapour continuum (400-560 cm^{-1}). The continuum is so-called because the absorption coefficient varies only slowly with wavelength, as opposed to the rapid fluctuations for line absorption (Paltridge and Platt 1976). The third interval represents the triple overlap between water vapour line and continuum absorption and the well-known 15μm band of CO_2 (560-800 cm^{-1}). The fourth (900-1100 cm^{-1}) and fifth (800-900 plus 1100-1200 cm^{-1}) intervals cover the contributions in the 10μm atmospheric window from weak water vapour lines, the water vapour continuum and the 9.6 μm band of ozone, which is important in the stratosphere. The sixth and final interval represents the 6.3 μm

vibration/rotation band of water vapour (1200 cm^{-1} upwards). Note that the weak 10 μm CO_2 band is ignored, although in principle it could easily be included as an additional term in the fourth interval.

4.4.2 Radiative Transfer Equation

The contributions to the longwave flux are calculated separately for each spectral band. Within each band, the equations for the downward and upward longwave fluxes at pressure p are;

$$F^{\downarrow}(p) = B(o).\epsilon(o,p) - \int_{p}^{o} a(p',p) \frac{dB(p')}{dp'} dp' \qquad (4.21)$$

$$F^{\uparrow}(p) = B(p_s) + \int_{p_s}^{p} a(p',p) \frac{dB(p')}{dp'} dp' \qquad (4.22)$$

where B(p) is the PLanck flux for the temperature of the air at pressure p, B(o) is thus the Planck flux for the top of the atmosphere, which is assumed to be the same as that for the top model level, and $B(p_s)$ is that for the surface. This formulation assumes that the air close to the surface is at the same temperature as the surface itself, which is a reasonable approximation in calculating the fluxes. The Planck fluxes are calculated from a third-order polynomial fit to the flux in each band as a function of temperature, which was obtained by numerical integration of the Planck function using 1 cm^{-1} spectral resolution for 5K intervals from 180K to 320K. $\epsilon(o,p)$ is the slab emissivity of the atmosphere from the top down to pressure p and a(p',p) is the slab absorptivity from the dummy pressure p' to p. Equations 4.21 and 4.22 are essentially the same as equations 2 and 3 of Ramanathan et al (1983), except for slight differences in nomenclature.

Equations 4.21 and 4.22 are solved numerically by a trapezoidal rule to calculate the fluxes at the layer boundaries. The terms which contribute to the upward and downward clear-sky fluxes at any level are illustrated on the left-hand-side of Figure 4.8. The notation is explained by the small diagram on the bottom right. The Planck fluxes are calculated at the 11 atmospheric levels and the surface and are assumed to vary linearly between these levels. The emissivities and absorptivities are calculated for each layer on the assumption that the mass mixing ratio of each gas is constant within the layer.

Evaluation of the integrals in these equations is complicated by the "half-layers", denoted by asterisks on Figure 4.8, which are found at both the upper and lower limits. The half-layers allow a more accurate calculation of the contribution to the integrals from the layer adjacent to the level at which the flux is required. This contribution can be large in regions of strong absorption. The contributions from the half-layers are calculated in a simple way to avoid excessive computation. For the half-layers closest to the level at which the fluxes are required, the dB term is one half that for the corresponding full layer (e.g. in the example shown it is $0.5(B_7 - B_6)$). The absorptivity should be calculated to the centre of the half-layer (as shown), but the version of the scheme on the Cyber 205 approximates this as one half the absorptivity to the edge of the half-layer. A factor of 0.25 thus appears in the program. This is obviously incorrect in calculating the downward flux at the surface (as the dB term does not need to be halved, so the factor should be 0.5), but the error may be ignored as the lowest sigma layer is very thin. Similar problems are posed by the half layers furthest from the level at which the fluxes are required. For the half-layer adjacent to the surface, the

absorptivity should be calculated to the centre of the half layer (as denoted by the cross), but it is taken to be that to the surface itself so that this term may be calculated in the same way as those from the higher layers. Note that the half layer at the top of the model makes no contribution to the fluxes as the atmosphere is taken to be isothermal above the top sigma level.

4.4.3 Gaseous absorption

a. Overlaps

The gaseous absorptivity in equations 4.21 and 4.22 is calculated from the transmissivity $\bar{\tau}$;

$$a(p',p) = 1 - \bar{\tau}(p',p) \qquad (4.23)$$

For a band in which water vapour is the only gaseous absorber (i.e. band 1 or 6), the emissivities and transmissivities are simply those for water vapour. For bands with two or more absorbers, the emissivities and transmissivities for each gas are combined by making the usual assumption that the transmissivities may be multiplied together to give the overlapped values. The first three bands of the scheme demonstrate the method. The subscripts on the following represent the separate contributions shown on Figure 4.7;

$$\begin{aligned} &\text{Band 1:} && \bar{\tau} = \bar{\tau}_1 \\ &\text{Band 2:} && \bar{\tau} = \bar{\tau}_2\,\bar{\tau}_9 \\ &\text{Band 3:} && \bar{\tau} = \bar{\tau}_3\,\bar{\tau}_7\,\bar{\tau}_{10} \end{aligned} \qquad (4.24)$$

Now $\epsilon \approx 1 - \bar{\tau}$, so the rules for combining emissivities are;

$$\begin{aligned} &\text{Band 1:} && (1-\epsilon) = (1-\epsilon_1) \text{ hence } \epsilon=\epsilon_1 \\ &\text{Band 2:} && (1-\epsilon) = (1-\epsilon_2)(1-\epsilon_9) \text{ hence } \epsilon = \epsilon_2 + \epsilon_9 - \epsilon_2\epsilon_9 \\ &\text{Band 3:} && (1-\epsilon) = (1-\epsilon_3)(1-\epsilon_7)(1-\epsilon_{10}) \end{aligned} \qquad (4.25)$$

hence $\epsilon = \epsilon_3 + \epsilon_7 + \epsilon_{10} - \epsilon_3\epsilon_7 - \epsilon_3\epsilon_{10} - \epsilon_7\epsilon_{10} + \epsilon_3\epsilon_7\epsilon_{10}$

b. Line absorption

The emissivities and transmissivities for the line absorption by water vapour, carbon dioxide and ozone are calculated from scaled absorber amounts for the given path by interpolation from look-up tables stored in the program. Pressure scaling is applied to the absorber amounts in the same way as described in section 4.3.2, the coefficient α having the value 0.9 for water vapour and carbon dioxide and 0.4 for ozone. Temperature scaling is applied only to the CO_2 data, as described layer.

The look-up tables were constructed by applying the version of the Goody (1952) random band model described by Hunt and Mattingly (1976) to the latest AFGL data tape (Rothman 1981). This gives, among other quantities, the line strength s_i and line width α_i for over 100,000 lines of various gases from a wavelength of less than 1 μm to the far infrared. A computer program was used to extract the data for each gas in each spectral interval. The line strengths and widths, listed on the tape for 296 K, were converted to values at 20 K intervals from 180 to 320 K using equations 4-7 of Hunt and Mattingly (1976). The quantities $\Sigma\, s_i$ and $\Sigma\, \sqrt{s_i \alpha_i}$ were then calculated in sub-intervals (typically 50 cm^{-1}) within which the Planck function may be taken to be constant. In the band model program, the transmission τ in each sub-interval at 30 K intervals from 203 to 323 K and at a pressure of 1000 mb was calculated for a range of absorber amounts u from 10^{-10} to 10^{2} g cm^{-2} in half-decade intervals. The band model approximation to τ in a direction $\cos^{-1} \mu$ to the normal is;

$$\tau = \exp\left\{ - \frac{c_1 u}{\mu} \left(1 + \frac{c_2 u}{\mu}\right)^{-1/2} \right\} \qquad (4.26)$$

where $C_1 = \sum_{i=1}^{M} S_i/\Delta\nu$ and $C_2 = \left[\frac{1}{2} \sum_{i=1}^{M} S_i \sum_{i=1}^{M} (S_i \alpha_i)^{1/2} \right]^2$

M is the number of lines in the sub-interval of width $\Delta\nu$. These transmissions were integrated over zenith angle by Gaussian quadrature to give the slab transmission τ', thus avoiding the need for a diffusivity factor in the radiation scheme.

The slab transmissions for each gas were weighted with the Planck function B(w,T) for wavenumber w and temperature T and integrated over w to give the mean transmissivity $\bar{\tau}_j$ and emissivity ϵ_j in each band j;

$$\bar{\tau}_j(u,T) = \int_j \tau'(w,u,T).\frac{dB(w,T)}{dT}\,dw \Big/ \int_j \frac{dB(w,T)}{dT}\,dw \qquad (4.27)$$

$$\epsilon_j(u,T) = \int_j (1 - \tau'(w,u,T)).B(w,T)dw \Big/ \int_j B(w,T)dw \qquad (4.28)$$

In the look-up tables, the emissivities and transmissivities given by 4.27 and 4.28 are stored for each term labelled 1-8 on Figure 4.7, for T = 263K only. The temperature dependence of the water vapour and ozone data is ignored but that of the CO_2 data is included by scaling the absorber amounts (Slingo and Wilderspin 1984b). Figure 4.9 shows curves of the emissivity of CO_2 in the 560-800 cm^{-1} band as a function of the absorber amount u for various temperatures T, as given by the band model (at 40 cm^{-1} resolution). The shape of the curves, which diverge steadily with increasing u, suggested that a reasonable approximation to the emissivity at any temperature could be obtained by using the curve for 263 K, but in addition scaling the absorber amounts with a temperature-dependent factor which is itself a function of absorber amount. After some experimentation, it was found that the following scaling of the absorber amount in each layer, Δu, was adequate;

$$\Delta u_{SCALED} = \Delta u . (T/263)^{POWER} \qquad (4.29)$$

where $POWER = 8.5 + 2 \log_{10}(\Delta u)$

where T is the layer temperature. At small Δu, POWER is forced to be zero rather than become negative. The dots on Figure 4.9 show the effective emissivities at the layer boundaries for a CO_2 concentration of 320 ppmv, obtained by using this scaling for temperatures of 203 and 323 K, which demonstrates the excellent fit to the data. Note that the dependence of the scaling on the absorber amount results in a shift of the effective emissivity curves as the CO_2 concentration is increased, but the effect on the sensitivity of the scheme to changing CO_2 amounts is very small.

c. Water vapour continuum absorption

In the original version of the longwave scheme (Walker 1977), the slab transmission for the water vapour continuum absorption was calculated from the data of Bignell (1970), taking into account the so-called e-type absorption but ignoring the dependence on temperature. The program included a large number of look-up tables of the emissivities and transmissitivies as a function of absorber amount for each of six values of the water vapour partial pressure. In the new version of the scheme these were removed and a simpler formulation substituted, which includes the strong temperature-dependence of the e-type absorption (Slingo and Wilderspin 1984b).

The distinction between emissivity and absorptivity is ignored and the transmissivity is taken to follow an exponential law, which is usually written as;

$$\bar{\tau} = \exp [- (k_1 u\ p + k_2\ u\ e)] \qquad (4.30)$$

where u is the water vapour absorber amount (gcm^{-2}), p is pressure (atmospheres, i.e. 1013 mb) and e the water vapour partial pressure (atmospheres). The foreign broadening coefficient k_1 arises from broadening of water vapour lines by collisions with other gases. The e-type coefficient k_2 is often attributed to the dimer molecule $(H_2O)_2$. Equation 4.30 can be re-arranged to give;

$$\bar{\tau} = \exp \left[- k_1 up \left(1 + \frac{k_2}{k_1} \cdot \frac{q}{0.622} \right) \right] \qquad (4.31)$$

Note that the humidity mixing ratio $q \approx 0.622\ e/p$. It is convenient to define a scaled absorber amount u_s so that we may write;

$$1 - \epsilon (p',p) = \bar{\tau} (p',p) = \exp [- k_1 u_s(p',p)] \qquad (4.32)$$

The contribution to u_s from layer k may then be written (same notation as in section 4.3.2);

$$u'_k = 1.66\ u_k \frac{p_k}{1013} \left(1 + \frac{k_2}{k_1} \frac{q_k}{0.622}\right) \qquad (4.33)$$

where the diffusivity factor (here taken to be 1.66) is required to calculate the slab transmissivity. Hence

$$u'_k = 1.66\ q_k\ \Delta\sigma_k\ p_*\ \frac{10}{g}\ \frac{\sigma_k\ p*}{1013} \left(1 + \frac{k_2}{k_1} \frac{q_k}{0.622}\right) \qquad (4.34)$$

Now k_1/k_2 is taken to be 0.005 in all four bands which include the continuum. In addition, the treatment of the temperature dependence of k_2 given by Roberts et al (1976) is included, using their best estimate of T_o = 1800 K for the temperature dependence parameter;

$$k_2(T) = k_2(296K) \exp[T_o/T - T_o/296] \qquad (4.35)$$

$$= k_2 (296K)\ f_2(T) \qquad (4.36)$$

$$\text{where } f_2(T) = \exp \left[\frac{1800}{T} - 6.081 \right] \qquad (4.37)$$

Hence equation (4.34) may be written;

$$u'_k = 1.671.10^{-3}\, q_k\, p_*^2\, \Delta\sigma_k\, \sigma_k\, (1 + 321.54\, f_2(T)\, q_k) \qquad (4.38)$$

The values of k_1 in bands 2-5 (terms 9-11 in Figure 4.7) are taken to be 0.35, 0.15 and 0.05 $g^{-1}\ cm^2\ atm^{-1}$.

4.4.4 Clouds

Just as they do for solar radiation, clouds can have a dominating effect on thermal emission. When they are present the longwave flux to space is reduced since they block the surface flux and emit at a lower temperature. Similarly, the downward surface flux is increased since the cloud radiates at a higher temperature than the equivalent black-body temperature of the radiation from clear air. Thus from the longwave standpoint both the planet and the surface tend to warm.

The effect of a typical cloud configuration on the infrared fluxes is shown in Fig 4.10. As in the solar scheme, the upward and downward fluxes each divide into five components, one from each cloud and that through the clear air either from space or the surface. The surface is assumed to act as a black-body so that the downward flux at the ground is completely absorbed. With the exception of high cloud which has an emissivity of 0.75, all clouds are treated as perfect absorbers and emitters of infrared radiation. In the scheme a cloud is assumed to be 'active' with respect to thermal radiation only near its edges, so that as a first approximation the thermal radiation leaving through the cloud surface can be identified with the black body emission at the temperature of the cloud boundary. This assumption is clearly not valid when a cloud is no longer 'black'. Then the radiation leaving the cloud will be part transmitted and part emitted. The emitted radiation will not be representative of the black body emission

at the cloud boundary temperature since it will comprise radiation from all parts of the cloud. At present the 'greyness' of high clouds is included in the scheme merely by reducing the cloud amount and then treating the cloud as a black body. When a cloud is modelled by the scheme it is assumed to occupy a whole layer or number of layers and the temperatures of the base and top of the cloud determined by taking a mean of the temperatures of the adjacent model levels.

The terms contributing to the downward fluxes at any level below a cloud layer are illustrated on the right hand side of Figure 4.8. Note that a factor 0.5 appears in the program for the half-layer adjacent to the cloud, because for convenience the dB term is calculated for the full layer (i.e. in this example to the centre of the cloudy layer). As with the half-layer adjacent to the surface, the absorptivity is calculated to the edge of the cloud. The terms contributing to the upward flux at any level above a cloud layer are calculated in the same way.

4.5 Cloud amounts used in model integrations

4.5.1 Interactive Cloud

As hinted at earlier, the major probem in incorporating interactive cloud and radiation in a numerical model is the prediction of cloud amount, height and thickness. The main reasons for this are firstly that the formation and dissipation processes for clouds are poorly understood and secondly that most clouds are sub-grid scale, both horizontally and vertically. Therefore practically all types of clouds need to be parametrized in terms of the dynamical-hydrological quantities of the model grid. For a discussion of the problems of cloud parametrization, and results from forecast integrations with interactive cloud in the limited-area tropical version of the 11-Layer Model, see J M Slingo (1978,

1980). Extension of the scheme to the global model is described by Slingo (1983, 1984) and Slingo and Wilderspin (1985). Similar work was carried out with the 5-Layer Model as described by J M Slingo (1981) and Wilson and Mitchell (1983, 1985).

4.5.2 Prescribed Cloud

Because of the problems associated with trying to generate realistic global cloud distributions with the interactive cloud scheme, many integrations are still performed with prescribed, zonally-meaned cloud amounts and heights. In versions of the model on the Meteorological Office IBM and ECMWF Cray-1 computers, the cloud climatology was the same as that used in integrations of the 5-layer Model (J. M. Slingo 1982, Bolton 1981). However, a study of the earth's radiation budget in the integration on the Cray-1 showed that there was an underestimate of the total cloud cover in the southern hemisphere (Slingo 1984/1985). In this region the data were taken from Sasamori et al (1972), who took the total cloud cover data compiled by van Loon (1972) and with various assumptions derived a breakdown into the component cloud amounts. However, the combination of these amounts and the assumption in the model of random overlap led to a significant underestimate of the total cloud cover compared with van Loon's original data. In the version of the model on the Cyber 205, the component amounts were therefore all increased so that van Loon's total cloud cover amounts are reproduced. These amounts are also in good agreement with the climatology of Berlyand et al (1980). The cloud amounts near the North Pole were also revised to be closer to the data of Huschke (1969).

The cloud amounts and heights are defined on a 10° latitude grid for mid-January, April, July and October (Tables 4.2 and 4.3). In annual-cycle integrations, the amounts are held constant for 15 days on either side of

the middle of each of the above months and at other times are linearly interpolated from the values given. The cloud heights are assigned the value from the month which is closest to the model date.

Table 4.2 Zonal-mean cloud amounts (percentage cover) used in the Interactive Radiation Scheme when running with prescribed cloudiness.

MONTH	CLOUD TYPE	N 90	80	70	60	50	40	30	20	10	0	10	20	30	40	50	60	70	80	S 90
									LATITUDE (DEGREES)											
JANUARY	H	18	20	18	20	21	19	16	13	15	20	17	16	15	17	23	28	25	18	20
	M	21	24	17	13	13	10	7	5	6	8	7	7	7	7	10	16	22	26	33
	L	12	14	25	43	44	38	28	20	25	32	34	32	32	43	62	74	54	26	14
	C	1	1	1	1	1	1	1	1	2	3	5	5	4	4	5	5	3	0	0
APRIL	H	21	21	23	26	26	24	20	17	21	20	16	14	14	14	20	22	19	12	12
	M	27	27	19	13	13	11	8	7	7	6	6	6	7	6	9	14	16	22	29
	L	26	26	31	37	35	30	23	19	24	28	31	30	34	46	61	69	51	22	12
	C	3	3	3	3	4	4	4	3	4	5	5	5	4	5	5	5	5	1	0
JULY	H	19	17	23	24	20	15	13	18	23	18	12	13	14	14	16	18	12	6	5
	M	37	33	23	11	10	7	6	7	8	7	7	6	6	6	7	10	12	13	18
	L	70	62	53	41	39	29	22	25	28	26	28	27	35	48	58	67	51	25	18
	C	4	4	5	5	5	4	3	4	7	5	5	4	5	5	6	6	5	2	0
OCTOBER	H	29	29	31	30	25	20	17	18	24	21	16	15	15	16	20	22	19	14	17
	M	38	38	26	15	14	10	7	8	8	7	7	7	7	6	9	13	12	15	18
	L	36	36	41	43	37	29	21	20	26	27	31	30	33	46	61	69	54	27	19
	C	3	3	3	4	4	4	4	4	6	5	4	3	4	4	5	5	4	1	0

Table 4.3 Same as Table 4.2 but for cloud heights (Sigma - layer boundaries counting upwards from the surface - see Figure 1.1).

MONTH	CLOUD TYPE	N 90	80	70	60	50	40	30	20	10	LATITUDE (DEGREES) 0	10	20	30	40	50	60	70	80	S 90
JANUARY	H	7	7	7	7	8	8	9	9	9	9	9	9	9	9	8	8	8	7	7
	M	5	5	5	5	5	5	5	5	5	5	5	5	5	5	5	5	5	5	5
	L	4	4	4	4	4	4	4	4	4	4	4	4	4	4	4	4	4	4	4
	C	4,3	5,3	5,3	5,3	5,3	5,4	5,4	6,4	7,4	7,3	7,3	7,4	7,4	6,4	6,4	6,4	5,3	5,3	5,3
APRIL	H	7	7	7	8	8	9	9	9	9	9	9	9	9	9	8	8	7	7	7
	M	5	5	5	5	5	5	6	6	6	6	6	6	6	5	5	5	5	5	5
	L	4	4	4	4	4	4	4	4	4	4	4	4	4	4	4	4	4	4	4
	C	5,3	5,3	5,3	5,3	5,4	6,4	6,4	7,4	6,4	6,3	6,4	7,4	6,4	6,4	5,4	5,3	5,3	5,3	5,3
JULY	H	7	7	8	8	8	9	9	9	9	9	9	9	9	8	8	7	7	7	7
	M	5	5	5	5	5	5	5	5	5	6	6	5	5	5	5	5	5	5	5
	L	4	4	4	4	4	4	4	4	4	4	4	4	4	4	4	4	4	4	4
	C	5,3	5,3	5,3	6,4	6,4	6,4	7,4	7,4	7,3	7,3	7,4	6,4	5,4	5,4	5,3	5,3	5,3	5,3	4,3
OCTOBER	H	7	7	7	8	8	9	9	9	9	9	9	9	9	9	8	8	7	7	7
	M	5	5	5	5	5	5	6	6	6	6	6	6	6	5	5	5	5	5	5
	L	4	4	4	4	4	4	4	4	4	4	4	4	4	4	4	4	4	4	4
	C	5,3	5,3	5,3	5,3	5,4	6,4	6,4	7,4	6,4	6,3	6,4	7,4	6,4	6,4	6,4	5,4	5,3	5,3	5,3

Cloud base is one level lower, except for convective cloud where the base height is also given.

4.6 Programme Details

These notes follow the logical path taken through the suite of eight subroutines which together make up the interactive radiation code.

4.6.1 COMMON Blocks

Data are communicated between individual subroutines and with the rest of the model through COMMON blocks. The radiation scheme uses eight COMMON areas of which three are especially important.

COMMON area /DCBA/ contains current values of all the model prognostic variables and supplies the radiation scheme with input data. As in all the 'physics' routines, COMMON area /IO/ is used as local work-space by the radiation code. The results from the radiation calculations are contained in COMMON block /R/ in the form of half precision, i.e. 32-bit, radiative temperature increments for the surface and atmosphere separately.

4.6.2 Subroutine Descriptions

1. RADINC

On each timestep, RADINC is called from the model master routine to add radiative increments to the model temperature fields. RADINC decides, by counting timesteps, whether to call subroutine HELIOS to re-calculate these increments. Increments are stored in half precision in arrays SRATE (surface) and RATE (atmosphere) in COMMON area /R/. They are used to update the temperature fields stored in the 'update' half of the 'A' store area in COMMON /DCBA/.

2. HELIOS

HELIOS is called by RADINC when it is necessary to do a full radiation calculation, i.e. every ID(18) timesteps. Typically, this occurs every three hours of model time. Model data required for the calculations are

passed to HELIOS through COMMON /DCBA/ and the udpated increments are returned to RADINC through COMMON /R/. On entry, HELIOS assumes the role of a master routine to organise and control the radiation calculations. These calculations conveniently divide into solar (shortwave) and terrestrial (longwave) parts which are treated independently. This separation strongly influences the organisation of the calculations.

Gather/Scatter

The model grid is divided into a number of equal length vectors (or arrays) which may be regarded as collections of grid points. The cornerstone of this organisation is a field-length bit vector called DAYBIT which is 1 at points receiving solar radiation during the period covered by the call to HELIOS and 0 otherwise. Data are gathered from /DCBA/ under DAYBIT control such that all the points which receive solar radiation are dealt with first, followed by those which do not. The first n vectors thus contain 'day' points only, the (n+1)th vector contains some 'day' followed by some 'night' points and subsequent vectors contain 'night' points only. This organisation allows vectors containing only 'night' points to bypass the solar calculations altogether, thereby minimizing computation. DAYBIT is used again when the calculations are complete to scatter heating rates back into COMMON /R/.

Preliminary calculations

The first task of HELIOS is to generate a look-up table of natural logarithms for the function routine VFLOG. These data are placed in arrays UPLK1 and UPLK2 in COMMON area /LOG/.

The incoming solar flux at the top of the atmosphere, OC, is calculated for the relevant day in the 360-day year (Slingo A 1982) and is then reduced by 3% to allow for Rayleigh Scatter (see section 4.3.1). OC is stored in COMMON /IO/. Various orbital constants for the 360-day year are set up in DATA statements near the beginning of HELIOS.

Subroutine HELIOS2 is called to calculate various quantities from data supplied in the block-data area named JRCDATA.

The DAYBIT vector (described earlier) is generated by a calculation at each grid point to determine whether any solar flux is going to be received between this and the next call to HELIOS. The number of 'day' vectors is determined by counting 1's in DAYBIT and dividing by the vector length (a prescribed quantity held in the PARAMETER statements. Vector IMK contains the beginning and end points of each collection (or vector) of grid points. The logical variable NIGHT in COMMON /NIGHT/ is initialized to .FALSE..

Main Loop Calculations ("DO 77777")

For each vector in the main loop, a subset of DAYBIT is used to gather data from COMMON /DCBA/ into radiation scheme workspace. Surface pressure and the atmospheric temperatures and specific humidities are gathered from A in /DCBA/ and placed in arrays PSTARX, TX and QX respectively.

If the current vector is a 'day' vector, i.e. NIGHT = .FALSE., the solar zenith angle averaged over the time between calls to HELIOS is calculated and placed in array COSZ in /IO/.

Surface temperature, soil moisture content and snowdepth are gathered from B in /DCBA/ and placed in arrays TSTARX, TTTARX and TUTARX respectively.

Cloud shortwave reflectivities are set explicitly (see table 4.1) and the surface albedo is initialized to zero. These quantities are held in array REFL in /IO/.

Subroutine LAYER is called to generate cloud amounts,bases and tops. These may be either from the zonal mean climatology or interactive clouds diagnosed from model variables (see section 4.5). On return to HELIOS the bit vector INDEX, in /IO/, is set to 1 at points where cloud is present.

Maximum and minimum cloud bases and tops are determined and stored in arrays MXCB, MXCT, MNCB and MNCT in COMMON /IO/. These are used later in the program to set limits of DO loops for the treatment of cloud-radiation interactions.

Vertical columns of atmospheric temperature, specific humidity and ozone mixing ratio are constructed in arrays TAEXP, CH and CO in COMMON /IO/. The temperatures in TAEXP are the means of the adjacent σ-level values stored in TX. They are used in subroutine CLOUD to calculate the longwave fluxes from the tops and bases of clouds (section 4.4.4). Specific humidities and ozone mixing ratios are not allowed to fall below 10^{-7} g/g and 10^{-8} g/g respectively. The ozone data from C in /DCBA/ are interpolated onto σ-levels above 200 mb from mean data for 40 mb thick layers.

The scaled pathlengths u_s (equation 4.11) for each radiatively-active gas are calculated from the surface (I=1) up to each layer boundary (I=12 is the top of the atmosphere) and placed in arrays TPATH (line absorption) and TTPVP (continuum) in COMMON /IO/. The CO_2 longwave temperature scaling (equation 4.29) is also applied. The continuum pathlengths are given by equations 4.38 and 4.37. For line absorption, everything after the first p_* in equation 4.13 is pre-calculated and stored in the following variables;

Index	Gas	Value of α	Variable
1	H_2O	0.9	PH
2	CO_2 longwave	0.9	PC
3	O_3 longwave	0.4	PO
4	O_3 shortwave	0	OS
5	CO_2 shortwave	0	PATHC

Note that PC and PATHC also include the mass mixing ratio (4.9×10^{-4}).

These data are used to calculate the scaled pathlengths EOD (continuum) and OD (line) between any two layer boundaries for each gas active in the longwave. There are 66 pathlengths (11 + 10 + ... 1). The final values in OD are 2 x $\log_{10}$ (the pathlengths) for later use by EMISS in accessing the look-up tables of emissivity and transmissivity, where the data are stored in half-decade intervals (section 4.4.3.b).

If NIGHT = .FALSE. the following solar calculations are made;

The magnification factor (eqn 4.14) is calculated for all 'day' points in the vector and stored in array XMAG in COMMON /IO/. Array AXMAG contains $\log_{10}$ (XMAG).

Subroutine CLEARAB is called to calculate the upward (reflected) and downward clear-sky solar absorptions as percentages of the effective incoming solar flux, OC, using the data shown in Figure 4.2. On return to HELIOS these percentages are changed into fluxes and stored in COMMON /IO/ in arrays RABSC and ABSC for upward and downward fluxes respectively.

The surface shortwave albedo is determined according to surface type and stored in array ALBEDO in COMMON /IO/. Some versions of the code simply use preset values for each surface type, whereas later versions contain a more realistic treatment (see section 4.3.4).

At this point HELIOS leaves the solar scheme to perform the bulk of the longwave calculations. Subroutine EMISS is called to calculate the gaseous contributions to the longwave fluxes (Wm^{-2}) for each model layer. On return to HELIOS, arrays E, TR and TRH in COMMON /IO/ contain slab emissions from each model layer, mean slab absorption for all possible (66) slabs and mean absorption for the half-layers, respectively. All are in units of Wm^{-2}. Arrays TR and TRH contain absorptions from longwave sources both above and below the slabs in question. These data are used to calculate the clear sky upward and downward longwave fluxes at each layer boundary. The results are placed in arrays DI (downward fluxes) and UI (upward fluxes) in COMMON /IO/.

Subroutine CLOUD is called to calculate upward and downward cloudy longwave and solar fluxes. On return to HELIOS the following arrays in COMMON /IO/ will have been affected; DS, B1, B2, B3, B4, CFDOWN, REFL, REF in the solar scheme and U, DB, DI and UI in the longwave scheme.

DS, B1, B2, B3, B4 are the downward solar clear-sky and diffuse fluxes at the layer boundaries from the four cloud types (see figure 4.3). CFDOWN is the sum of these components, i.e. the downward solar flux at each model layer boundary. Array REF contains the upward (reflected) solar fluxes at the layer boundaries from each of the four cloud types and the surface. The effective surface albedo, after allowance is made for multiple reflections between surface and clouds (see figure 4.4), is contained in array REFL.

The longwave clear sky upward and downward fluxes in UI and DI are adjusted for clouds. Upward and downward longwave fluxes from clouds at each layer boundary are contained in arrays U and DB respectively.

Solar calculations are now completed by including the effects of surface reflections. Upward and downward solar fluxes at each model layer boundary are contained in arrays CFUP and CFDOWN in COMMON /IO/.

Total upward and downward fluxes at the layer boundaries are calculated by adding the components and are placed in arrays B1 and B2 in COMMON /IO/ respectively. These fluxes are used to calculate atmospheric and surface heating rates by flux differencing (equations 4.1 and 4.2). In current versions of the scheme the surface heating rates over sea points are explicitly set to zero. All the radiation calculations for this pass through the main loop are now complete so any radiation diagnostics required are generated and stored in workspace in COMMON /IO/.

The final operation in the main loop is to scatter the heating rates and any diagnostics back into field form to COMMON /R/ and the diagnostic area of /DCBA/ respectively. Addresses of the beginning and end points of the vector and logical variables such as NIGHT are reset for the next vector.

Final Calculations

Having left the main loop calculations for the last time, the arrays SRATE and RATE in common area /R/ are updated with the new heating rates. These data are changed into radiative temperature increments by multiplying by the relevant time step (forward or leap frog) ready for passing back to the calling routine RADINC.

3. HELIOS2

This subroutine is called by HELIOS to calculate various quantities from data supplied in the block-data area JRCDATA.

Differences between successive elements of the emissivity and transmissivity look-up tables in arrays EM and TBAR are calculated and stored in arrays EMA and TBARA in COMMON /RADCONST/. Transmissivities of all cloud combinations are claculated from the individual cloud values and stored in TS12 to TS1234 in COMMON /RADCONST/. Look-up tables of solar absorptivity differences are calculated from data in arrays AH2OAB, ACO2AB and AO3AB and stored in arrays ADH2OAB, ADCO2AB and ADO3AB in COMMON /RADCHEM/.

4. LAYER

Subroutine LAYER is called by HELIOS to calculate cloud amounts, bases and tops. These are either interpolated values from the zonal-mean cloud climatology (Tables 4.2 and 4.3) or diagnosed from model variables in the interactive scheme.

Prescribed clouds are interpolated twice; first, onto the models latitudinal grid from the 10° data (loop 10) and then to the relevant day (loop 50) from the four mid-month values (see section 4.5.2).

The interactive cloud scheme calculates convective cloud amounts, bases and tops from data passed to it from the convection scheme. The relative humidity of each model layer is adjusted to represent the value for the environmental air outside the (saturated) convective tower. Layer cloud amounts are calculated in layers where the modified relative humidity exceeds some prescribed threshold value. These layer clouds are then sorted into high, medium and low on the basis of the maximum amounts in specified layers, typically σ-layers 11 to 9 for low cloud, 8 to 6 for medium cloud and 5 to 2 for high cloud.

Both the fixed and interactive cloud schemes pass amounts, bases and tops back to HELIOS in arrays CA, CB and CT respectively in COMMON /IO/.

5. CLEARAB

Subroutine CLEARAB is called by HELIOS to calculate upward and downward clear-sky shortwave absorptions as percentages of the effective incoming solar flux, OC.

The downward clear-sky absorption is calculated in loop 10, which cycles round the model layer boundaries from the surface upwards. The vertical pathlengths from the top of the atmosphere down to each layer boundary are calculated for each absorber and stored in array ODC in COMMON /IO/. The zenith angle dependence is then included by multiplying the vertical pathlengths by the magnification factor stored in array AXMAG (equation 4.14). The percentage shortwave absorption for each gas is calculated from the look-up tables. The range of reference path-lengths for each absorber in these tables is indicated on Figure 4.2 and listed below;

GAS	RANGE ($\log_{10}$)	INCREMENT	NO. OF POINTS
H_2O	-5.4 to 3.0	0.2	43
CO_2	-6.2 to 0.8	0.5	15
O_3	-6.6 to -1.7	0.1	50

The solar absorptions down to the layer boundaries by each gas are summed into array ABSC in COMMON /IO/.

The upward clear-sky absorptions to each layer boundary above each of the five reflecting surfaces (four clouds and the surface), are calculated in loop 100. Pathlengths for the direct beam from the top of the atmosphere down to the level of each reflector and from the surface to the layer boundaries above the reflectors are gathered from arrays ODC and

TPATH respectively. The latter are used to calculate the diffuse pathlengths between the reflectors and the overlying layer boundaries in loop 2000. These diffuse pathlengths are added to the direct pathlengths gathered from ODC to form the total pathlengths from the top of the atmosphere down to each surface (direct), and back up to each of the overlying layer boundaries (diffuse). Gaseous absorptions are determined from look-up tables as before and summed into array RABSC in COMMON /IO/ for each reflecting surface.

6. EMISS

Subroutine EMISS is called by HELIOS to calculate the longwave gaseous emissivities and absorptivities for each model layer (i.e. the gaseous contributions to equations 4.21 and 4.22). The Planck fluxes at the surface and for each σ-level (B_1 to B_{12} in Fig. 4.8) are calculated for each spectral band (see fig. 4.7) using a third-order polynomial in temperature. Fluxes and flux differences (dB in fig. 4.8) are placed in arrays PF and PFD in COMMON /IO/.

There are three sections in the main loop (DO loop 1) calculations. Mean slab emissivities are calculated and stored in array E, mean slab absorptivities for all 66 possible slabs are stored in array TR and slab absorptivities for the 'half-layers' are stored in array TRH.

Absorber amounts are gathered from arrays OD and EOD, in COMMON /IO/, for atmospheric slabs progressively increasing in depth from the top of the atmosphere down to each layer boundary. Gaseous emissivities in each spectral band are interpolated from look-up tables of emissivity (array EM) and emissivity differences (array EMA) and stored in the workspace array EEV in COMMON /IO/. Water vapour continuum emissivities (terms 9 to 11 in fig. 4.7) are calculated directly from eqn. 4.32. Overlapped band

emissivities (see eqn. 4.25) are weighted by the Planck flux in each band and summed into array E as the longwave emission at the layer boundaries (i.e. term $B(o)\epsilon(o,p)$ in eqn. 4.21).

The Planck flux gradient, dB, is different for the top and bottom of each slab, so the absorptivity terms ($a(p',p).dB(p')$ in equations 4.21 and 4.22) have to be calculated separately for the downward (IDNUP=1) and upward (IDNUP=2) fluxes (in the DO 52 and DO 54 loops).

Nested loop 5 calculates these terms for all 66 possible slabs. Absorber amounts in each slab are gathered from arrays OD and EOD. Slab transmissivities in each band are calculated from look-up tables of transmissivity (array TBAR) and transmissivity differences (array TBARA) and from eqn. 4.32 (for water vapour continuum). These are overlapped (eqn. 4.24) to obtain band transmissivities which are then weighted by PFD in the up and down directions. They are summed over the bands and using equation 4.23 are transformed into absorptivities which are stored in array TR in COMMON /IO/.

The absorptivity calculations are repeated for halved absorber amounts in each model layer gathered from arrays OD and EOD (see section 4.4.2 for discussion of 'half-layers'). The calculated 'half-layer' slab absorptivities in the downward and upward directions are stored in array TRH in COMMON /IO/.

7. CLOUD

Subroutine CLOUD is called by HELIOS to calculate the effect of clouds on the upward and downward longwave and shortwave fluxes. It is in two parts, dealing with solar fluxes first, followed by longwave fluxes.

The solar part is entered if .NIGHT. is set .FALSE. . Subroutine CLOUDAB is called to calculate upward and downward diffuse solar absorptions. These are stored in arrays RABSD (upward fluxes) and ABSD (downward fluxes) in COMMON /IO/.

The direct and diffuse components of the solar beam at the layer boundaries (D, B1, B2, B3 and B4 in fig. 4.3) are first calculated in the absence of the convective tower (loop 14). They are then adjusted for the position of the convective cloud top (loop 990) and base (loop 160). The components are summed together to form the downward solar flux at each layer boundary and stored in array CFDOWN in COMMON /IO/.

Effective surface albedos are calculated to allow for multiple reflections between clouds and the surface. These are stored in array REFL in COMMON /IO/.

Do loop 90 cycles round the five reflecting surfaces using data gathered from arrays ABSD and ABSC to calculate the total solar absorption to the level of each reflector, ABSTOT, and the solar flux incident on each reflector, FLUXT. Loop 97 uses data gathered from arrays RABSD and RABSC to calculate the total solar absorptions to each layer boundary above the reflectors, and stores them in RBSTOT. The upward solar fluxes at layer boundaries above each reflecting surface are calculated from FLUXT, ABSTOT and RBSTOT and stored in array REF in COMMON /IO/.

The solar part of CLOUD is now complete (77774 CONTINUE) and attention turns to the effect of clouds on the longwave fluxes.

Cloud-free upward and downward fluxes, calculated in HELIOS and stored in arrays UI and DI, are adjusted by the clear-sky fraction in each layer to allow for clouds.

The upward and downward fluxes emitted from clouds are calculated at the layer boundaries above and below each cloud in turn. Cloud top and base temperatures are gathered from array TAEXP and slab absorptivities are gathered from arrays TR and TRH in COMMON /IO/. These data are used in loops 23 and 309 to calculate downward cloudy fluxes and in loop 29 to calculate upward cloudy fluxes. The upward and downward cloudy fluxes at the layer boundaries above and below each cloud are stored in arrays U and DB respectively in COMMON /IO/.

8. CLOUDAB

Subroutine CLOUDAB is called from subroutine CLOUD to calculate upward and downward diffuse solar absorptions as percentages of the effective incoming solar flux, OC. Downward diffuse solar absorptions to the layer boundaries below clouds are calculated in loop 100. Direct pathlengths for each absorber from the top of the atmosphere down to cloud top and from the surface up to cloud top are gathered from arrays ODC and TPATH respectively. Diffuse pathlengths between cloud top and underlying layer boundaries are calculated in loop 20 and stored in array ODD in COMMON /IO/. These pathlengths are summed with the direct pathlengths gathered from ODC to form the total pathlengths from the top of the atmosphere to the layer boundaries below cloud top. Percentage absorptivities are interpolated from look-up tables for each absorber and summed into array ABSD in COMMON /IO/.

Upward diffuse solar absorptions to layer boundaries above clouds and the surface are calculated in loop 3100. The technique for constructing total pathlengths is the same as before. Total pathlengths for each absorber from the top of the atmosphere to layer boundaries above cloud top are calculated in loops 2000 and 200 using pathlength data gathered from

arrays ODC, ODD and TPATH. Percentage absorptivities are interpolated from loop-up tables for each absorber and summed into array RABSD in COMMON /IO/.

9. JRCDATA (Block Data)

Longwave emissivity and transmissivity data for 25 reference values of absorber amount (path-length) are placed in arrays EM and TBAR respectively in COMMON/RADCONST/. There are a total of eight tables; six are for H_2O in each band of the longwave spectrum (see fig. 4.7) with one each for CO_2 (term 7) and O_3 (term 8).

Absorber amount data are placed in arrays PH, PC, PO, OS and PATHC in COMMON /RADCONST/ (see table on page 80).

Cloud transmissivities for high, medium, low and convective cloud are stored in TRANS1 to TRANS4 respectively in COMMON /RADCONST/.

Solar absorptivity data for each gas at various reference pathlengths (see Fig. 4.2 and Table on page 84) are stored in arrays AH2OAB (H_2O), ACO2AB (CO_2) and AO3AB (O_3) in COMMON /RADCHEM/.

The coefficients required by the polynomial fits to the Planck flux in each band are stored in PFCO and their sum in PFSUM.

10. VFLOG (Function)

This is a function routine called throughout the radiation scheme to calculate natural logarithms. It is faster than the system routine because it derives logarithms from look-up tables contained in arrays UPLK1 and UPLK2 in COMMON /LOG/. Zero arguments are replaced by 1.0 E-50 and negative arguments cause termination of the integration.

5. SURFACE AND BOUNDARY LAYER

5.1 SCIENTIFIC BASIS

5.1.1 Introduction

The boundary layer subroutine treats not only the effects of turbulent mixing through the atmospheric boundary layer on the atmospheric variables, but also those of the surface turbulent fluxes on the surface prognostic variables. Three boundary layer schemes were used in the 11-Layer Model on the IBM 360/195 computer (Heasman 1983,1984). These have identical treatments of the interactions between the surface and the lowest model layer (Carson 1982a) and differ only in the treatment of the turbulent exchanges between the model layers in the boundary (Ekman) layer. The schemes are called;

1. CLARKE : based on the ideas of Clarke (1970), See Carson (1982b)

2. RICHARDS: An extension of the method of Clarke described in Richards (1980a,b),

3. EXPLICIT-TOP: So-called because the depth through which turbulent mixing occurs is predicted explicitly (Richards 1980b, Heasman 1983) and may take any value independent of the vertical grid. This scheme is not available in the Cyber model.

The treatment of the surface and the calculation of the surface turbulent exchanges with the atmosphere are described in sections 5.1.2 and 5.1.3 respectively. The treatment of the turbulent exchanges within the Ekman layer itself is discussed in section 5.1.4 for the CLARKE and RICHARDS schemes.

5.1.2 Treatment of the surface

The surface prognostic variables are the temperature T_* (in K), soil moisture content SMC (in cm. of water) and snow depth SNODEP (in cm. of water when melted). They are held at all points on the model's grid,

although updating of a given variable takes place only for certain surface types. Where the variable is not to be updated, as for example for soil moisture over the sea, it may be assigned a value which acts as an indicator of the surface type. The four surface types used by the model are land, sea, land-ice and sea-ice. The range of values which the surface variables are allowed to take and the values used to indicate the surface type are shown in Table 5.1.

TABLE 5.1 - SURFACE VARIABLES AS A FUNCTION OF SURFACE TYPE

Surface type	T_* (K)	SMC (cm)	SNODEP (cm)
SEA	PRESCRIBED	100*	0
SEA-ICE	≤ 271.2	1000*	SNODEP ≥ 0
LAND-ICE	≤ 273	10000*	SNODEP ≥ 100
LAND	ANY VALUE	$0 \leq$ SMC ≤ 15	SNODEP ≥ 0

*Used as an indicator of the surface type.

In the standard version of the model, the soil moisture content and snow depth are allowed to vary over the land as determined by budget equations for water, snow and heat. The snow depth is increased by snowfall from the large scale precipitation and the convection schemes and decreased either by sublimation or by snow-melt (if the surface temperature exceeds 273K). The soil moisture content is increased by rainfall from the large scale precipitation and convection schemes and by snow-melt. It is decreased by evaporation and is limited to an assumed maximum field

capacity of 15 cm, above which runoff is assumed to occur. The soil moisture content is used to control the evaporation from the land surface (see below).

The sea surface temperatures (SSTs) are prescribed when the model is run without an interactive ocean surface. In seasonal integrations these temperatures are updated every 5 days by reading pentad SST datasets derived from the same bi-monthly data used to set up such integrations with the 5-Layer Model (J M Slingo 1982, section 2(c)). In the pentad datasets, the sea-ice points are flagged by SST < 271.3K, which is used in subroutine CLIMAT (see Hinds 1985) to set the soil moisture indicator as shown in Table 5.1.

The surface temperatures for land-ice, sea-ice and land points are calculated from the surface energy balance equation;

$$\Delta T_* = \frac{\Delta t}{C*} \left[R_N - H - Q + Q_F + H_I \right] \qquad (5.1)$$

where Δt is the timestep, $C*$ is the effective surface thermal capacity, R_N is the surface net radiation, H is the surface sensible heat flux (positive into the atmosphere), $Q = LE$ is the latent heat flux due to surface evaporation (or sublimation), Q_F is the latent heat release associated with the freezing or melting of snow cover and H_I is the heat flux through sea-ice from the underlying ocean. R_N is calculated and used to update $T*$ in the radiation subroutine. All other terms are applied in the boundary layer subroutine.

H_I is calculated according to

$$H_I = \frac{(271.2 - T*)\ \text{conductivity}}{(\text{thickness})} \qquad (5.2)$$

with an assumed sea ice thickness of 2m, and a conductivity of 2.09 Wm^{-1} K^{-1}. The temperature of the sea beneath the ice is assumed to be 271.2K. The thermal capacity of the land surface is assumed to be equivalent to 5 cm of water. In the program, $1/C_*$ is set to be 4.8 10^{-6} J^{-1} m^2K.

5.1.3 Surface turbulent fluxes

a. Introduction

Let F_χ represent the mean vertical turbulent flux of some conservative quantity whose mean value is χ. Then $F_\chi = \overline{w'\chi'}$ in conventional turbulence notation is the eddy covariance of χ and the vertical velocity component w.

It is standard practice at the surface (σ=1) to express F_χ by the bulk formula;

$$F_\chi = (\overline{w'x'})_* = -\rho_* C_\chi |V(Z_{11})| \Delta\chi$$
$$= -\rho_* C_\chi |V(Z_{11})| [\chi(z_{11}) - \chi_*] \qquad (5.3)$$

where C_χ is a bulk transfer coefficient, $V(Z_{11})$ is the wind velocity at height Z_{11}, taken as that of the lowest atmospheric level (σ=0.987), $\Delta\chi$ is the difference between $\chi(z_{11})$, the value of χ at height z_{11} and its surface value χ_*. ρ_* is the density of the air at the surface.

The form of this equation for Evaporation (χ = q) is;

$$E = -\rho_* C_E |V(z_{11})| [q(z_{11}) - q_*] \qquad (5.4)$$

where q_* is the "surface specific humidity".

The problem then reduces to the determination of q_* from the saturation surface specific humidity q_{sat} (T_*). A few models have prescribed a surface relative humidity r_* and defined

$$q_* = r_* q_{sat} (T_*) \qquad (5.5)$$

More commonly a potential evpaoration (E_p) is defined by the right hand side of (5.4) with $q_* = q_{sat}(T_*)$ and evaporation taken as

$$E = \beta E_p \qquad (5.6)$$

with β a linear function often modelled as a function of the soil moisture with a maximum value of unity. This can be interpreted as representing a fraction β of the surface as saturated and the remainder as having the same specific humidity as the air (Rowntree 1983b);

$$q_* = \beta\, q_{sat}(T_*) + (1-\beta)\, q(z_{11}) \qquad (5.7)$$

In the 11-Layer Model, β=1 if the soil moisture content is equal to or greater than 5 cm. If the soil is drier then;

$$\beta = SMC/5 \qquad (5.8)$$

In the latest version of the model (as used in the Third Control Annual Cycle integration), a surface resistance to evaporation of r_s = 60sm^{-1} is included over land points by replacing $C_E|V(z_{11})|$ in equation (5.4) by $(1/C_E|V(z_{11})| + r_s)^{-1}$. This was first incorporated into the operational fine mesh model to reduce evaporation over land (thereby increasing the sensible heat flux) and reduce a tendency for too much rainfall from shallow convection over the UK in summer. The term was included in the 11 Layer-Model partly for consistency with the operational model and partly because it improves (ie increases) the ratio of sensible to latent heat flux from land surfaces, which has tended to be too low.

For more discussion on the calculation of surface evaporation in numerical models see Carson (1982b) and Rowntree (1983b).

b. Surface layer bulk transfer coefficients used

Theoretical and field observational studies indicate that, in general, C_χ is different for each χ and is a complicated function of height, atmospheric stability, surface roughness and other physical and physiological characteristics of the surface vegetation. The surface layer bulk transfer coefficients for momentum (C_D), heat (C_H) and moisture (C_E)

transfer used in the 11-Layer Model are illustrated in Figure 5.1 and have been derived from Monin-Obukhov similarity theory. They are expressed as functions of the surface roughness length, z_o (assumed to be 0.1 m over the land and 10^{-4} m over the sea), and a suitably defined stability parameter (the bulk Richardson number, RIB, for the layer approximately 100 m thick, from the surface to layer 11). For a full description of the general method and the assumptions implicit in it see, for example, Carson and Richards (1978). For further particular details for the 11-Layer Model see Carson (1982b). The following description is taken from Heasman (1983).

For the turbulent surface layer, Monin-Obukhov similarity theory states that

$$\frac{\partial x}{\partial z} = \frac{x*}{kz} \Phi_x (z/L) \qquad (5.9)$$

where Φ_x is a universal similarity function, $x*$ is a scaling parameter for x in the surface layer and k is von Karman's constant (taken to be 0.4). The Monin-Obukhov length is given by (Carson and Richards 1978);

$$L = - \frac{u*^3}{\frac{kg}{T}\left[\frac{H}{\rho c_p} + \frac{0.61TE}{\rho}\right]} \qquad (5.10)$$

$u*$ is the friction velocity and g the acceleration due to gravity. Integration of (5.9) gives:

$$\frac{k \Delta x}{x*} = \int_{\zeta_o}^{\zeta} \frac{\Phi_x (\zeta') \, d\zeta'}{\zeta'}$$

$$\equiv \Phi_x (\zeta, \zeta_o) \qquad (5.11)$$

where $\zeta_o = z_o/L$ and $\zeta = z/L$, z_o is the characteristic surface roughness length.

The surface scaling parameter x_* is related to the vertical turbulent flux through

$$F_X \equiv - u_* X_* \qquad (5.12)$$

so, from (5.3):

$$C_X = \left[\frac{u_*}{V(z)} \right] \left[\frac{X_*}{\Delta X} \right] \qquad (5.13)$$

Thus C_X can be expressed in terms of the functions defined by (5.11);

$$C_X = k^2 / \left[\Phi_m (\zeta, \zeta_o) \; \Phi_x (\zeta, \zeta_o) \right] \qquad (5.14)$$

The Bulk Richardson Number (RIB) of the surface layer gives a measure of its stability. It is defined by

$$RIB = \frac{z_{11}}{|\underline{V}_{11}|^2} \frac{g}{T_{11}} \left[(\theta_{11} - \theta_*) + 0.61 \, \beta \, (q_{11} - q(T_*)) \right] \qquad (5.15)$$

where β is given by (5.8).

On the stable side (RIB > 0) the 11-Layer Model uses values of ϕ suggested by Webb (1970). On the unstable side, the values of ϕ given by Dyer and Hicks (1970) are used.

In the model the values of C_D and C_H evaluated from (5.14) are tabulated as functions of RIB for the values of roughness length used. Calculation of C_D and C_H is then done by linear interpolation using this table.

5.1.4 The treatment of the Ekman layer

a. Introduction

Both the Clarke and the Richards schemes use the concept of eddy diffusivity to represent the turbulent exchanges in the boundary layer. By analogy with molecular diffusivity, it is assumed that the flux F_χ of a quantity is related to the vertical gradient of that quantity:

$$F_\chi = - K_\chi \frac{\partial \chi}{\partial z} \qquad (5.16)$$

and that one can write

$$K_\chi = l_m l_\chi \left| \frac{\partial V}{\partial z} \right| = \Lambda_\chi^2 \left| \frac{\partial V}{\partial z} \right| \qquad (5.17)$$

where $\underline{V}$ is the horizontal wind velocity, l_m, l_χ are the mixing lengths for the vertical transfer of momentum and χ respectively, and

$$\Lambda_\chi = (l_m l_\chi)^{1/2} \qquad (5.18)$$

In reality the specification of appropriate functions for K_χ (or Λ_χ) is very difficult. However, in practice in the CLARKE boundary layer scheme the mixing-lengths were assumed to vary very simply with height and stability as detailed in Method I of Clarke (1970).

A comprehensive study of the eddy diffusivity approach to the parametrization of the turbulent transfer processes in the boundary-layer was later made by Richards (1980a) who developed and tested more detailed functional forms for the mixing-lengths and incorporated these into the RICHARDS scheme.

b. Clarke scheme

In the Clarke scheme (see Carson 1982a), the boundary layer is assumed to occupy the lowest three model layers (9, 10 and 11), as shown in Figure 5.2. The mixing lengths for momentum, heat and water vapour are assumed to

be all the same. The Clarke scheme is summarised in Figure 5.3, where l_1, l_2 are the mixing lengths used to calculate the transfers between levels 11 to 10, and 10 to 9 respectively. In very stable conditions (Clarke's class IV), l_1 = 15m and l_2 = 30m. In moderately stable conditions (Clarke's class III) and in moderately unstable conditions (Clarke's class II) l_1 = l_2 = 30m. The boundary layer scheme 'mixes' u, v, θ and q for these three cases. In unstable conditions when both the surface and the lowest pair or lowest two pairs of layers are convectively unstable (Clarke's class I), the vertical mixing of heat and water vapour is handled by whichever convection scheme is employed in the model and only momentum is mixed by the boundary layer scheme. In these conditions the mixing lengths vary linearly between $l_1 = l_2$ = 30m and l_1 = 100m, l_2 = 200m according to the degree of instability L_* (= u^*/f). The depth of convection is taken to be 515m when only the lowest two atmospheric layers are unstable with respect to each other and 1360m when all three are unstable, ie. convection is occurring throughout the boundary layer.

The formulation of the boundary layer diffusion equations is given below.

(i) Momentum:

$$\frac{\partial u}{\partial t} = -\frac{1}{\rho}\frac{\partial \tau_z}{\partial z} = \frac{g}{p_*}\frac{\partial \tau_z}{\partial \sigma} \qquad (5.19)$$

where

$$\tau_z = -\rho K\frac{\partial u}{\partial z} = -\rho\left[\frac{g\rho}{p_*}\right]^2 l^2 \left|\frac{\partial u}{\partial \sigma}\right| \frac{\partial u}{\partial \sigma} \qquad (5.20)$$

The hydrostatic and gas equations imply:

$$\tau_z = p_*\left[\frac{\partial \phi}{\partial \sigma}\right]^{-3} g^2 l^2 \left|\frac{\partial u}{\partial \sigma}\right| \frac{\partial u}{\partial \sigma} \qquad (5.21)$$

Hence

$$\frac{\partial u}{\partial t} = -\frac{\partial}{\partial \sigma}\left[\left[\frac{g}{\partial \phi/\partial \sigma}\right]^3 l^2 \left|\frac{\partial u}{\partial \sigma}\right| \frac{\partial u}{\partial \sigma}\right] \qquad (5.22)$$

In finite difference form this is

$$u_k = u'_k - 2\Delta t\ \delta_\sigma \left[\left[\frac{g}{\Delta\phi} \right]^3 l^2 \left| \Delta u \right| \Delta u\ \Delta\sigma \right]_k \qquad (5.23)$$

where u'_k is the value of u at the kth grid point obtained after the model has been integrated from time $(t-2\Delta t)$ but before applying the boundary layer equations.

(ii) Heat transfer:

The equation is written in terms of potential temperature, θ. Mixing length theory implies

$$\frac{\partial\theta}{\partial t} = \frac{-1}{\rho} \frac{\partial}{\partial z} \left[\frac{H}{Cp} \right] \qquad (5.24)$$

$$= \frac{g}{p*} \frac{\partial}{\partial\sigma} \left[\frac{H}{Cp} \right] \qquad (5.25)$$

$$\text{Now } \frac{H}{\rho Cp} = K \frac{\partial\theta}{\partial z} \qquad (5.26)$$

Substituting (5.26) into (5.25) and using the hydrostatic equation to change from ∂z to $\partial\sigma$ gives

$$\frac{\partial\theta}{\partial t} = -\frac{\partial}{\partial\sigma} \left[l^2 \left[\frac{g\rho}{p*} \right]^3 \left| \frac{\partial u}{\partial\sigma} \right| \frac{\partial\theta}{\partial\sigma} \right] \qquad (5.27)$$

or in terms of temperature, T:

$$\frac{\partial T}{\partial t} = -\sigma^K \frac{\partial}{\partial\sigma} \left[l^2 \left[\frac{g}{\partial\phi/\partial\sigma} \right]^3 \left| \frac{\partial u}{\partial\sigma} \right| \frac{\partial}{\partial\sigma} \left[\frac{T}{\sigma^K} \right] \right] \qquad (5.28)$$

The finite difference form is analogous to (5.23)

(iii) Water vapour:

Similar arguments to those used in (i) and (ii) lead to:

$$\frac{\partial q}{\partial t} = -\frac{\partial}{\partial\sigma} \left[l^2 \left[\frac{g}{\partial\phi/\partial\sigma} \right]^3 \left| \frac{\partial u}{\partial\sigma} \right| \frac{\partial q}{\partial\sigma} \right] \qquad (5.29)$$

c. Richards scheme (Richards 1980a,b)

In principle, this method is an extension of the Clarke scheme, using more detailed functional forms for the mixing lengths and allowing some variation in the boundary layer depth. The diagnosed boundary layer top (which is always at a layer boundary) is defined by the position of the lowest inversion. In unstable conditions, the turbulent mixing occurs through the lowest three layers, as in the Clarke scheme. In stable conditions, the mixing is restricted to those layers below the diagnosed boundary layer top. This scheme is used in the operational numerical weather prediction model (Dickinson and Temperton 1984). In neutral conditions, the diffusion coefficients are calculated according to (5.17) with the mixing length taken as its neutral value l_N (Blackadar 1962);

$$l_N = \frac{kz}{(1 + kz/\lambda)} \qquad (5.30)$$

where λ is a scaling length which is calculated from the ratio of the surface roughness to the depth of the boundary layer z_h

Defining

$$P \equiv \log_{10} (z_h/z_o) \qquad (5.31)$$

λ is given by:

$$\lambda = 0.01 \frac{(41.26 - 3.46P)}{(5.06 - 0.46P)} \qquad (5.32)$$

Away from neutral conditions, it is assumed that one can write

$$\Lambda_\chi^2 = l_N^2 f(R_i) \qquad (5.33)$$

where R_i is the Richardson number

and $$f_\chi(R_i) = \frac{\Phi_m^2(0)}{\Phi_m(\zeta)\,\Phi_\chi(\zeta)} \qquad (5.34)$$

Ri and ζ are related through the equation

$$Ri = \zeta\Phi_H(\zeta)/[\Phi_m(\zeta)]^2 \qquad (5.35)$$

In unstable conditions, Φ_m, Φ_H are determined from the formulae of Dyer and Hicks (1970) which give

$$f_m\,(Ri) = (1 - 16\ Ri)^{-1/2}$$

$$f_H\,(Ri) = (1 - 16\ Ri)^{3/4} \qquad (5.36)$$

but it is assumed that the mixing of heat and moisture are treated in the convection scheme, so $f_H(Ri)=0$ when $Ri<0$.

On the stable side, Carson and Richards (1978) preferred the formulation of Hicks (1976);

$$\Phi_m(\zeta) = \Phi_H(\zeta) = 1 + \alpha\zeta \qquad (\zeta \leqslant 0.5)$$

$$= 8 - 4.25\ \zeta + 1/\zeta^2 \qquad (0.5 < \zeta < 10)$$

$$= 0.76\ \zeta \qquad (\zeta > 10) \qquad (5.37)$$

Note that for $\zeta > 0.5$ one cannot write out an explicit form for $f_m(Ri)$ or $f_H(Ri)$ and iteration is necessary. The need for iteration is removed from the final version of the scheme on the IBM 360/195 (HRBLMIX3) and the version on the CYBER 205 by the use of a tabulation for f_m and f_H as a function of Ri for $Ri > 0$.

Note that the above formulation implies that Ri cannot become greater than 1.32 however large ζ is. Carson and Richards argued that this may be interpreted as a critical Richardson number, Ri_C for the suppression of turbulence and that for $Ri > Ri_C$, $f_\chi\,(Ri) \equiv 0$, although they noted the

difficulty of representing weak intermittent turbulence over a model grid square.

5.2 Program details for the boundary layer schemes

The purpose of this section is to provide a bridge between the physics, as described in section 5.1, and the CYBER 205 computer code. These program details do not stand alone and are not intended as a comprehensive documentation of the code; they can only be informative when used in conjunction with both Section 5.1 and the code.

The COMMON area DCBA holds all the basic data. COMMON area IO holds the work arrays PERM, IPERM, BITP, TEMP, ITEMP and BITT. A-store data are block-gathered into array PERM at the start of the routine and block-scattered back to the A-stores after updating at the end.

The processing of NROWS = ID(37) rows is done at one time starting at the beginning of row NROW1 = ID(38). The value of ID(37) is internally computed from parameters (both in the boundary layer and master routines) to fit available workspace. NBL = ID(39) is the number of layers on which the scheme operates; for the Clarke scheme this is always 3 but in the Richards scheme it can be set at will from 2 to 10 (3 is standard). NPR is the number of rows processed at a time (NROWS) multiplied by the number of points in a row (NPTS = ID(12)).

The following tables indicate the correspondence between the physical variables, the descriptors in the code and the storage locations in the work arrays. Where, within a particular section of the code, the same work area or descriptor is used for a number of different purposes, the relevant descriptors are listed in order of usage. To simplify notation p = NPR and b = NBL are used.

(i) Richards scheme

Array PERM

Surface section

Physical quantities	Descriptors	Start	Length
block-gathered quantities	BLVD	1	(1 + 4b)p
p^*	PSTARD	1	p
u_{11}	UD	p+1	p
v_{11}	VD	(1+b)p + 1	p
T_{11}	TD	(1+2b)p + 1	p
q_{11}	QD	(1+3b)p + 1	p

Ekman section

Physical quantity	Levels	Descriptors	Start	Length
	11 → 13-b	VARMD	p + 1	(b-1)p
u	10 → 12-b	VARPD	2p + 1	(b-1)p
	11 → 12-b	UD	p + 1	bp
	11 → 13-b	VARMD	(1+b)p + 1	(b-1)p
v	10 → 12-b	VARPD	(2+b)p + 1	(b-1)p
	11 → 12-b	VD	(1+b)p + 1	bp
	11		(1+2b)p + 1	p
T	:	TD	:	:
	12-b		3bp + 1	p
T	11 → 12-b	TD	(1+2b)p + 1	bp
	11 → 13-b	VARMD	(1+3b)p + 1	(b-1)p
q	10 → 12-b	VARPD	(2+3b)p + 1	(b-1)p
	11 → 12-b	QD	(1+3b)p + 1	bp

Array IPERM contains only one vector with descriptor IBLVD. The integers in it are used in block-gathering and scattering the A-stores.

Array BITP

Physical quantity	Descriptor	Start	Length
Sea indicator	BITSEAD	1	p
Sea ice indicator	BITSICED	p+1	p
land ice indicator	BITLICED	2p+1	p
Snow indicator	BITSNOWD	3p+1	p
Land indicator	BITLAND	4p+1	p

Array TEMP

Surface section (→ Ekman denotes a surface quantity transferred to Ekman section).

Physical quantity	Descriptor	Start	Length
T_*	TMPTSTD	1	NMELT
soil moisture content	TMPSMCD	NMELT + 1	NMELT
snow depth	TMPSNDD	2*NMELT + 1	NMELT
snow-melt	SMELTD	3*NMELT + 1	NMELT
	PLEFTD		
$(1000/p_{11})^{\kappa}$	CONST2D		
$q_{sat}(T_*)$	QSATD	1	p
Ri_b	RIBD		
E (→ Ekman)	ED		
	TEMP2D		
$\Delta\theta$	DTHETAD	p + 1	p
H (→ Ekman)	HD		
	TEMP3D		
θ_{11}	TH11D		
C_D	CDD	2p + 1	p
	TEMP3D		
τ_x (→ Ekman)	TAUXD		
temporary quantity in QSAT	W1D		
Δq	DQD	3p + 1	p
	TEMP4D		
τ_y (→ Ekman)	TAUYD		
temporary quantity in QSAT	W2D		
$\lvert\underline{v}_{11}\rvert$	VMODD	4p + 1	p
	TEMP5D		
temporary quantity in QSAT	W3D		
$\lvert\underline{v}_{11}\rvert^2$	VMOD2D	5p + 1	p
C_H	CHD		
			NDTICE
	TEMPTD	5p + 1	NLAN
			NSNOW
	TEMP7D	6p + 1	p
ρ_*	ROSTARD		
	TEMP8D	7p + 1	p
"τ" = $\rho_* C_D \lvert\underline{v}_{11}\rvert$	TAUD		
	TEMPUD		NFREE
	TEMP9D	8p + 1	NLAN
	TEMPUD		NSNOW
	TEMPVD	8p+NSNOW+1	NSNOW
	TEMPQD	8p+2*NSNOW+1	NSNOW

Array TEMP: Ekman section

(surface - denotes a quantity computed in and transferred from the surface section; $F\chi = \rho w'\chi'$).

Physical quantities	Levels	Descriptors	Start	Length
	$10^1/_2$		1	p
	:	ZHALFD	:	:
heights of	$11^1/_2$-b		(b- 1)p+1	p
layer boundaries	$10^1/_2$-$11^1/_2$-b	ZHALFD	1	bp
Z_{half}	$10^1/_2$	ZHALFD	1	p
	$10^1/_2$-$12^1/_2$-b	ZHF1D	1	(b-1)p
	$9^1/_2$-$11^1/_2$-b	ZHF2D	p+1	(b-1)p
	11		bp+1	p
	:	THETAD	:	:
potential	12-b		(2b-1)p+1	p
temperatures	11-13-b	VARMD	bp+1	(b-1)p
θ	10-12-b	VARPD	(b+1)p+1	(b-1)p
	11-12-b	THETAD	bp+1	bp
Richardson nos. Ri	$10^1/_2$-$12^1/_2$-b	RID	bp+1	(b-1)p
Layer thicknesses	11	DZD	bp+1	p
$\Delta Z_j = Z_{j-1/2} - Z_{j+1/2}$	10-12-b	DZD	(b+1)p+1	(b-1)p
	11-13-b	DZD	bp+1	(b-1)p
	11		bp+1	p
$2\Delta t$	:	DTDZD	:	:
$\rho_j \Delta Z_j$	12-b		(2b-1)p+1	p
	11-12-b	DTDZD	bp+1	bp
	11		bp+1	p
$2\Delta t$	:	TEMP24D		
$\rho_j \Delta Z_j \sigma_j$	12-b		(2b-1)p+1	p
τ_x (surface -)	$11^1/_2$		2bp+1	p
Δu	$10^1/_2$-$12^1/_2$-b	DUD	(2b+1)p+1	(b-1)p
	$10^1/_2$-$12^1/_2$-b	FUD	(2b+1)p+1	(b-1)p
$-F_u$	$11^1/_2$-$13^1/_2$-b	FUPD	2bp + 1	(b-1)p
	$12^1/_2$-b	FTOPD	(3b-1)p+1	p
	$10^1/_2$-$12^1/_2$-b	FDND	(2b+1)p+1	(b-1)p
τ_y (surface -)	$11^1/_2$		3bp + 1	p
Δv	$10^1/_2$-$12^1/_2$-b	DVD	(3b+1)p+1	(b-1)p
	$10^1/_2$-$12^1/_2$-b	FVD	(3b+1)p+1	(b-1)p
$-F_v$	$11^1/_2$-$13^1/_2$-b	FUPD	3bp+1	(b-1)p
	$12^1/_2$-b	FTOPD	(4b-1)p+1	p
	$10^1/_2$-$12^1/_2$-b	FDND	(3b+1)p+1	(b-1)p

H (surface -)	$11^1/_2$		4bp+1	p
$\Delta\theta$	$10^1/_2$-$12^1/_2$-b	DTHETAD	(4b+1)p+1	(b-1)p
	$10^1/_2$-$12^1/_2$-b	FTD	(4b+1)p+1	(b-1)p
F_θ	$11^1/_2$-$13^1/_2$-b	FUPD	4bp+1	(b-1)p
	$12^1/_2$-b	FTOPD	(5b-1)p+1	p
	$10^1/_2$-$12^1/_2$-b	FDND	(4b+1)p+1	(b-1)p

E (surface -)	$11^1/_2$		5bp+1	p
Δq	$10^1/_2$-$12^1/_2$-b	DQD	(5b+1)p+1	(b-1)p
	$10^1/_2$-$12^1/_2$-b	FQD	(5b+1)p+1	(b-1)p
F_q	$11^1/_2$-$13^1/_2$-b	FUPD	5bp+1	(b-1)p
	$12^1/_2$-b	FTOPD	(6b-1)p+1	p
	$10^1/_2$-$12^1/_2$-b	FDND	(5b+1)p+1	(b-1)p

$1/\Delta Z_{half}$	$10^1/_2$-$12^1/_2$-b	RDZHD		
$\lvert\Delta\bar{v}\rvert/\Delta Z_{half}$	$10^1/_2$-$12^1/_2$-b	DVDZD	6bp+1	(b-1)p
$f(\bar{Ri})$	$10^1/_2$-$12^1/_2$-b	FRID		
	$10^1/_2$		6bp+1	p
f(Ri)	:	FRIZHD	:	:
	$12^1/_2$-b		(7b-2)p+1	p
K_m	$10^1/_2$-$12^1/_2$-b	AKD	6bp+1	(b-1)p
$(\Delta F_\chi)_j=(F_\chi)_{j-1/2}-(F\chi)_{j+1/2}$	11-13-b	FLUXD	6bp+1	(b-1)p
$(\Delta F_\chi)_{top}=-(F_\chi)_{121/2-b}$	12-b	FLTPD	(7b-1)p+1	p
$\Delta_t\chi$	11-12-b	XINCD	6bp+1	bp

$(\Delta v/\Delta z)^2$	$10^1/_2$-$12^1/_2$-b	TEMP21D	(7b-1)p+1	(b-1)p
	$10^1/_2$		(7b-1)p+1	p
ℓ	:	ELD	:	:
	$12^1/_2$-b		(8b-3)p+1	p
$\ell^2(\Delta\underline{v}/\Delta z)^2$	$10^1/_2$-$12^1/_2$-b	AKKD	(7b-1)p+1	(b-1)p
	$10^1/_2$		(7b-1)p+1	p
$\rho\ell^2(\Delta\underline{v}/\Delta z)^2$		TEMP22D	:	:
	$12^1/_2$-b		(8b-3)p+1	p
$\rho\ell^2(\Delta\underline{v}/\Delta z)^2$	$10^1/_2$-$12^1/_2$-b	AKKD	(7b-1)p+1	(b-1)p

[Note overwriting (level $10^1/_2$ only) by $(\Delta F_\chi)_{top}$].

---

f_h (Ri)	$10^1/_2$-$12^1/_2$-b	FRIHD	(8b-2)p+1	(b-1)p
K_h	$10^1/_2$-$12^1/_2$-b	HKD	(8b-2)p+1	(b-1)p

---

mid-layer	$10^1/_2$		(9b-3)p+1	p
separations	:	DZHALFD	:	:
ΔZ_{half}	$12^1/_2$-b		(10b-5)p+1	p
	$10^1/_2$-$12^1/_2$-b	DZHALFD	(9b-3)p+1	(b-1)p

---

z_{half} ($z_{111/2}$=0)	$11^1/_2,..,11^1/_2$-b	ZXD	(10b-3)p+1	p
z_h/z_o = height b.l.top/rough.length	-	ZHMD	(10b-3)p+1	p
λ = asymptotic mixing length	-	ELAMDAD	(10b-3)p+1	p

temporary quantities used in calculation of f(Ri) from table [Note overwriting of λ if b > 2]	$10^1/_2$-$12^1/_2$-b	FRILD TEMP22D	(10b-4)p+1	(b-1)p

Array ITEMP: Surface section

Contents	Descriptor	Start	Length
temporary quantity in QSAT	ITEMP1D I1D ITEMP1D	1	p
temporary quantity in QSAT	ITEMP2D I2D ITEMP2D	p+1	p

Array ITEMP: Ekman section

Contents	Descriptor	Start	Length
temporary quantities used in calculation of f(Ri).	ITEMP21D ITEMP22D	1 (b-1)p+1	(b-1)p (b-1)p
number of mixing layers	IZHD ITEMP21D	1 p+1	p p

Array BITT: Surface section

Contents	Descriptor	Start	Length
	BITT1D		
bit vector in QSAT	BIT1D	1	p
	BITT1D		
bit vector in QSAT	BIT2D	p+1	p
	BITT2D		
			NMELTD
	BITT3D	2p+1	NPR
			NLAN
			NSNOW
	BITT4D	3p+1	NSNOW
	BITT5D	4p+1	NSNOW

Array BITT: Ekman section

Contents	Descriptor	Start	Length
	BITT21D		
indicator for Ri $\leq$ 0	BITRID	1	(b-1)p
	BITT31D	1	p
	BITT32D	p+1	p

(ii) Clarke Scheme

Array PERM: Surface section - same as for the Richards scheme.

Array PERM: Ekman section

Physical quantity	Descriptors	Start	Length
U_{11}	UD	p+1	p
U_{10}	UUD, UD	2p+1	p
U_9	UUD, UD	3p+1	p
V_{11}	VD	(b+1)p+1	p
V_{10}	VUD, VD	(b+2)p+1	p
V_9	VUD, VD	(b+3)p+1	p
T_{11}	TD	(2b+1)p+1	p
T_{10}	TD, TUD, TD	(2b+2)p+1	p
T_9	TD, TUD, TD	(2b+3)p+1	p
q_{11}	QD	(3b+1)p+1	p
q_{10}	QUD, QD	(3b+2)p+1	p
q_9	QUD, QD	(3b+3)p+1	p

Array IPERM - same as for the Richards scheme.

Array BITP - same as for the Richards scheme.

Array ITEMP - same as for the Richards scheme in the surface section. Not used in the Ekman section.

Array BITT: Surface section - same as for the Richards scheme.

Array BITT: Ekman section

Descriptor	Start	Length
BIT1D	1	p
BIT2D	p+1	p
BIT3D	2p+1	p
BIT4D	3p+1	p
BIT5D	4p+1	p
BIT6D	5p+1	p

Array TEMP: Surface section

Physical quantity	Descriptor	Start	Length
T_*	TMPTSTD	1	NMELT
soil moisture content	TMPSMCD	NMELT+1	NMELT
snow depth	TMPSNDD	2*NMELT+1	NMELT
snow-melt	SMELTD	3*NMELT+1	NMELT
	PLEFTD		
$(1000/p_{11})^K$	CONST2D	1	p
$q_{sat}(T_*)$	QSATD		
Ri_b (- Ekman)	RIBD		
	TEMP2D		
$\Delta\theta$	DTHETAD	p+1	p
	TEMP3D		
θ_{11}	TH11D	2p+1	p
C_D	CDD		
	TEMP3D		
temporary quantity in QSAT	W1D		
Δq	DQD	3p+1	p
	TEMP4D		
temporary quantity in QSAT	W2D		
$\lvert\underline{v}_{11}\rvert$	VMODD	4p+1	p
	TEMP5D		
temporary quantity in QSAT	W3D		
$\lvert\underline{v}_{11}\rvert^2$	VMOD2D	5p+1	p
C_H	CHD		
			NDTICE
	TEMPTD	5p+1	NLAN
			NSNOW

		TEMP7D	6p+1	p
ρ_*		ROSTARD		
		TEMP8D	7p+1	p
		TEMPUD		NFREE
		TEMP9D	8p+1	NLAN
		TEMPUD		NSNOW
		TEMPVD	8p+NSNOW+1	NSNOW
		TEMPQD	8p+2*NSNOW+1	NSNOW
"τ" = $\rho_* c_D \lvert \underline{v}_{11} \rvert / p_*$		TAUD	(4b+1)p + 1	p
H		HD	(5b+1)p + 1	p
E	(→ Ekman)	ED	(6b+1)p + 1	p
$c_D^{1/2}$		RTCD	7bp+1	p
u_* then l_*		ELSTAD	(7b+1)p+1	p
			(7b+1)p+1	NPTS
$l_* = u_*/\lvert f \rvert$		ELROWD	:	:
(f depends on row no.)			(7b+1)p+(NROWS-1)*NPTS+1	NPTS

Array TEMP: Ekman section

Physical quantity	Level	Descriptors	Start	Length
Ri_b (surface →)	$11\frac{1}{2}$	RIBD	1	p
ℓ_1, ℓ	$10\frac{1}{2}$	EL1D, ELD	p+1	p
ℓ_2, ℓ	$9\frac{1}{2}$	EL2D, ELD	2p+1	p
$g/\Delta\phi$	$10\frac{1}{2}$	ACD	3p+1	p
	$9\frac{1}{2}$		4p+1	p
		TEMPC1D	5p+1	N1D,p
		TEMPC2D	6p+1	N1D,p, N5D,p
		TEMPC3D	7p+1	N5D,p
		TEMPC4D	8p+1	N5D,p
		ZND	9p+1	p
	$11\frac{1}{2}$	UFLUXLD	10p+1	p
	$10\frac{1}{2}$	UFLUXUD	11p+1	p
$-(g/p_*) F_u$		UFLUXLD		
	$9\frac{1}{2}$	UFLUXUD	12p+1	p
		UFLUXLD		
τ (surface →)	$11\frac{1}{2}$	TAUD	13p+1	p
	$11\frac{1}{2}$	VFLUXLD		
	$10\frac{1}{2}$	VFLUXUD	14p+1	p
$-(g/p_*) F_v$		VFLUXLD		
	$9\frac{1}{2}$	VFLUXUD	15p+1	p
		VFLUXLD		
H (surface →)	$11\frac{1}{2}$	HD	16p+1	p
	$11\frac{1}{2}$	TFLUXLD		
	$10\frac{1}{2}$	TFLUXUD	17p+1	p
$-(g/p_*) F_\theta$		TFLUXLD		
	$9\frac{1}{2}$	TFLUXUD	18p+1	p
		TFLUXLD		
E (surface →)	$11\frac{1}{2}$	ED	19p+1	p
	$11\frac{1}{2}$	QFLUXLD		
	$10\frac{1}{2}$	QFLUXUD	20p+1	p

$-(g/p*)\ F_q$	$9^1/_2$	QFLUXLD QFLUXUD QFLUXLD	21p+1	p
$C_D{}^{1/2}$ (surface -) (overwritten after use by level $9^1/_2$ q-flux)		RTCD	21p+1	p
$\ell*$		ELSTAD	22p+1	p

6. LARGE-SCALE PRECIPITATION

6.1 Introduction

Large-scale or dynamic precipitation is produced when the air at model gridpoints becomes supersaturated as a result of convergence or radiative cooling. The parametrization scheme removes this excess moisture and allows it to fall as rain or snow. The effects of evaporation (see later) and the melting of snow on the falling precipitation are also taken into account.

6.2 The formation of precipitation through condensation

Starting at the top of the model, the following calculation is performed for each level k in turn. First, the specific humidity, q_k, is compared with the saturation specific humidity, $q_s(T_k)$, corresponding to the temperature T_k at that gridpoint. If $q_k \leq q_s(T_k)$ and there is no precipitation falling from higher levels, then we proceed to the next level below.

If $q_k > q_s(T_k)$, then the excess moisture is removed and the temperature is increased through the release of latent heat. Defining adjusted values of q_k and T_k by $q_s(T'_k)$ and $T'_k = (T_k + \Delta T_k)$, we have

$$\Delta T_k = \frac{L}{C_p} \left(q_k - q_s(T'_k)\right) \qquad (6.1)$$

where L is the latent heat of condensation and C_p is the specific heat of dry air at constant pressure. The adjustment is made so that the gridpoint is just saturated at the new temperature. On using the Clausius-Clapeyron relation, we have

$$q_s(T'_k) = q_s(T_k) + \frac{\partial q_s}{\partial T}(T_k)\, \Delta T_k = q_s(T_k) \left[1 + \frac{L\, \Delta T_k}{R_v T_k^2}\right] \qquad (6.2)$$

where R_v is the gas constant for water vapour (i.e. R/ϵ where R is the gas constant for dry air and ϵ is the ratio of the molecular weights of water and dry air). Equations (6.1) and (6.2) can be solved simultaneously for ΔT_k and $q_s(T'_k)$, the new value of $q_s(T'_k)$ being given by

$$q_s(T'_k) = q'_k = q_k - (q_k - q_s(T_k)). \left[1 + \frac{L^2 q_s(T_k)}{C_p R_v T_k^2} \right]^{-1} \qquad (6.3)$$

If the temperature is below freezing, the precipitation formed is assumed to freeze. A further contribution to the temperature increment is then derived from the additional latent heat released using L_f, the latent heat of fusion.

The precipitation per unit mass resulting from the adjustment at this level, given by

$$P_k = q_k - q_s(T'_k) \qquad (6.4)$$

is added to any precipitation reaching this level from above.

6.3 Evaporation

At present, the 11-Layer Model does not include this process, but it was implemented in the operational model (Dickinson and Temperton 1984). It will be included in the next version of the model and is reproduced here for completeness.

If $q_k < q_s(T_k)$, that is the air is not saturated at level k, and precipitation is falling from higher levels, a proportion is evaporated. The evaporation formula is designed to give evaporation rates which are typically of the order of 7 mm per day per 100 mb. The evaporation per unit mass, E_k, is given by

$$E_k = \min [\beta(q_s(T_k) - q_k) \Delta t, P_k] \qquad (6.5)$$

where $\beta = 2 \times 10^{-5}\ s^{-1}$. Δt is the timestep and P_k is the precipitation falling through the layer.

New values of q_k and T_k, say q_k'' and T_k'', as a result of the above evaporation are given by

$$q_k'' = q_k + E_k \qquad \text{and} \qquad T_k'' = T_k - L\,E_k/C_p\ ,$$

where L is the latent heat appropriate to the phase of the precipitation.

6.4 The melting of snow

An ice-phase is introduced into precipitation in the 11-Layer Model. The motivation behind this was largely the decision to allow an interactive snow cover in the model. Snow lying on the ground is melted whenever the surface temperature rises above 273K, the amount melted being determined by the temperature and the latent heat of fusion of water. If latent heat is not released when rain turns to snow in the atmosphere there will be a spurious sink of heat at the ground.

Snow is melted in a layer whose temperature is greater than 273°K. All the precipitation falling into this layer is assumed to melt immediately. The accompanying change in temperature is therefore given by

$$\Delta T_k = -\frac{L_f}{C_p} \sum_{n=k+1}^{TOP} (P_n - E_n) \qquad (6.6)$$

A similar adjustment is made to the temperature field if the precipitation changes from rain to snow.

6.5 The precipitation reaching the surface

From the above the amount of dynamic precipitation reaching the surface in one timestep, A_*, may be calculated. Expressed in mm per unit area

$$A_* = \frac{10^2}{g}\, p_* \sum_{n=1}^{TOP} (P_n - E_n)\, \Delta\sigma_n \qquad (6.7)$$

The rate of precipitation R^* in mm per hour is then given by

$$R^* = (3600 / \Delta t) A^* \qquad (6.8)$$

7. CONVECTION

7.1 Introduction Source: Rowntree (1984) and Dickinson and Temperton (1984).

The original version of the 11-Layer Model used a convective adjustment scheme described by Saker (1975). This was replaced by the penetrative convection scheme, which was described in detail by Rowntree (1973) while Lyne and Rowntree (1976) discuss its development using GATE data. It is based on the concept of parcel theory modified by entrainment (Riehl 1954 pp 143 ff, Scorer 1958 pp 155 ff, Ludlam 1963 p 19) with a treatment of detrainment based partly on Ceselski (1972 p 102) and his discussion of the scheme of Arakawa (1969). We imagine an ensemble of buoyant plumes of varying characteristics (temperature, humidity, cross-sectional area) starting at one level and extending upwards to different heights depending on their characteristics. The plumes entrain environmental air over their leading and side surfaces as they push into the environmental air; the less buoyant plumes terminate through lack of buoyancy and detrain at a lower level than more buoyant ones which, perhaps because of their original large cross-section or the more favourable nature of the local environment into which they have risen, have led more protected lives and may even reach the heights accessible to an undilute parcel. Since detrainment is generally assumed to occur with zero buoyancy, the heating of the environment occurs, as in Arakawa's scheme, mainly through the mass descent which compensates the ascent of the buoyant plumes, although moistening by detrainment and re-evaporation of condensed moisture do mitigate the drying and warming effects of this descent.

In more detail, for each model column we work upwards until we find a level at which a parcel starting with a small excess buoyancy relative to the environment will still be buoyant after rising to the next level and

entraining some environmental air en route. If at this next level it still has an excess buoyancy greater than a certain lower limit (equal to that given to the starting parcel) the convective process is initiated.

At each level the ensemble reaches we calculate whether, after allowing for entrainment between that level and the next the mean ensemble will still be buoyant. If it is not we find what proportion of the less buoyant part of the ensemble needs to be detrained, at a density equal to that of the environment, at the lower level to allow the residue of the ensemble to be buoyant at the next level. (The effects of moisture on density are allowed for both in detrainment and in the buoyancy test). Because the detrainment allows an indefinite extrapolation towards greater buoyancy it is necessary to limit it. A simple restriction is that even the most buoyant plumes should not rise higher than an undilute parcel would. It also seems reasonable to place a lower limit on the mass flux on the assumption that an ensemble of small total cross-section will be destroyed by entrainment. Where these restrictions bring the convective process to an end, it is simplest to detrain the residual air with non-zero buoyancy although a scheme has been worked out in which this is avoided by splitting the detrainment between two layers. The search for further mutually unstable layers is resumed in the layer above that in which this final detrainment occurs (or in the new scheme in the upper of the two layers in which the final detrainment occurs).

The scheme is applicable equally to dry and moist convection, although it is obviously necessary to know which is appropriate at any particular level as certain terms (eg latent heat release) are absent in dry convection and the moisture content of detrained air is defined differently in the two cases.

A major revision of the scheme was undertaken during 1984. This resulted in the inclusion of a further detrainment term designed to provide a better modelling of the mixing processes which take place at the leading and side surfaces of convective cells as they push into the environmental air. In addition, the precipitation-forming parts of the scheme were reformulated in order to limit the amount of summer convective precipitation over land, which had been too widespread in early operational fine-mesh forecasts.

Several arbitrary parameters are incorporated within the scheme allowing adjustments to be made and the scheme to be "tuned". Many of these have been modified in the light of experience from the values originally quoted by Lyne and Rowntree (1976). The values in current use are shown in Table 7.1. Note that in the following the levels are numbered from the surface upwards, whereas in the rest of this handbook (and in the model itself) the numbering is from the top of the atmosphere downwards.

7.2 The buoyancy equations

The scheme assumes that in each grid box there is an ensemble of buoyant convective plumes with varying characteristics (temperature, humidity, cross-sectional area) which entrain air from the surrounding environment and ascend until they are no longer buoyant. Within the ensemble the virtual potential temperatures of the plumes are further assumed to be distributed about an average value

$$(\theta_v^P)_k = \theta_k^P(1 + 0.61\, q_k^P) \qquad (7.1)$$

Here q_k^P is the average specific humidity of the plumes with $q_s^P \leq q_k(\theta_k^P)$.

TABLE 7.1 VALUES OF ADJUSTABLE PARAMETERS USED IN THE DEEP CONVECTION SCHEME

Parameter	Meaning	Value
b	Excess buoyancy of parcel for continuance of convection.	0.2°K
$\epsilon_{k+1/4}$	Fractional entrainment rate at level $k+^1/_4$.	$3A_E\sigma_k(\sigma_k-\sigma_{k+1/2})$
$\epsilon_{k+3/4}$	Fractional entrainment rate at level $k+^3/_4$.	$3A_E\sigma_{k+1/2}(\sigma_{k+1/2}-\sigma_{k+1})$
c	Constants in initial	$3.33 \times 10^{-4}s^{-1}K^{-1}$
d	mass flux formula.	0.0
M_{MIN}	Minimum mass flux	$10^{-3}c\ E_{MIN}\ \Delta t$
S_θ S_q	Excess of initial parcel values over the environment.	0.2°K 0.0 Kg/Kg
E_{MIN}	Minimum parcel buoyancy	1°K
A_E	Entrainment factor	Original scheme: 1 k≥1 New scheme: 1 k=1 1.5 k>1
η_k	Fractional mixing detrainment rate at level k	$(\epsilon_{k+1/4}+\epsilon_{k+3/4})(1-A_E^{-1})$ (N.B. $\eta_k = 0$ for $A_E = 1$)
e	Evaporation constant (original scheme only)	3

The finite difference treatment of the ensemble is best understood by reference to Figure 7.1. We define δ_k as the fractional rate of forced detrainment at level k, η_k as the fractional rate of detrainment due to mixing and $\epsilon_{k+1/4}$, $\epsilon_{k+3/4}$ as the fractional entrainment rates at levels $k+^1/_4$, $k+^3/_4$. The entrainment and mixing detrainment rates are specified empirically (see Table 7.1), whilst the forced detrainment rate is

diagnosed by the convection scheme. Forced detrainment occurs at those levels where it is necessary to maintain buoyancy and may be interpreted as the fraction of the ensemble whose plumes terminate at that level. The effects of entrainment and mixing detrainment, on the other hand, are assumed to act at all levels and represent the mixing processes near the edges of updraughts which transfer air both into and out of a plume. In the original version of the scheme the detrainment due to mixing was not included. This can be recovered by setting $A_E=1$ which gives $\eta_k = 0$ (see Table 7.1).

The vertical mass flux at level k, M_k, gives a measure of the size of the ensemble and is predicted by

$$M_{k+1} = (1 + \epsilon_{k+1/4}) (1 + \epsilon_{k+3/4}) (1 - \delta_k) (1 - \eta_k) M_k \qquad (7.2)$$

The treatment of the ensemble as it passes from level k to level k+1 is independent of η_k and is described by the following equations:

$$(1 + \epsilon_{k+1/4}) (1 + \epsilon_{k+3/4}) (1 - \delta_k) q^P_{k+1} =$$

$$q^P_k - \delta_k q^R_k + \epsilon_{k+1/4}(1 - \delta_k) q^E_k + \epsilon_{k+3/4} (1 + \epsilon_{k+1/4})(1 - \delta_k) q^E_{k+1} \qquad (7.3)$$

$$(1 + \epsilon_{k+1/4}) (1 + \epsilon_{k+3/4})(1 - \delta_k)(\theta^P_{k+1} - \frac{L'}{c_p} \gamma_{k+1}(q^P_{k+1} - q_s(\theta^P_{k+1})\sigma^{-\kappa}_{k+1} =$$

$$\theta^P_k - \delta_k \theta^R_k + \epsilon_{k+1/4} (1 - \delta_k) \theta^E_k + \epsilon_{k+3/4} (1 + \epsilon_{k+1/4}) (1 - \delta_k) \theta^E_{k+1} \qquad (7.4)$$

where q^P_k is the specific humidity of the ensemble before condensation and $\gamma_k = 1$ if $q^P_k \geq q_s(P_k)$; otherwise $\gamma_k = 0$. A superscript E refers to environmental values whilst a superscript R refers to detrainment values. L' is the latent heat of condensation L if $\frac{1}{2}(T^E_k + T^E_{k+1}) \geq 263K$ or the latent heat of deposition $L+L_F$ if $\frac{1}{2}(T^E_k + T^E_{k+1}) < 263$ K.

7.3 Forced detrainment

No forced detrainment takes place at the lowest convective level. At higher levels this process only takes place when it is necessary to make the ensemble buoyant at the next level.

The ensemble is first raised from level k to level k+1 without the effects of forced detrainment. This is done by solving equations (7.3) and (7.4) with $\delta_k = 0$. The Clausius–Clapeyron relation is used to approximate $q_s(\theta^P_{k+1})$ in equation (7.4) by

$$q_s(\theta^P_{k+1}) = q_s(\theta^E_{k+1}) \left[1 + \frac{L}{R_v} \frac{(\theta^P_{k+1} - \theta^E_{k+1})}{(T^E_{k+1})^2} \sigma_{k+1} \right] \qquad (7.5)$$

If it is found that the virtual potential temperature of the ensemble is greater by a quantity b than that of the environmental air, that is

$$(\theta^P_v)_{k+1} - b > (\theta^E_v)_{k+1} \qquad (7.6)$$

then the ensemble is assumed to be buoyant at this level and no forced detrainment occurs. The minimum excess buoyancy b allows for the spread of θP_v in the ensemble. Thus the characteristics of the ensemble at level k are now known.

If (7.6) is not satisfied, then it is assumed that sufficient detrainment has occurred at level k at a virtual potential temperature of θE_v to raise the minimum θ_v of the plumes to that of the environment. Therefore defining the virtual potential temperature of detraining air by

$$(\theta^R_v)_k = \theta^R_k (1 + 0.61\, \gamma_k q_s(\theta^R_k) + 0.61\,(1 - \gamma_k)\, q^P_k) \qquad (7.7)$$

we can set

$$(\theta^R_v)_k = (\theta^E_v)_k \qquad (7.8)$$

The potential temperature of detraining air may now be derived from equations (7.7) and (7.8) by using the Clausius–Clapeyron relationship (see equation (7.5) with the approximation

$$\theta^R_k q_s(\theta^R_k) = \theta^E_k q_s(\theta^R_k)$$

whence

$$\theta^R_k = \theta^E_k \left[1 + \frac{0.61\,(q^E_k - q_s(\theta^E_k))}{1 + 0.61\,L/(R_v T^E_k)\,q_s(\theta^E_k)} \right] \qquad (7.9)$$

The forced detrainment rate δ_k may now be determined from equations (7.3) and (7.4) together with equation (7.9) by choosing a value for θp_{k+1} such that the ensemble is just buoyant: the buoyancy test (7.6) is treated in the same way as the derivation of equation (7.9) to give

$$\theta^R_{k+1} = \theta^E_{k+1} + \frac{0.61\;\theta^E_{k+1}\,(q^E_{k+1} - q_s(\theta^E_{k+1})) + b}{1 + 0.61\,L/(R_v T^E_{k+1})\,q_s(\theta^E_{k+1})} \qquad (7.10)$$

When dry convection is necessary, that is $\gamma_k = \gamma_{k+1} = 0$, this reduces to

$$\theta^P_{k+1} = \frac{\theta^E_{k+1}\,(1 + 0.61\,q^E_{k+1}) + b}{1 + 0.61\,q^P_{k+1}} \qquad (7.11)$$

7.4 Initiation of convection

The model atmosphere is tested from the bottom upwards for convective instability by taking a parcel from level k to level k+1 with

$$\theta^P_k = \theta_I = \theta^E_k + S_\theta \quad \text{and} \quad q^P_k = q_I = q^E_k + S_q$$

where S_θ and S_q are constants (see Table 7.1). Convection is then initiated if the buoyancy test

$$(\theta_v^P)_{k+1} - (\theta_v^E)_{k+1} - b \geq E_{MIN}\Delta\sigma_{k+1/2} \qquad (7.12)$$

is satisfied. Here E_{MIN} is a constant and represents the minimum buoyancy required by the ensemble for convection to begin.

The initial mass flux ascribed to the ensemble is based on the excess buoyancy occurring in a timestep and is given by

$$M_I = 10^{-3}\Delta t \left[d + c \frac{(\theta_v^P)_{k+1} - (\theta_v^E)_{k+1} - b}{\Delta\sigma_{k+1/2}} \right] \qquad (7.13)$$

Here d and c are constants (see Table 7.1). The parameter d is designed to allow some convection to take place independently of the amount of excess buoyancy. M_I is additionally constrained to be smaller than the depth of the thinnest model layer to prevent over-stabilisation.

7.5 Termination of convection

Convection continues upwards through the model atmosphere until the ensemble is no longer buoyant. This occurs when the upward mass flux becomes so small (less than a critical mass flux M_{MIN}) that the effects of convection would be negligible. Convection is therefore terminated when the residual mass flux

$$(1 - \eta_k)(1 - \delta_k) M_k < M_{MIN} \qquad (7.14)$$

Convection is also terminated at level k if an undilute parcel rising from the first convective layer (I) is stable in layer k+1. This happens when

$$(\theta_v^E)_{k+1} + b > (\theta_I^P + \frac{L}{c_p}(q_I^P - q_s(\theta_{k+1}^E))\sigma_{k+1}^{-\kappa})(1 + 0.61 q_s(\theta_{k+1}^E)) \qquad (7.15)$$

This test prevents the detrainment from leading to excessive buoyancy.

In the original scheme complete detrainment ($\delta_{k=1}$) takes place with parcel values θp_k and $q p_k$. A modified scheme (undergoing tests) detrains partially ($\delta_k \leq 1$) with neutral buoyancy at level k with the remainder of the plume ensemble detraining at the level above. This modification is designed to represent the effect of the penetration of an inversion by a proportion of the more buoyant plumes. It provides an important mechanism by which the boundary layer and the free atmosphere may interact. (Slingo and Wilderspin 1985).

7.6 Effects on the environment

At those levels where convection has taken place the model's temperature and humidity fields are modified to take account of the changes in the nature of the environmental air. The latent heat released during condensation/deposition is added to the parcel temperature and so does not appear explicitly in the environmental heat budget. The changes described here are due to entrainment, detrainment and the subsidence which compensates for the parcel's upward mass flux. The effects of evaporation are considered in the next section.

For layer k the effects of the fluxes on the mass of the environmental air are

(i) Entrainment: a loss of

$$\frac{\epsilon_{k-1/4}}{1 + \epsilon_{k-1/4}} + \epsilon_{k+1/4}(1 - \delta_k)(1_k - \eta_k) M_k$$

at the environmental values of θ^E_k and q^E_k. In the lowest convective layer this transfer takes place with the values $\theta^E_k + S_\theta$ and $q^E_k + S_q$.

(ii) Mixing detrainment: a gain of

$$\eta_k M_k$$

at the parcel values of θ^P_k and q^P_k.

(iii) Forced detrainment: a gain of

$$\delta_k (1 - \eta_k) M_k$$

at the detrainment values of θ_k^R and $\gamma_k q_s(\theta_k^R) + (1 - \gamma_k) q_k^P$, except in the top layer where values of θ_k^P and q_k are used.

(iv) Downward mass flux into layer k: a gain of

$$(1 + \epsilon_{k+1/4}) (1 - \delta_k) (1 - \eta_k) M_k$$

at the environmental values of θ_{k+1}^E and q_{k+1}^E

(v) Downward mass flux out of layer k: a loss of

$$M_k \; / \; (1 + \epsilon_{k-1/4})$$

at the environmental values of θ_k^E and q_k^E. Note that this flux will be zero in the bottom convective layer.

On combining the effects (i) - (v) the net change in the values of the environmental potential temperature and specific humidity at level k may be calculated. These are given by

$$\Delta\theta_k = \frac{M_k}{\Delta\sigma_k} \left[(1 + \epsilon_{k+1/4}) (1 - \delta_k) (1 - \eta_k) (\theta_{k+1}^E - \theta_k^E) \right.$$

$$\left. + \delta_k (1 - \eta_k) (\theta_k^R - \theta_k^E) + \eta_k(\theta_k^P - \theta_k^E) \right] \qquad (7.16)$$

$$\Delta q_k = \frac{M_k}{\Delta\sigma_k} \left[(1 + \epsilon_{k+1/4}) (1 - \delta_k) (1 - \eta_k) (q_{k+1}^E - q_k^E) \right.$$

$$\left. + \delta_k(1 - \eta_k) (q_k^R - q_k^E) + \eta_k(q_k^P - q_k^E) \right] \qquad (7.17)$$

7.7 Condensation, evaporation and precipitation

The original scheme (with $A_E = 1$ and $\eta_k = 0$ in the above) treated condensation, evaporation and precipitation processes in the manner described in (a) below. In the operational weather prediction model this produced too much precipitation from summer convective clouds. The alternative treatment to overcome this problem is described in (b) below.

(a) The original scheme

The condensation, in mm per unit area, produced by taking the ensemble from level k to level k+1 is given by

$$P_k = \gamma_{k+1}(r^P_{k+1} - r_s(\theta^P_{k+1}))\, M_{k+1} \left[\frac{10^2 p_*}{g} \right] \qquad (7.18)$$

This is assumed to be converted immediately into precipitation and is allowed to fall as snow or rain depending on the sign of

$$\frac{1}{2}\left(T^E_k + T^E_{k+1} \right) - 263$$

Here 263°K is assumed to be the temperature at which the effects of deposition of water vapour into ice become pronounced. If $\gamma_{k+1} = 1$ the parcel humidity is then adjusted so that $r^P_{k+1} = r_s(\theta^P_{k+1})$.

In order to allow for cloud dissipation and the effects of unsaturated downdraughts on the falling precipitation, some evaporation takes place at level k. This is done according to the formula

$$E_k = e \left[r_s(\theta^E_k) - r^E_k \right] M_{k+1} \left[\frac{10^2 p_* \Delta\sigma_k}{g} \right] \qquad (7.19)$$

where e is a constant. The evaporation is further constrained so that

$$E_k \leq P_k$$

The environmental temperature and humidity are then incremented by

$$\Delta r_k = \frac{g E_k}{p_* \Delta\sigma_k} \quad \text{and} \quad \Delta T_k = - \frac{L / g E_k}{C_p p_* \Delta\sigma_k}$$

The falling precipitation changes state as it crosses the freezing level (273 K) and the model temperature fields are changed accordingly.

The total convective precipitation reaching the surface may now be calculated from equations (7.18) and (7.19) by summing over the model levels in essentially the same way as in the large-scale precipitation scheme.

(b) The new scheme

Detrained cloud water is evaporated into the environment. This leads to further environmental temperature and humidity increments of the form

$$\Delta q_k = (\delta_k + \eta_k(1 - \delta_k)) \frac{M_k X_k^P}{\Delta\sigma_k} \qquad (7.20)$$

$$\Delta\theta_k = - \frac{L}{C_p} \Delta q_k \qquad (7.21)$$

Here X_k^P is the mixing ratio of cloud water at level k predicted by

$$X_{k+1}^P = \frac{X_k^P}{(1 + \epsilon_{k+1/4})(1 + \epsilon_{k+3/4})} + \gamma_{k+1} (q_{k+1}^P - q_s(\theta_{k+1}^P)) \qquad (7.22)$$

and $\gamma_k = 1$ if $q_k^P > q_s(\theta_k^P)$; otherwise $\gamma_k = 0$.

Observations of summer convection suggest that precipitation does not occur until clouds attain a substantial depth. This depends on the aerosol size spetrum and is much greater for nucleus-rich continental air than for maritime air which has fewer but typically larger nuclei. At low temperatures, on the other hand, ice crystal growth through the Bergeron-Findeisen process allows precipitation to form more readily and

winter showers often result from quite shallow clouds. The convection scheme takes account of these effects by inhibiting precipitation unless the cloud depth, D_k, measured from the bottom of the first convective layer with a saturated parcel to the top of layer k, exceeds a critical value D_{crit}. The values used for D_{crit} are based on observational data (Ludlam 1980):

$$D_{crit} = \begin{cases} 4 \text{ km over land points} \\ 1.5 \text{ km over sea points} \\ 1 \text{ km if } T_{k+1} < 263°K \end{cases} \qquad (7.23)$$

After fall-out of precipitation commences, some water is retained in the cloud by specifying a minimum cloud water content, X_{MIN}. This is taken as 1 g/Kg or the local saturation specific humidity where it is less.

Precipitation of cloud water occurs if $D_k > D_{crit}$ and $X^P_k > X_{MIN}$. This is assumed to fall out of the cloud immediately. The amount produced, in mm per unit area, by taking the ensemble from level k to k+1 is given by

$$P_k = (X^P_{k+1} - X_{MIN}) M_{k+1} \frac{10^2 p*}{g} \qquad (7.24)$$

The falling precipitation changes state as it crosses the freezing level (273 K) and the model temperature fields are changed accordingly.

The total amount of precipitation falling from the base of the convective cloud is then given by

$$J_b = \sum_{m=c_b}^{m=c_t} P_m \qquad (7.25)$$

where c_t is the cloud top, as defined by section 7.5 and c_b is the cloud base: that is the first convecting layer for which $X^P > 0$.

The precipitation falling below cloud base is now evaporated at those levels where the precipitation is diagnosed as rain. No evaporation of falling snow is carried out. The formula assumes an evaporation rate of $(q - q_s)$ Kg Kg^{-1} s^{-1}, derived using the Marshall-Palmer drop size distribution (Bennetts and Rawlins 1981, Liu and Orville 1969) and is constructed by integrating the fractional evaporation of the falling precipitation J (mm) over a layer of depth dz. This is given by

$$\frac{dJ}{J} = \frac{(q - q_s)}{Q} \rho \, dz \qquad (7.26)$$

where ρ is the density of air and Q (mm/s) is the local rate of rainfall. Q is estimated by assuming that the precipitation covers 10% of a gridbox and that little change occurs in the rainfall rate between cloud base and the ground. It then follows that

$$Q = \frac{10 \, J_b}{\Delta t} \qquad (7.27)$$

where suffix b refers to the level of cloud base and Δt is the timestep.

On converting to model coordinates the formula is applied by first starting at the level below cloud base and examining each level of the model in turn down to the surface. If $q_k < q_s(T_k)$, that is the air is not saturated, the precipitated water, J_{k+1}, reaching level k is evaporated according to

$$J_k = J_{k+1} \exp(- \Delta t \, p_* \Delta\sigma [q_s(T_k) - q_k]/[10^2 J_b g]) \qquad (7.28)$$

7.8 Check on the energy budget

The convection scheme as described above redistributes air and water in a column with latent heating being the only diabatic process. If Δ represents the change during a timestep due to the processes represented in the convection scheme then by forming the mass weighted integral of the thermodynamic equation over the column we obtain:

$$C_p \int_o^1 \Delta T \, d\sigma + L \int_o^1 \Delta q d\sigma = L_F \int_o^1 \Delta_s q_f d\sigma \qquad (7.29)$$

or

$$C_p \int_o^1 \Delta T d\sigma + (L+L_F) \int_o^1 \Delta q d\sigma = - L_F \int_o^1 \Delta_s q_l d\sigma \qquad (7.30)$$

L is the latent heat of condensation, L_F the latent heat of fusion, q_l the specific liquid water content (cloud and rain), and q_f is the specific frozen water content (cloud and snow/ice). $\Delta_s$represnets the increment due to changes of state only. Equations (7.29) and (7.30) are equivalent because of the conservation of water substance during phase changes:

$$\Delta q + \Delta_s q_l + \Delta_s q_f = 0$$

Now if T < 273 K in the bottom model layer then

$$\int_o^\infty \rho \, \Delta_s q_l dz = 0$$

i.e. any liquid water formed by condensation of vapour or melting of frozen water will have evaporated or frozen before reaching the ground.

Similarly if T $\geq$ 273 K in the bottom model layer then

$$\int_o^\infty \rho \, \Delta_s q_f \, dz = 0$$

Thus, in finite differences, we should have

$$\sum_{m=1}^{NLEV} [C_p \Delta T_m + L \Delta q_m] \Delta\sigma_m = 0 \quad \text{if } T_{bottom} \geq 273 \text{ K} \qquad (7.31)$$

or

$$\sum_{m=1}^{NLEV} [C_p \Delta T_m + (L+L_F) \Delta q_m] \Delta\sigma_m = 0 \quad \text{if } T_{bottom} < 273 \text{ K} \qquad (7.32)$$

In the final stage of the scheme the environmental temperature increments are adjusted to satisfy (7.31) and (7.32) by equalising the vertically integrated temperature increments of each sign.

7.9 PROGRAMME DETAILS

Source: Notes by M K Hinds

The details in this section apply to the original scheme only.

There are three versions of the routine on the basic Cyber 205 libraries (e.g. DCPL32M) with DECK-names as follows:-

SQUALL — All arithmetic in 64-bits

SQUALL64 — All arithmetic in 64-bit Q8 calls (otherwise identical to SQUALL)

SQUALL32 — All arithmetic in 32-bit Q8 calls

They all assume that D and B stores are 64-bit and A-stores are 32-bit (C-stores are not used).

For each timestep of the model there are a number of entries to the convection scheme ("CALL SHOWER"), each processing ID(40) rows of the grid, starting with row ID(38). The last batch of rows will, if necessary, be shorter. The batching of rows is organised in the master routine. The

calculation of ID(40)=ISROWPAR is done in Parameter statements at the beginning of SHOWER and the master routine.

The number of rows in a batch for SQUALL32 will be approximately twice as many as for the 64-bit versions and MUST BE AN EVEN NUMBER. There is an IDENT on the library which alters the master routine part of this calculation from 64-bit to 32-bit. If the 64-bit versions are required, this IDENT must be YANKed, as follows:-

*YANK MASTSQ32 for MASTER

or *YANK MST5SQ32 for MASTER5

A scalar version of this routine exists as HRSQUL3 on IBM libraries or as SQUALL on the scalar Cyber 205 library DCLIB.

The vector version has no argument list and all working space is in the COMMON area IO, which is normally two large pages. The COMMON area DCBA which holds all the basic data is also used. The use of working space is described below.

The in-line routines COMQSAT (for 64-bit) or COMQST32 (for 32-bit) are used to compute saturation vapour pressure e_s times 0.622 and they need constants in COMSVPTB or COMSVP32. They use descriptors W1D, W2D, W3D, I1D, I2D, QSATD. The basic vector-length in SHOWER is NPR which is the number of rows in a batch (ID(40)) times the number of points in a row (ID(12)).

Most of the routine is within the DO-loop

```
DO 100 KI=1,NLEVP
```

where NLEVP=ID(11)-1 or one less than the number of layers in the model. For each sweep through the DO-loop an adjacent pair of layers is considered, starting with the lowest pair.

There are four sections of programme within the DO-loop, and vector-lengths in the first and last section are NPR. The descriptors for most vectors in use in these sections end with the characters 1D.

In the second section very stable cases are omitted. The bit-vector BITSKP1D (length NPR) contains ones for those grid points which are included in the vectors in section two. The number of ones in BITSKP1D is NSKP1 and this will be the vector-length in section two. The descriptors for most vectors in use in section two end with the characters 2D.

The third section includes only those parcels buoyant at the next level. The bit-vector BITSKP2D (length NSKP1) contains ones for those grid-points which are included in section three. The number of ones in BITSKP2D is NSKP2 and this will be the vector-length in section three. The descriptors for most vectors in use in section three end with characters 3D.

If NSKP2 is zero, section three will be skipped. If NSKP1 is zero, sections two and three will be skipped. Within section three NSKP3 is the number of grid-points for which detrainment is necessary, and a considerable amount of calculation is skipped if NSKP3 is zero (eg KI=1).

BITSKP1D is changed so that it only contains ones for grid-points which are included in section three, and it can therefore be used at the end of section three to merge various values back into the vectors in use in section one and used again in section four.

Work-space storage in COMMON area IO

assuming NPR=n, NSKP1=m, NSKP2=ℓ Array TEMP

Section	Start	Length	Descriptors		Contents
1 and 4	1	n	THKI1D,QSUMD) Swopping for		θ^e_k
	n+1	n	THJI1D,TSUM1D) alternate levels		θ^e_{k-1}
	2n+1	n	QSJ1D,QSATD,TSUM2D		$q_s(\theta^e_{k-1})$
	3n+1	n	THPK1D		θp_k
	4n+1	n	QPK1D		qp_k
	5n+1	n	RPRESS1D		$(1/p*)$
	6n+1	n	EM1D		m
	7n+1	n	DLTA1D		δ_k
	8n+1	n	QSK1D (QSATD)		$q_s(\theta^e_k)$
	9n+1	n	E1D,X1D		$\theta p_v-\theta^e_v-b,x$
	10n+1	n	QDIFF1D		$q^e_k-q_s(\theta^e_{k-1})$
	11n+1	n	W1D	}	over-written
	12n+1	n	W2D,TEMP1D	}	in
	13n+1	n	W3D,PPNET1D,W2D	}	Section 2
	(Section 2 storage here)				
	33n+1	n	QPI1D		q_I,qp_I
	34n+1	n	THPI1D		$\theta_I,\theta p_I$

Section 2	Start	Length	Descriptors		Contents
	11n+1	m	W1D		
	12n+1	m	W2D		
	13n+1	m	W3D		
	14n+1	m	W4D		
	15n+1	m	QST2D		
	16n+1	m	TUK2D		T^e_k
	16n+m+1	m	TUJ2D		T^e_{k-1}
	16n+2m+1	m	THPK2D	}	as 1D
	16n+3m+1	m	QPK2D	}	as 1D
	16n+4m+1	m	RPRESS2D (1/p*)	}	
	16n+5m+1	m	THKI2D	}	as 1D
	16n+6m+1	m	THJI2D	}	as 1D
	16n+7m+1	m	QSJ2D	}	as 1D
	16n+8m+1	m	X2D	} COMP2D	as 1D
	16n+9m+1	m	QPJ2D	}	qp_{k-1}

	16n+10m+1	m	QK2D		q^e_k
	16n+11m+1	m	QUJ2D		q^e_{k-1}
	16n+12m+1	m	THPJ2D		θp_{k-1}
	16n+13m+1	m	RTJ52D		$L(R_v\ T^e_{k-1})$
	16n+14m+1	m	Z2D		
	16n+15m+1	m	E2D		as 1D
	16n+16m+1	m	CLCP2D		L/C_p
Section 3	Start	Length	Descriptors		Contents
	35n+1	ℓ	EM3D		as 1D
	36n+1	ℓ	DLTA3D		as 1D
	37n+1	ℓ	QSK3D		as 1D
	38n+1	ℓ	THPK3D		as 1D
	38n+ℓ+1	ℓ	QPK3D		as 1D
	38n+2ℓ+1	ℓ	RPRESS3D (1/p*)		as 1D
	38n+3ℓ+1	ℓ	THKI3D		as 1D
	38n+4ℓ+1	ℓ	THJI3D		as 1D
	38n+5ℓ+1	ℓ	QSJ3D		as 1D
	38n+6ℓ+1	ℓ	X3D		as 1D
	38n+7ℓ+1	ℓ	QPJ3D	COMP3D	as 2D
	38n+8ℓ+1	ℓ	QK3D		as 2D
	38n+9ℓ+1	ℓ	QUJ3D		as 2D
	38n+10ℓ+1	ℓ	THPJ3D		as 2D
	38n+11ℓ+1	ℓ	RTJ53D		as 2D
	38n+12ℓ+1	ℓ	Z3D		
	38n+13ℓ+1	ℓ	E3D,X13D,S3D,PPND		
	38n+14ℓ+1	ℓ	CLCP3D		as 2D
	38n+15ℓ+1	ℓ	QP13D,QV3D		
	38n+16ℓ+1	ℓ	THP13D,TEMP3D		
	38n+17ℓ+1	ℓ	THPI3D		as 1D
	38n+18ℓ+1	ℓ	QPI3D		as 1D
	38n+19ℓ+1	ℓ	THR3D,DQ3D		θr_k
	38n+20ℓ+1	ℓ	TUK3D,W1D		as 2D
	38n+21ℓ+1	ℓ	A3D,W2D,PPNET3D,ZZ3D		
	38n+22ℓ+1	ℓ	W3D,EPSDLT3D		

38n+23ℓ+1	ℓ	DQR3D,W4D,PSG3D	
38n+24ℓ+1	ℓ	TD	T
38n+25ℓ+1	ℓ	ADDT3D,QSATD	
38n+26ℓ+1	ℓ	ADDQ3D,W2D	

(X13D,QP13D,THP13D are values of X3D,QPJ3D,THPJ3D before detrainment)

Array PERM (within COMMON area IO) (n=NPR)

This area is primarily used to block-gather the data into partial fields. It also contains the increments for T and q and the convective precipitation.

Start	Length	Descriptors		Contents	
1	n	PSTARD		p*	PERMD
n+1	11.n	TD,TUK1D,TUJ1D	(length n)	T	PERMD
12n+1	11.n	QK1D,QUJ1D	(length n)	q	PERMD
23n+1	11.n	ADDT1D	(length n)	T increments	ADDTD
34n+1	11.n	ADDQ1D	(length n)	q increments	ADDTD
45n+1	n	TOTALRD		convective rain	
46n+1	n	TOTALSD		convective snow	

Note that in the 32-bit version TOTALRD and TOTALSD are expanded to 64-bit in I1D and I2D and the descriptors are then reset.

Array IPERM (within COMMON area IO) (n = NPR)

Start	Length	Descriptors
1	n	IID indicates level where convection starts (1=level 11)
n+1		IPERMD index for block-gather

Array ITEMP (within COMMON area IO)

Start	Length	Descriptors	Contents
		Section 1 (n=NPR)	
1	n	I1D	
n+1	n	I2D	
2n+1	n	LMDAK1D	λ_k
		Section 2 (m=NSKP1)	
1	m	I1D	
m+1	m	I2D	
n+1	m	II2D	
3n+1	m	LMDAJ2D	λ_{k-1}

Section 3 (ℓ=NSKP2)

1	ℓ	II3D,I1D	
n+1	ℓ	I2D	
2n+1	ℓ	LMDAJ3D	λ_{k-1}
3n+1	ℓ	LMDA13D	
4n+1	ℓ	LMDAK3D	λ_k

Array BITP (in COMMON area IO) (n=NPR, ℓ=NSKP2, m=NSKP1)

Start	Length	Descriptors	Contents
1	n	BITIID	
n+1	n	BITSKP1D	control vector sections 1 to 2, later 1 to 3
2n+1	m	BITSKP2D	control vector sections 2 to 3

Array BITT (in COMMON area IO)

Start	Length	Descriptors
		Section 1 (n=NPR)
1	n	BITT1D,BITWATRD,BITADDTD,BITTERRD,BIT1D
n+1	n	BITFRZED,BITTSM1D,BIT2D
2n+1	n	BITMELTD,BITTSM2D
3n+1	n	BITTFACD
4n+1	n	BITSM12D
		Section 2 (m=NSKP1)
1	m	BITT21D, BIT1D
m+1	m	BITT22D, BIT2D
2m+1	m	BITT23D
		Section 3 (ℓ=NSKP2)
1	ℓ	BITE3D,BITDQD,BITCOM1D → BITCOM1D
ℓ+1	ℓ	BITLMDKD,BITCOM2D → BITCOM1D
2ℓ+1	ℓ	BITT31D → BITCOM2D → BITCOM1D
3ℓ+1	ℓ	BITLMD3D → BITCOM2D → BITCOM1D
4ℓ+1	ℓ	BITT32D → BITCOM2D
5ℓ+1	ℓ	BITX3D → BITCOM2D
6ℓ+1	ℓ	BITT33D → BITCOM2D
7ℓ+1	ℓ	BITTHD → BITCOM2D
8ℓ+1	ℓ	BITZZD
9ℓ+1	ℓ	BITTH1D
10ℓ+1	ℓ	BITZZ1D
11ℓ+1	ℓ	BITDLTD
12ℓ+1	ℓ	
13ℓ+1	ℓ	
14ℓ+1	ℓ	
15ℓ+1	ℓ	

BITCOM1D = B I T C O

BITCOM2D = M 1 D

BITCOMD = B I T C O M 1 D

BITCOM = B I T C O M

8. REFERENCES

Arakawa, A., 1969: Parametrization of cumulus convection. Proceedings of WMO/IUGG Symposium on Numerical Weather Prediction, Tokyo. Japan Met. Agency Tech. Report 67, pp. IV - 8-1 to IV - 8-6.

Asselin, R., 1972: Frequency filter for time integrations. Mon. Wea. Rev., 100, 487-490.

Bennetts, D.A., and Rawlins, F., 1981: Parametrization of the ice-phase in a model of mid-latitude cumulonimbus convection and its influence on the simulation of cloud development. Quart. J.R. Met. Soc., 107, 477-502.

Berlyand, T.G., Strokina, L.A., and Greshnikova, L.E., 1980: Zonal cloud distribution on the earth. Soviet Meteorology and Hydrology, No. 3, 9-15.

Bignell, K.J., 1970: The water-vapour infra-red continuum. Quart. J.R. Met. Soc., 96, 390-403.

Blackadar, A.K., 1962: The vertical distribution of wind and turbulent exchange in a neutral atmosphere. J. Geophys. Res., 67, 3095-3102.

Bolton, J.A., 1977: Monthly estimates of the mean distribution of ozone in the atmosphere as a function of latitude. Met O 20 Technical Note No. II/117, Meteorological Office, Bracknell.

Bolton, J.A., 1981: The estimation of zonally-averaged climatological cloud data for use in the 5-level model radiation scheme. Met O 20 Technical Note II/136, Meteorological Office, Bracknell.

Bourke, W., McAvaney, B., Puri, K. and Thurling, R., 1977: Global modelling of atmospheric flow by spectral methods. Methods in Computational Physics, 17, "General Circulation of the Atmosphere". Ed. J. Chang, Academic Press.

Bryan, K., 1966: A scheme for numerical integration of the equations of motion on an irregular grid free of non-linear instability. Mon. Wea. Rev., 94, 39-40.

Carson, D.J., 1982a: Comments on the sensitivity of numerical simulations to different parametrizations of the boundary layer properties and processes, Workshop on Planetary Boundary Layer Parametrization, 25-27 November 1981, ECMWF. Also appears as Met O 20 Technical Note II/136, Meteorological Office, Bracknell.

Carson, D.J. 1982b Current parametrizations of land-surface processes in atmospheric general circulation models. Land Surface Processes in atmospheric general circulation models, ed. P.S. Eagleson, Cambridge University Press. Also appears as Met O 20 Technical Note No. II/152, Meteorological Office, Bracknell.

Carson, D.J., and Richards, P.J.R., 1978: Modelling surface turbulent fluxes in stable conditions. Boundary-Layer Met., 14, 67-81.

Cattle, H., 1985: Atmospheric general circulation model simulation of the climate of the Mediterranean region. Dynamical Climatology Technical Note No. 17, Meteorological Office, Bracknell.

Ceselski, B.F. 1972 A comparison of cumulus parametrization techniques in numerical integrations of an easterly wave. Report 72-1 (Part 4), Dept. Met. Florida State University, Tallahassee, U.S.A.

Clarke, R.H. 1970 Recommended methods for the treatment of the boundary layer in numerical models. Austr. Met. Mag., 18, 51-73.

Corby G.A., Gilchrist A., and Newson R.L. 1972 A general circulation model of the atmosphere suitable for long period integrations. Quart. J.R. Met. Soc., 98, 809-832.

Corby G.A., Gilchrist, A. and Rowntree, P.R. 1977 United Kingdom

Meteorological Office five-level general circulation model. Methods in Computational Physics, 17, 67-110, Academic Press, New York.

Cunnington, W.M., 1983a: The sensitivity of the Saharan region in a general circulation model. Met O 20 Technical Note No. II/205, Meteorological Office, Bracknell.

Cunnington, W.M. 1983b An annual-cycle integration of the 11-layer model. Met O 20 Technical Note II/212, Meteorological Office, Bracknell.

Cunnington, W.M., and Rowntree, P.R., 1985: The sensitivity of the Saharan region in a general circulation model. Dynamical Climatology Technical Note No. 19, Meteorological Office, Bracknell.

Dickinson, A., and Temperton, C., 1984: The operational numerical weather prediction model. Met O 11 Technical Note No. 183, Meteorological Office, Bracknell.

Dyer, A.J., and Hicks, B.B., 1970: Flux gradient relationships in the constant flux layer. Quart. J.R. Met. Soc., 96, 715-721.

Dyson, J.F., 1984: An intercomparison of the Met O 11 N45 model and the Met O 20 11 level model on the Cyber 205. Dynamical Climatology Technical Note. No. 10, Meteorological Office, Bracknell.

Dyson, J.F., 1985: On time smoothing and high-latitude filtering. Met O 20 Internal Note No. 38, Meteorological Office, Bracknell.

Gadd, A.J., 1983: Some thoughts on diffusion. Met O 20 Internal Note No. 13, Meteorological Office, Bracknell.

Gates, W.L., and Nelson, A.B., 1973: A new tabulation of the Scripps topography on a 1° global grid. Part 1: Terrain heights. R-1276-ARPA, Rand Corporation, Santa Monica, California, U.S.A.

Gilchrist, A., 1975: Note on the integral form of the hydrostatic equation used in the 11-layer Model. Met O 20 Technical Note No. II/45, Meteorological Office, Bracknell.

Gilchrist, A. and White P.W. 1982 The development of the Meteorological Office new operational forecasting system. Met. Mag., 111, 161-179.

Goody, R.M., 1952: A statistical model for water vapour absorption. Quart. J.R. Met. Soc., 78, 165-169.

Gordon, C., and Bottomley, M., 1984: A scheme for incorporating the thermodynamic sea-ice model into a coupled ocean-atmosphere model. Dynamical Climatology Technical Note No. 1, Meteorological Office, Bracknell.

Heasman, C.C. 1983 Boundary layer schemes used in the 11-layer model. Met O 20 Technical Note II/215, Meteorological Office, Bracknell.

Heasman, C.C., 1984, The sensitivity of the 11-layer Model to boundary layer parametrization schemes. Met O 20 Technical Note No. II/219, Meteorological Office, Bracknell.

Hicks, B.B., 1976: Wind profile relationships from the 'Wangara' Experiment. Quart. J.R. Met. Soc., 102, 535-551.

Hills, T.S., 1982: The use of a numerical filter to control stability in a general circulation model. Met O 20 Technical Note II/179, Meteorological Office, Bracknell.

Hinds, M.K., 1981 Computer Story. Met. Mag., 110, 69-81.

Hinds, M.K., 1985: Handbook of the Meteorological Office 11-Layer Atmospheric General Circulation Model. Volume 2.

Houghton, J.T., 1963: The absorption of solar infra-red radiation by the lower stratosphere. Quart. J.R. Met. Soc., 89, 319-331.

Houghton, J.T., 1977, The physics of atmospheres. Cambridge University Press.

Hunt G.E. and Mattingly S.R. 1976 Infrared radiative transfer in planetary atmospheres - I Effects of computational and spectroscopic economies on thermal heating/cooling rates. J. Quant. Spectrosc, Radiat. Transfer., 16, 505-520.

Huschke R.E. 1969 Arctic cloud statistics from "air calibrated" surface weather observations. RAND Corp. memo. RM-6173-PR.

Kershaw, R., 1984: Forecasts and analyses of the onset of the Southwest monsoon, Dynamical Climatology Technical Note No. 12, Meteorological Office, Bracknell.

Liou, K.-N., 1976: On the absorption, reflection and transmission of solar radiation in cloudy atmospheres. J. Atmos. Sci., 33, 798-805.

Liou, K.-N. 1980 An introduction to atmospheric radiation. International Geophysics Series, 26, Academic Press.

Liu, J. V., and Orville, H.D., 1969: Numerical modelling of precipitation and cloud shadow effect on mountain induced cumuli. J. Atmos. Sci., 26, 1283-1298.

Louis, J.-F. (editor), 1984: Research Manual 3: ECMWF Forecast Model Physical Parametrization, ECMWF.

Ludlam, F.H. 1963 Severe local storms - a review. Meteorological Monographs, 5, 1-30.

Ludlam, F.H., 1980: Clouds and Storms. Pennsylvania State University Press.

Lyne W.H. and Rowntree P.R. 1976 Development of a convective parametrization using GATE data. Met O 20 Technical Note II/70, Meteorological Office, Bracknell.

Lyne W.H., Rowntree P.R., Temperton C. and Walker Julia 1976 Numerical modelling using GATE data. Met. Mag., 105. 261-271.

Lyne W.H., Swinbank R. and Birch N.T. 1982 A data assimilation experiment and the global circulation during the FGGE special observing periods. Quart. J.R. Met. Soc., 108, 575-594.

Manabe S. and Möller F. 1961 On the radiative equilibrium and heat balance of the atmosphere. Mon. Weath. Rev., 89, 503-532.

Mattingly, S.R., 1975: The report of the Committee on Meteorological Effects of Stratospheric Aircraft (COMESA) 1972-1975. COMESA Report, Vol. II, 422-429.

Mitchell J.F.B. 1983 The seasonal response of a general circulation model to changes in CO_2 and sea temperatures. Quart. J.R. Met. Soc., 109, 113-152.

Mitchell, J.F.B., 1984: On modelling the effects of CO_2 on climate. To appear in Proceedings of the E.C. Climatology Programme Symposium, 2-5 October 1984, Sophia Antipolis, France. Also appears as Dynamical Climatology Technical Note No. 13, Meteorological Office, Bracknell.

Mitchell, J.F.B., Wilson, C.A., and Price, C.M., 1984: On the specification of surface fluxes in coupled atmosphere-ocean general circulation models. Dynamical Climatology Technical Note No. 7, Meteorological Office, Bracknell.

Neckel H. and Labs D. 1981 Improved data of solar spectral irradiance from 0.33 to 1.25 micron. Solar Phys., 74, 231-249.

O'Neill, A., 1974: The eleven level radiation scheme. Part I Theory. Met O 20 Technical Note No. II/27, Meteorological Office, Bracknell.

Palmer, T.N., and Mansfield, D.A., 1984: Response of two atmospheric general circulation models to sea-surface temperature anomalies in the tropical east and west Pacific. Nature, 310, 483-485.

Palmer, T.N., and Shutts, G.J., 1984: Preliminary results of the effect of a parametrization of gravity wave drag in the Meteorological Office 11-Layer general circulation model. Met O 13 branch memorandum No. 149, Meteorological Office, Bracknell.

Paltridge G.W. and Platt C.M.R. 1976 Radiative processes in meteorology and climatology. Developments in atmospheric science, 5, Elsevier.

Ramanathan, V., Pitcher, E.J., Malone, R.C., and Blackmon, M.L., 1983, The response of a spectral general circulation model to refinements in radiative processes. J. Atmos. Sci., 40, 605-630.

Richards, P.J.R., 1977: A comparison of an interactive radiation scheme and one based on climatology for use in the high-resolution model. Met O 20 Technical Note II/98, Meteorological Office, Bracknell.

Richards, P.J.R., 1980a: An objective assessment of specifications of boundary-layer eddy diffusion coefficients. Met O 20 Technical Note No. II/140, Meteorological Office, Bracknell.

Richards, P.J.R. 1980b The parametrization of boundary layer processes in general circulation models. Ph.D. thesis, Department of Meteorology, University of Reading.

Ricketts, J.N., 1973: An investigation into a relationship between upper-air relative humidity and cloud cover. Met. Mag., 102, 146-153.

Riehl, H. 1954 Tropical Meteorology. McGraw Hill, New York.

Roberts, R.E., Selby, J.E.A., and Biberman, L.M., 1976: Infrared continuum absorption by atmospheric water vapour in the 8-12 μm window. Applied Optics, 15, 2085-2090.

Rothman, L.S., 1981: AFGL atmospheric absorption line parameters compilation: 1980 version. Applied Optics, 20, 791-795.

Rowntree, P.R., 1971: Proposed vertical resolution in the new Met O 20 model. Met O 20 Technical Note No. 1, Meteorological Office, Bracknell.

Rowntree, P.R. 1973 Proposed convection scheme for the 11-layer tropical model. Unpublished typescript, Met O 20, Meteorological Office, Bracknell.

Rowntree, P.R., 1975: The representation of radiation and surface heat exchange in a general circulation model. Met O 20 Technical Note No. II/58, Meteorological Office, Bracknell.

Rowntree P.R. 1976 Response of the atmosphere to a tropical Atlantic ocean temperature anomaly. Quart J.R. Met. Soc., 102, 607-625.

Rowntree, P.R., 1983a: Eddy kinetic energies in July integrations with the Meteorological Office General Circulation Model. Met O 20 Technical Note No. II/204, Meteorological Office, Bracknell.

Rowntree, P.R., 1983b: Land surface processes in climate models - parametrization and model sensitivity. Met O 20 Technical Note No. II/201, Meteorological Office, Bracknell.

Rowntree, P.R., 1984: Sensitivity of global simulations to the formulation of the evaporation of convective condensates. Workshop on convection in large-scale numerical models, 28 November - 1 December 1983, ECMWF. Also appears as Met O 20 Technical Note II/226, Meteorological Office, Bracknell.

Rowntree P.R. and Bolton J.A. 1983 Simulation of the atmospheric response to soil moisture anomalies over Europe. Quart. J.R. Met. Soc., 109, 501-526.

Rowntree, P.R., and Cattle, H., (editors), 1983: The Meteorological Office GATE Modelling Experiment. Meteorological Office Scientific Paper No. 40, HMSO, London.

Rowntree, P.R., and Mitchell, J.F.B., 1982: Preliminary analyses of 50-day integrations of the Met O 20 Cyber Model. Met O 20 Technical Note No. II/194, Meteorological Office, Bracknell.

Rowntree, P.R., and Walker, J.M., 1977: Radiation schemes in Met O 20 models. Met O 20 Technical Note No. II/93, Meteorological Office, Bracknell.

Saker N.J. 1975 An 11-layer general circulation model. Met O 20 Technical Note II/30, Meteorological Office, Bracknell.

Sasamori T., London J., and Hoyt D.V. 1972 Radiation Budget of the southern hemisphere. Meteorology of the Southern Hemisphere, Meteorological Monographs, 13, no 35.

Scorer, R.S. 1958 Natural Aerodynamics Pergamon Press, London.

S.D.C.B. (Staff of the Dynamical Climatology Branch) 1984: An 8-year integration of the 11-layer GCM. W.C.R.P. Numerical Experimentation Programme, Research activities in atmospheric and oceanic modelling, Report No. 7, p. 9.5 - 9.7.

Shine, K.P., Henderson-Sellers, A., and Slingo, A., 1984: The influence of the spectral response of satellite sensors on estimates of broadband albedo. Quart. J.R. Met. Soc., 110, 1170-1179.

Slingo A. 1982 Insolation calculations for a 360-day year. Met O 20 Technical Note II/184, Meteorological Office, Bracknell.

Slingo A. 1983 Clouds and radiation in the Meteorological Office 11-layer general circulation model. Met O 20 Technical Note II/203, Meteorological Office, Bracknell.

Slingo, A., 1984: The cloudy marine boundary layer in the Meteorological Office Climate Model. Report of the WMO/CAS Expert Meeting on Atmospheric Boundary Layer Parametrization over the Oceans for Long Range Forecasting and Climate Models. WCP-74, WMO.

Slingo, A., 1984/1985: Simulation of the earth's radiation budget with the 11-layer general circulation model. Met O 20 Technical Note No. II/214, Meteorological Office, Bracknell. A slightly revised version appears in Met. Mag., 114, 121-141 (May 1985).

Slingo, A., and Pearson, D.W., 1985: A comparison of the impact of an envelope orography and of a parametrization of gravity-wave drag on simulations with an atmospheric general circulation model. In preparation.

Slingo, A., and Schrecker, H.M., 1982: On the shortwave radiative properties of stratiform water clouds, Quart. J.R. Met. Soc., 108, 407-426.

Slingo, A., and Wilderspin, R.C., 1984a: Development of an improved GCM radiation scheme. Submitted to the Proceedings of the International Radiation Symposium 1984, Perugia, Italy. Also appears as Dynamical Climatology Technical Note No. 6, Meteorological Office, Bracknell.

Slingo, A., and Wilderspin, R.C., 1984b: Development of a revised longwave radiation scheme for an atmospheric general circulation model. Dynamical Climatology Technical Note No. 14, Meteorological Office, Bracknell.

Slingo, A., and Wilderspin, R.C., 1985: Simulation of cloudiness with the U.K. Meteorological Office 11-layer AGCM. Workshop on cloud cover parametrization in numerical models, 26-28 November 1984, ECMWF. Also appears as Dynamical Climatology Technical Note No. 22, Meteorological Office, Bracknell.

Slingo, A., and Wilson, H., 1984: Simulation of European Climate with an Atmospheric General Circulation Model. To appear in Proceedings of the E.C. Climatology Programme Symposium, 2-5 October 1984, Sophia Antipolis, France.

Slingo, J.M., 1978: The effect of interactive clouds and radiation on convective activity in a numerical model of the tropics. Workshop on the parametrization of cumulus convection, 23-25 October 1978, ECMWF. Also appears as Met O 20 Technical Note II/130, Meteorological Office, Bracknell.

Slingo, J.M., 1980 A cloud parametrization scheme derived from GATE data for use with a numerical model. Quart. J.R. Met. Soc., 106, 747-770.

Slingo, J.M., 1981: Interactive cloud and radiation in the Meteorological Office General Circulation Model. Workshop on radiation and cloud-radiation interaction in numerical modelling, 15-17 October 1980, ECMWF. Also appears as Met O 20 Technical Note II/157, Meteorological Office, Bracknell.

Slingo, J.M., 1982 A study of the earth's radiation budget using a general circulation model. Quart. J.R. Met. Soc., 108, 379-405.

Smith, R.N.B., 1985: An integrated approach to the representation of cloud processes. Workshop on cloud cover parametrization in numerical models, 26-28 November 1984, ECMWF. Also appears as Dynamical Climatology Technical Note No. 23, Meteorological Office, Bracknell.

Somerville, R.C.J., and Remer, L.A., 1984: Cloud optical thickness feedbacks in the CO_2 climate problem. J. Geophys. Res., 89, 9668-9672.

Stephens, G.L., 1984: The parametrization of radiation for numerical weather prediction and climate models. Mon. Wea. Rev., 112, 826-867.

Umscheid, L., and Sankar-Rao, M., 1971: Further tests of a grid system for global numerical prediction. Mon. Wea. Rev., 99, 686-690.

Vanderman, L.W., 1972: Forecasting with a global, three-layer primitive-equation model. Mon. Wea. Rev., 100, 856-868.

Van Loon H. 1972 Cloudiness and precipitation in the southern hemisphere. Meteorology of the Southern Hemisphere, Meteorological Monographs, 13, no 35.

Walker J.M. 1977 Interactive cloud and radiation in the 11-layer model. Part I: Radiation Scheme. Met O 20 Technical Note II/91, Meteorological Office, Bracknell.

Wallace, J.M., Tibaldi, S., and Simmons, A.J., 1983: Reduction of systematic forecast errors in the ECMWF model through the introduction of an envelope orography. Quart. J.R. Met. Soc., 109, 683-717.

Webb, E.K., 1970: Profile relationships: the log-linear range and extension to strong stability. Quart. J. R. Met. Soc., 96, 67-90.

Welch, R.M., Cox, S.K., and Davis, J.M., 1980: Solar radiation and clouds. Amer. Met. Soc., Met. Mon., 17, No. 39.

Williamson, D.L., 1976: Linear stability of finite difference approximations on a uniform latitude-longitude grid with Fourier Filtering. Mon. Wea. Rev., 104, 31-41.

Wilson, C.A., and Mitchell, J.F.B., 1983: Interactive cloud in the 5-level model. Met O 20 Technical Note II/195, Meteorological Office, Bracknell.

Wilson, C.A., and Mitchell, J.F.B., 1985: Diurnal variation and cloud in a general circulation model. Dynamical Climatology Technical Note No. 18, Meteorological Office, Bracknell.

Wilson, H., 1984a: A study of the July climatology of the 11-Layer Model over the European area. Met O 20 Technical Note No. II/222, Meteorological Office, Bracknell.

Wilson, H., 1984b: The effects on the January circulation of the 11-Layer Model due to increasing orographic heights, Met O 20 Technical Note No. II/223, Meteorological Office, Bracknell.

Wilson, H., and Slingo, A., 1983: A study of the January climatology of the 11-Layer Model over the European area. Met O 20 Technical Note No II/214, Meteorological Office, Bracknell.

Wilson, M.F., 1984: The construction and use of land surface information in a general circulation climate model. Ph.D. Thesis, University of Liverpool.

Wilson, M.F. and Henderson-Sellers, A., 1985: A global archive of land cover and soils data for use in general circulation climate models. J. Climatology, 5, 119-143.

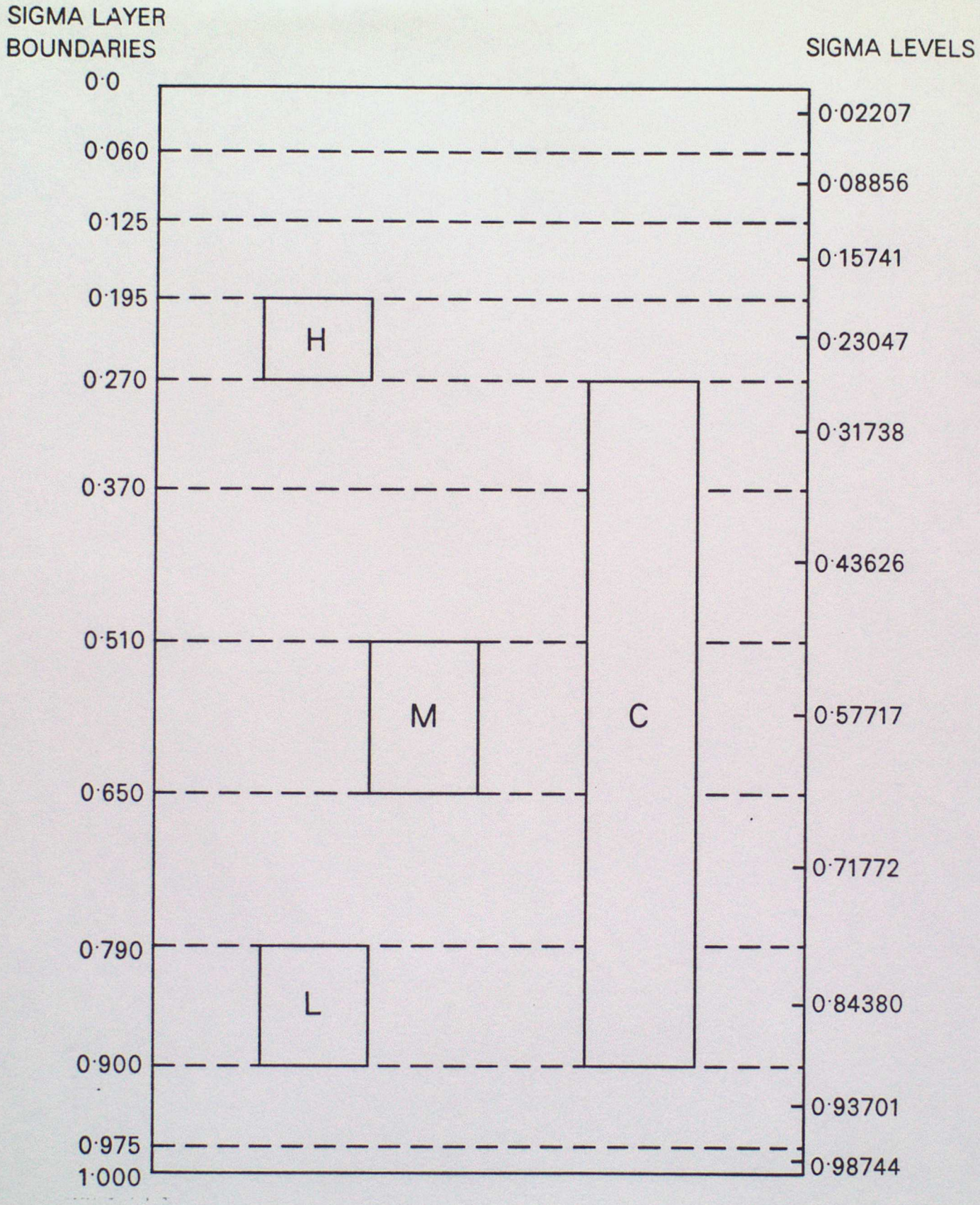

Figure 1.1 **Vertical resolution of the 11-Layer Model. A possible configuration of the High (H), Medium (M) and Low (L) layer clouds and the convective tower (C), as used in the interactive radiation scheme, is also shown.**

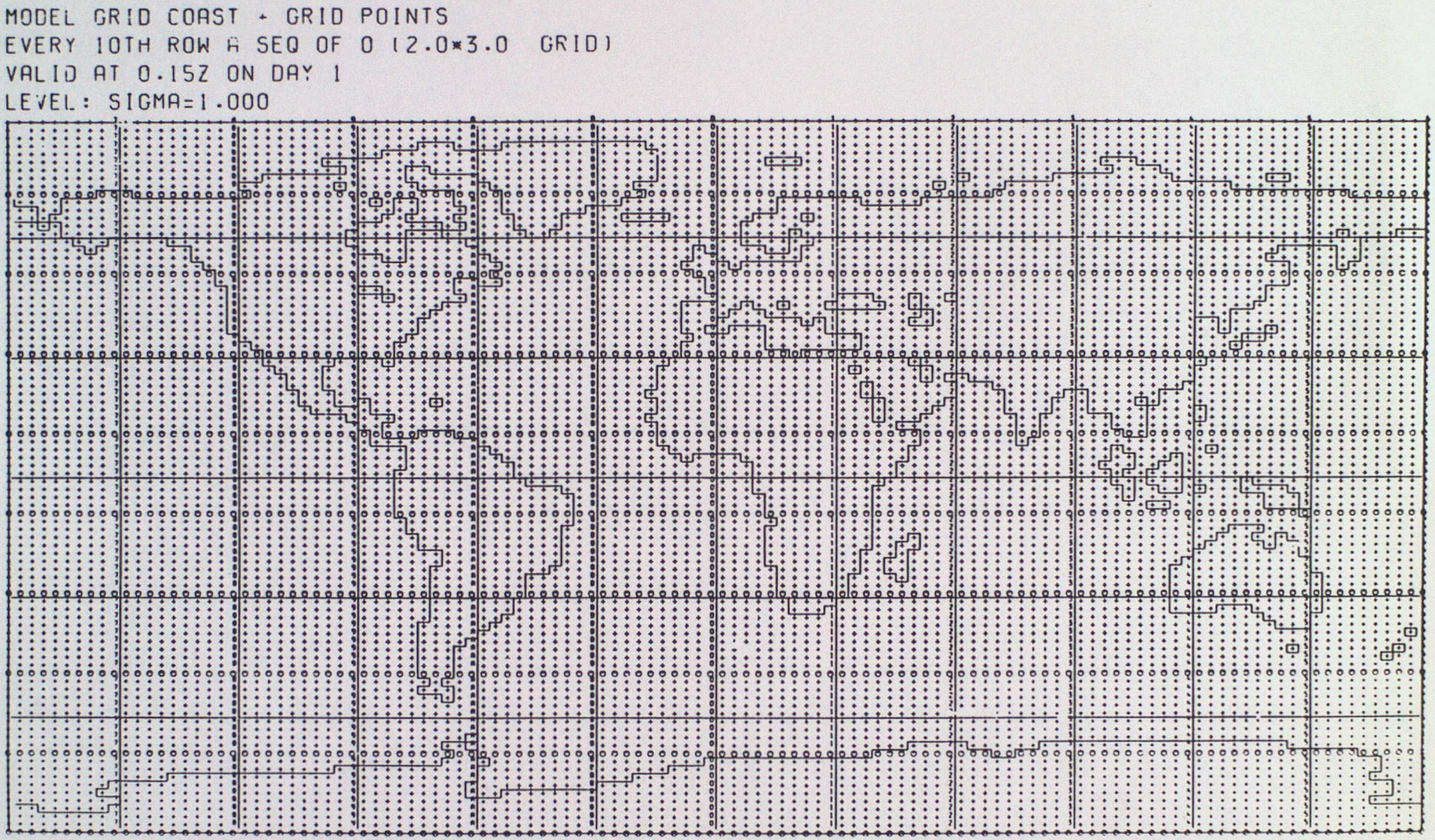

Figure 1.2 Horizontal resolution of the 11-Layer Model when integrated on the 2 x 3 degree latitude-longitude grid.

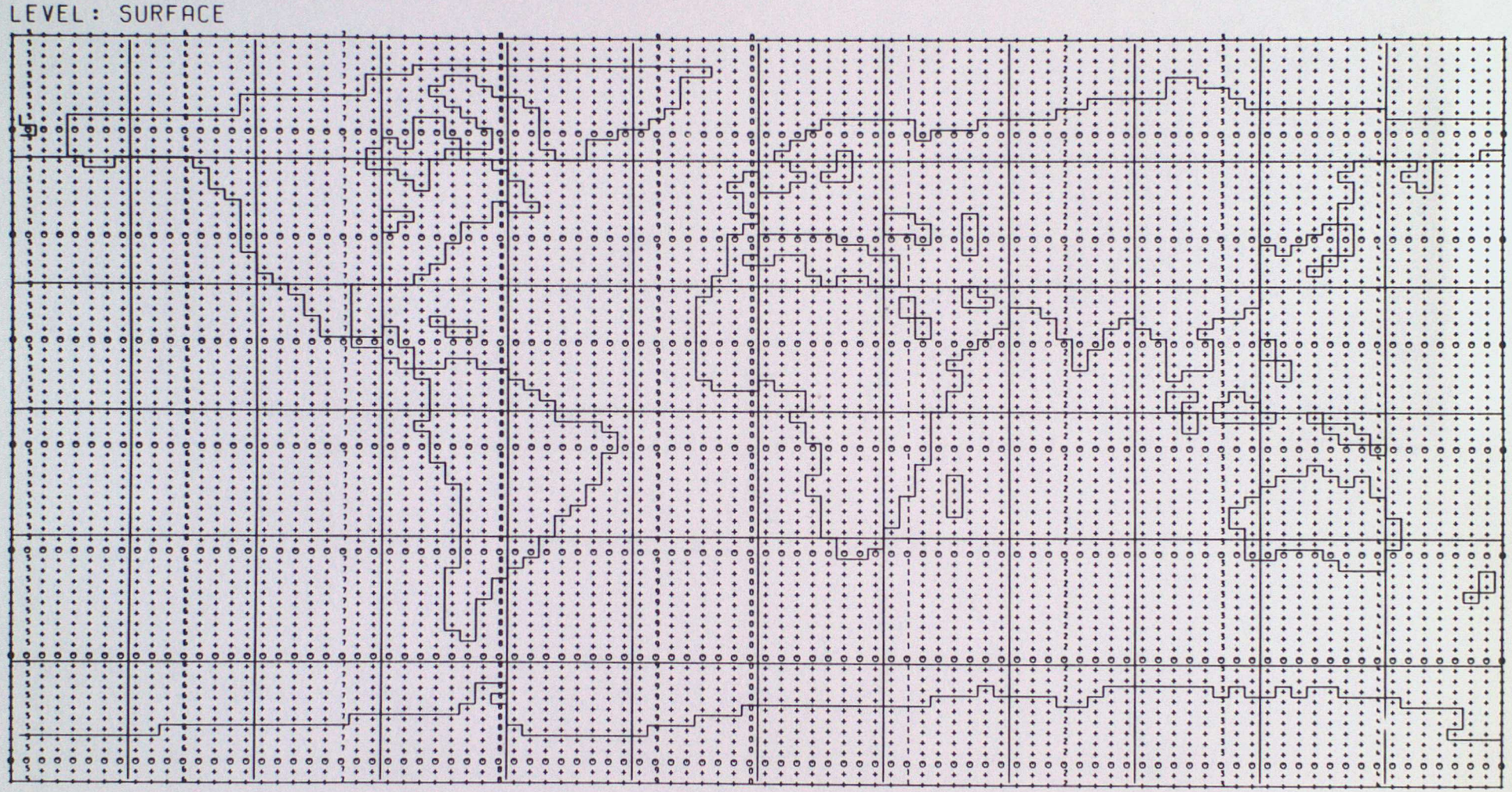

Figure 1.3 Horizontal resolution of the 11-Layer Model when integrated on the 2.5 x 3.75 degree latitude-longitude grid.

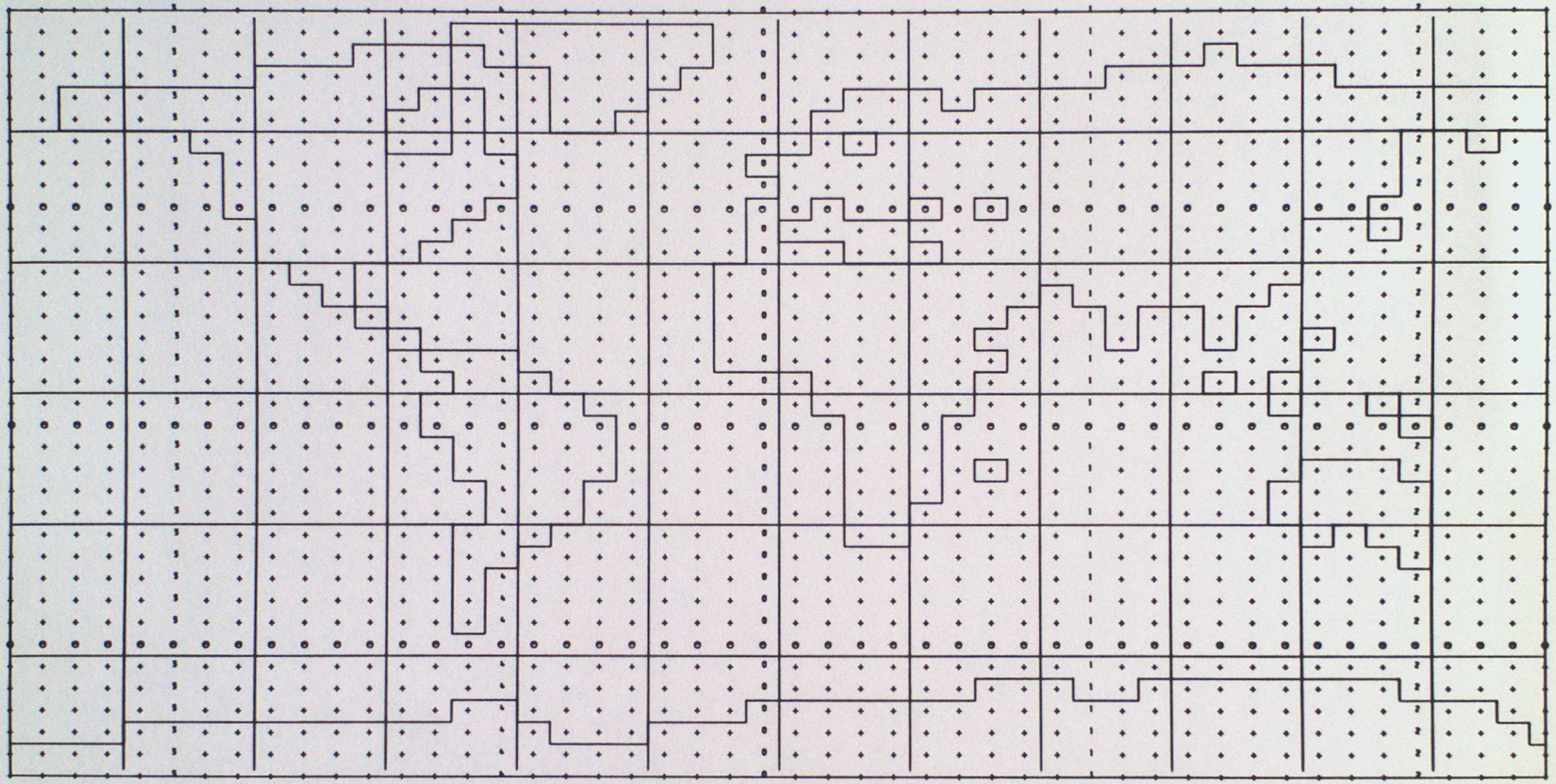

Figure 1.4 Horizontal resolution of the 11-Layer Model when integrated on the 5 x 7.5 degree latitude-longitude grid.

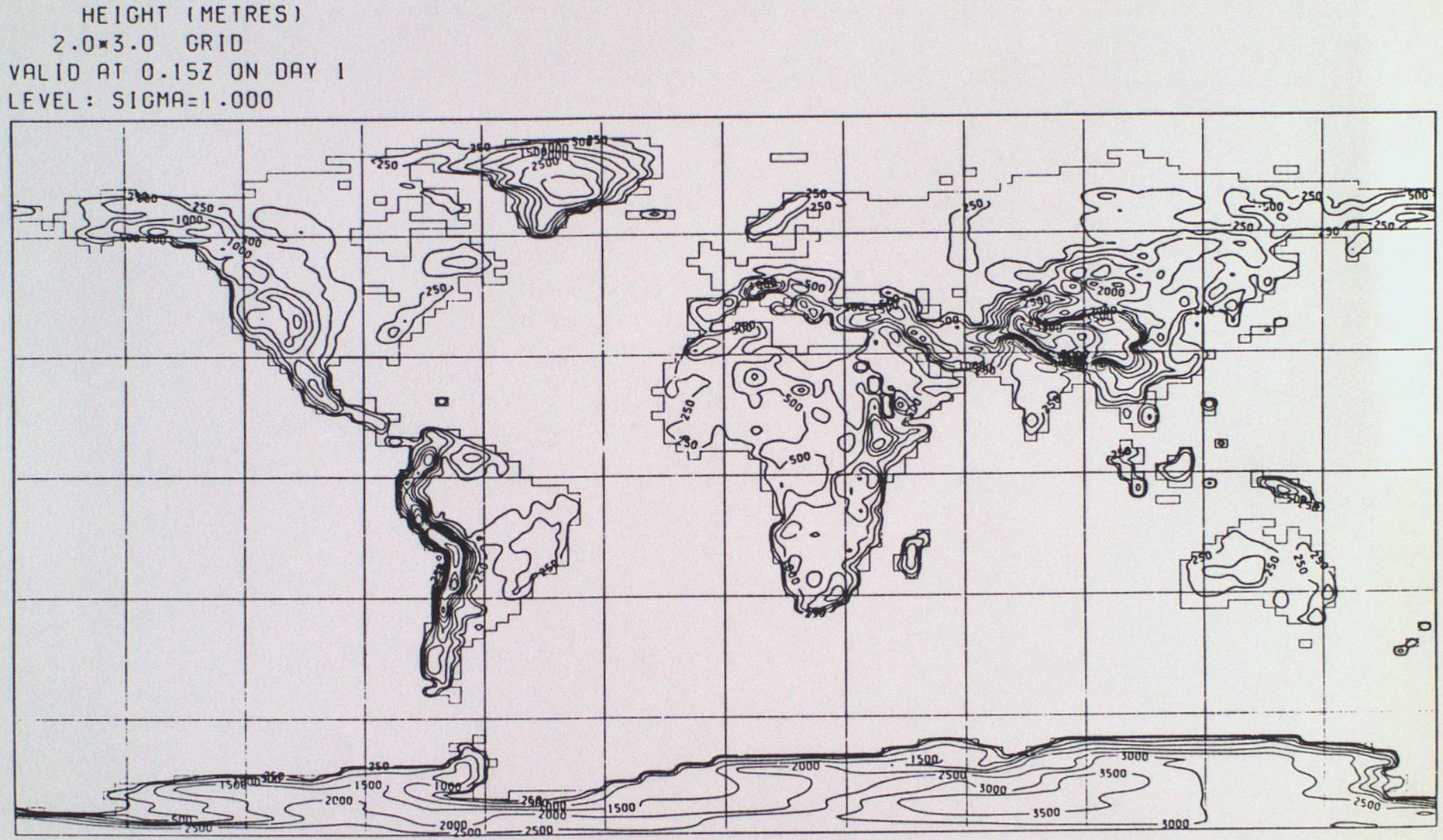

Figure 1.5 Surface elevations for the 2 x 3 degree latitude-longitude grid.

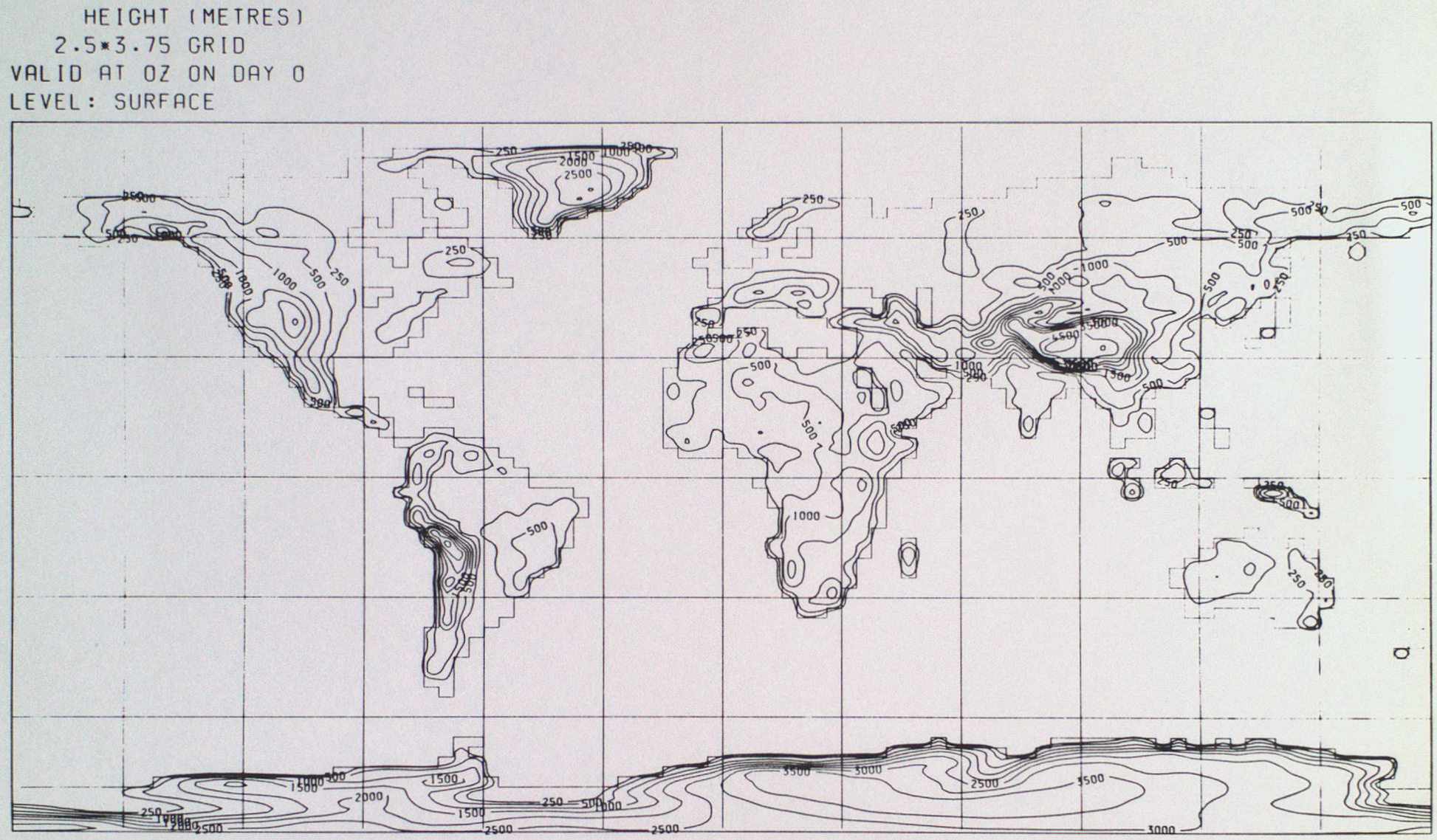

Figure 1.6 Surface elevations for the 2.5 x 3.75 degree latitude-longitude grid.

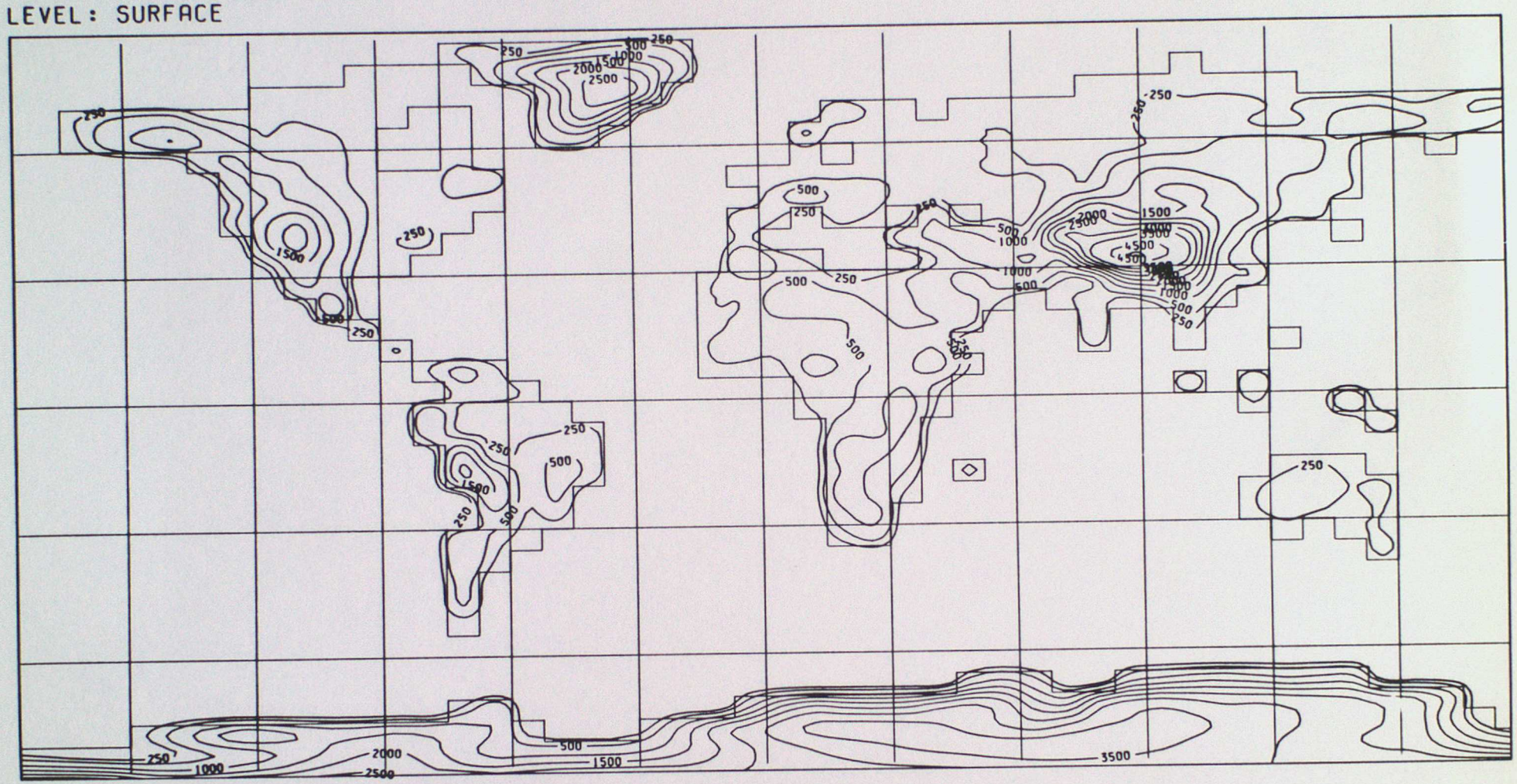

Figure 1.7 Surface elevations for the 5 x 7.5 degree latitude-longitude grid.

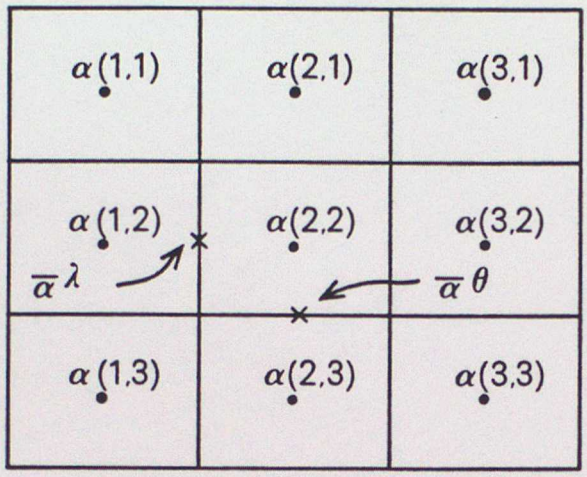

Figure 2.1 Illustration of terms used in section 2.6.

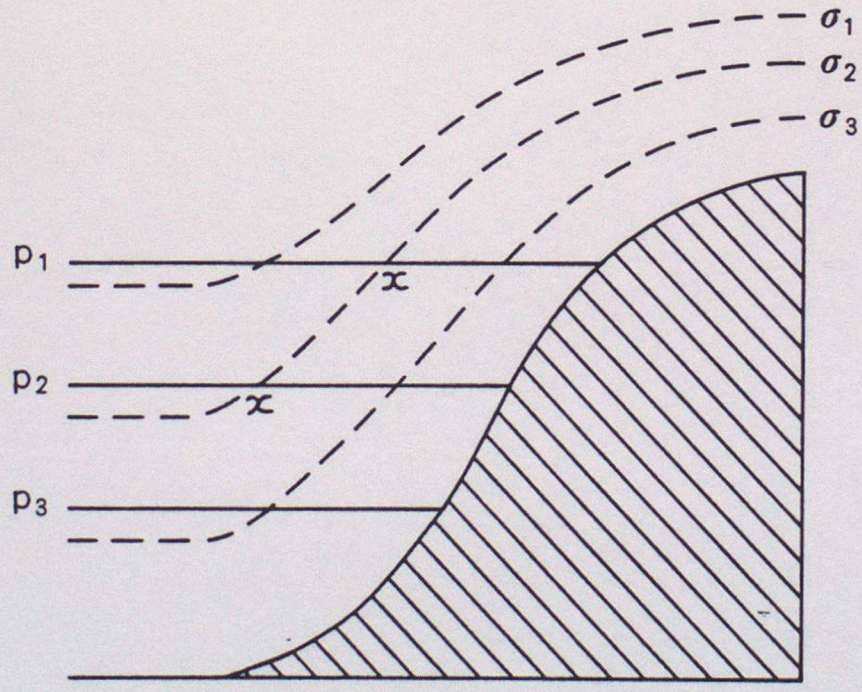

Figure 2.2 Pressure and sigma levels near changes in the surface elevation (see section 2.6 (iv)).

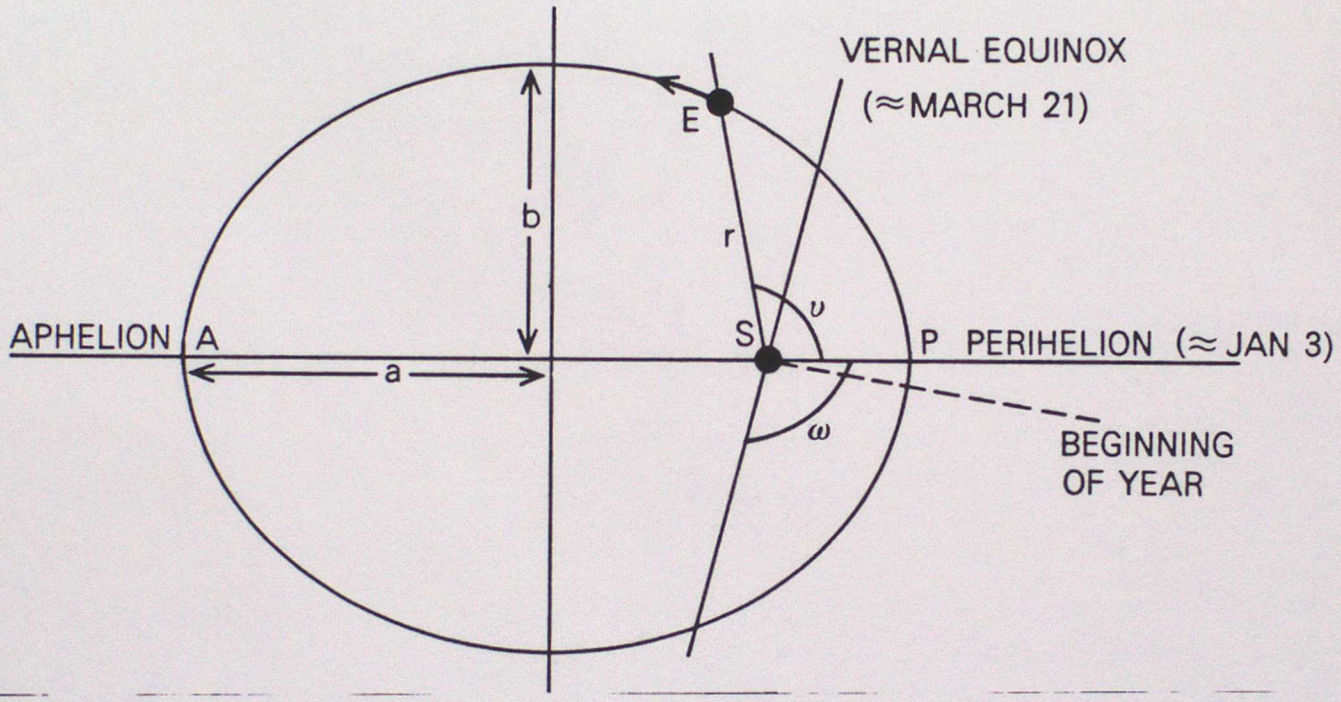

Figure 4.1 Schematic diagram of the earth's orbit. The meaning of the symbols is as follows;

S Sun

E Earth

A Aphelion (Earth furthest from Sun)

P Perihelion (Earth closest to Sun)

a Semi-major axis

b Semi-minor axis

r Length of radius vector SE

w Longitude of perihelion. Note that this is defined such that the angle between perihelion and the vernal equinox is $(\pi - w)$.

v True Anomaly, which is the angle around the orbit from perihelion.

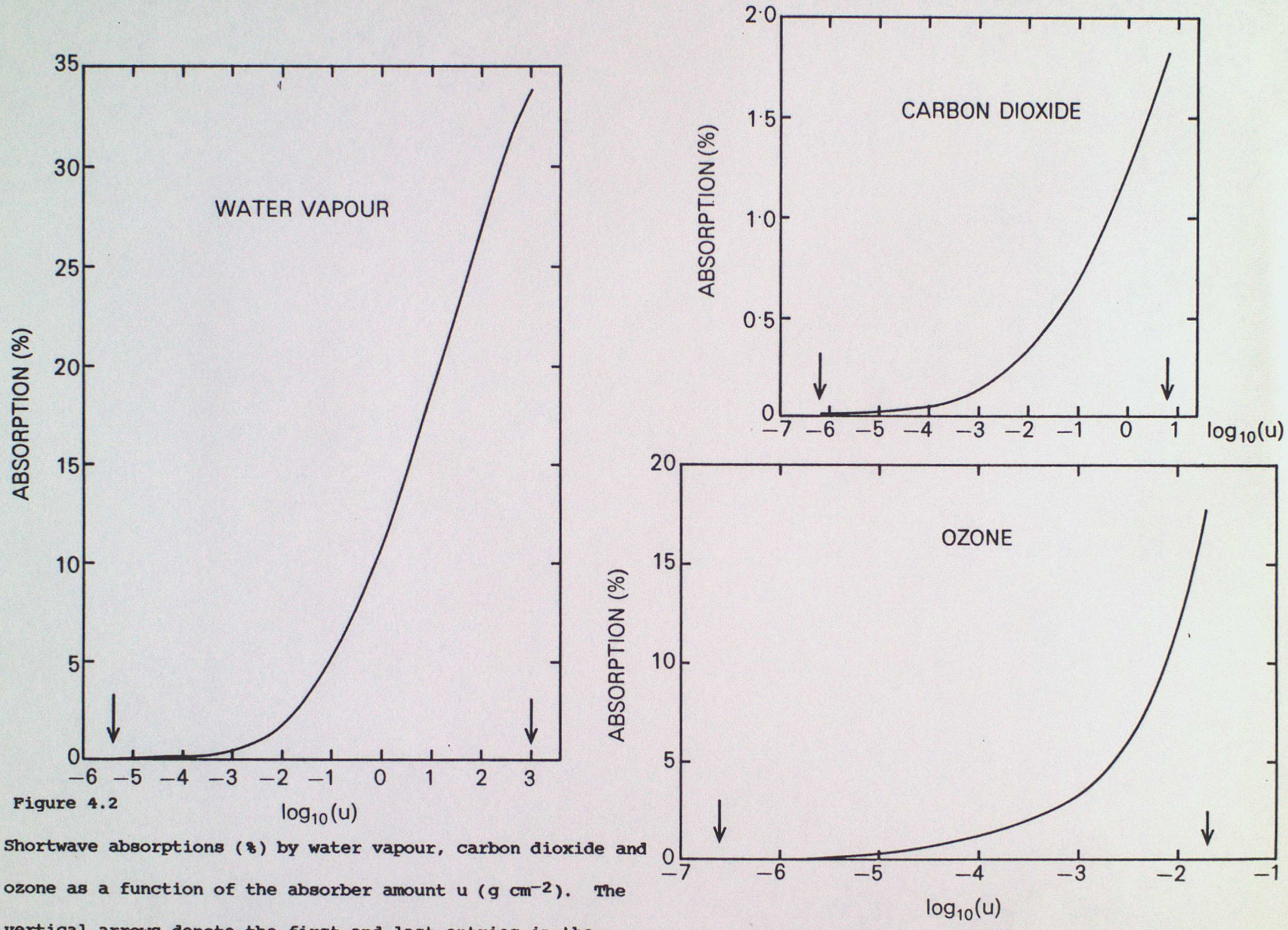

Figure 4.2

Shortwave absorptions (%) by water vapour, carbon dioxide and ozone as a function of the absorber amount u (g cm^{-2}). The vertical arrows denote the first and last entries in the look-up tables stored in the program.

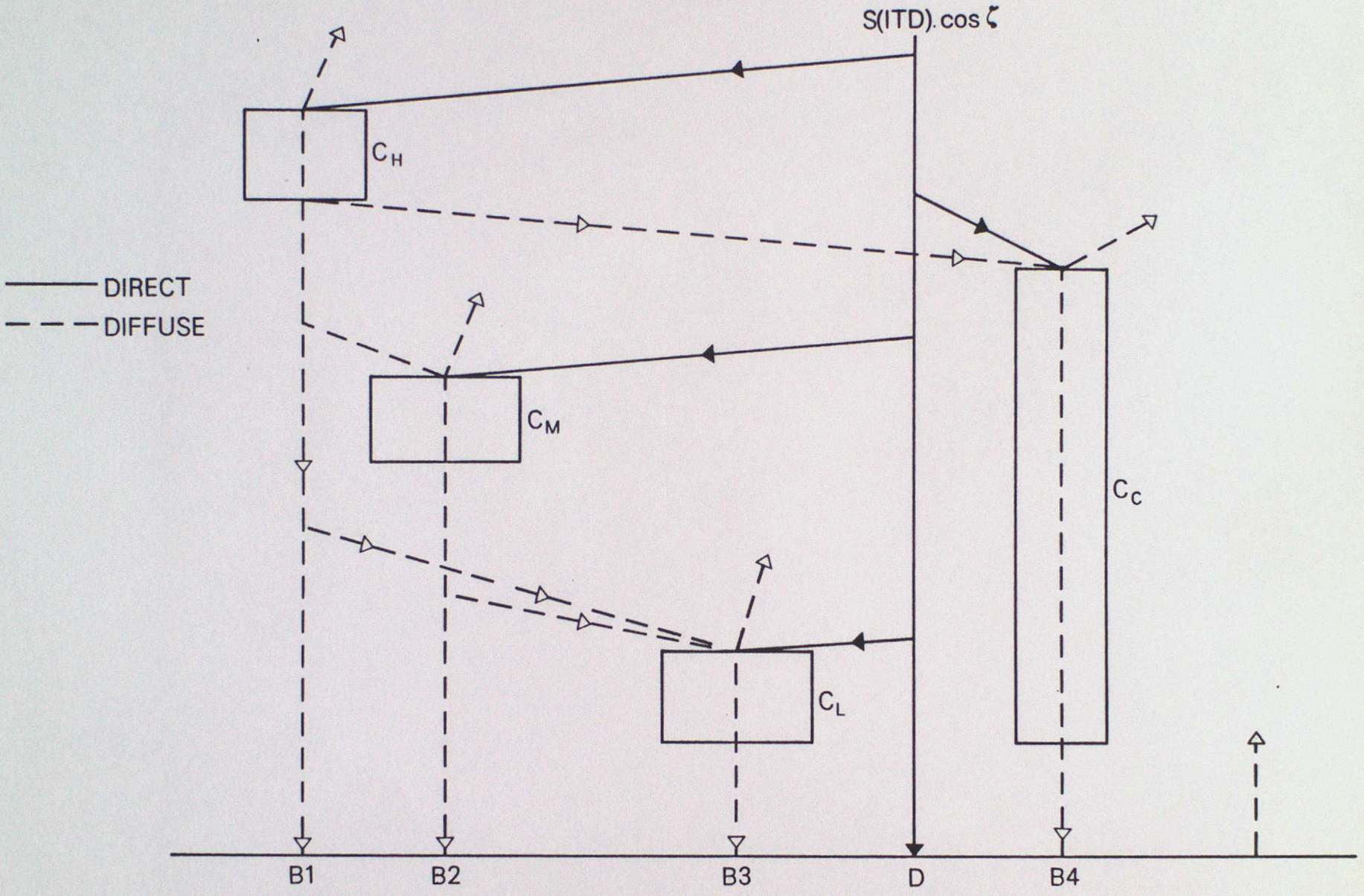

Figure 4.3 Division of the solar beam during its passage through a cloudy atmosphere.

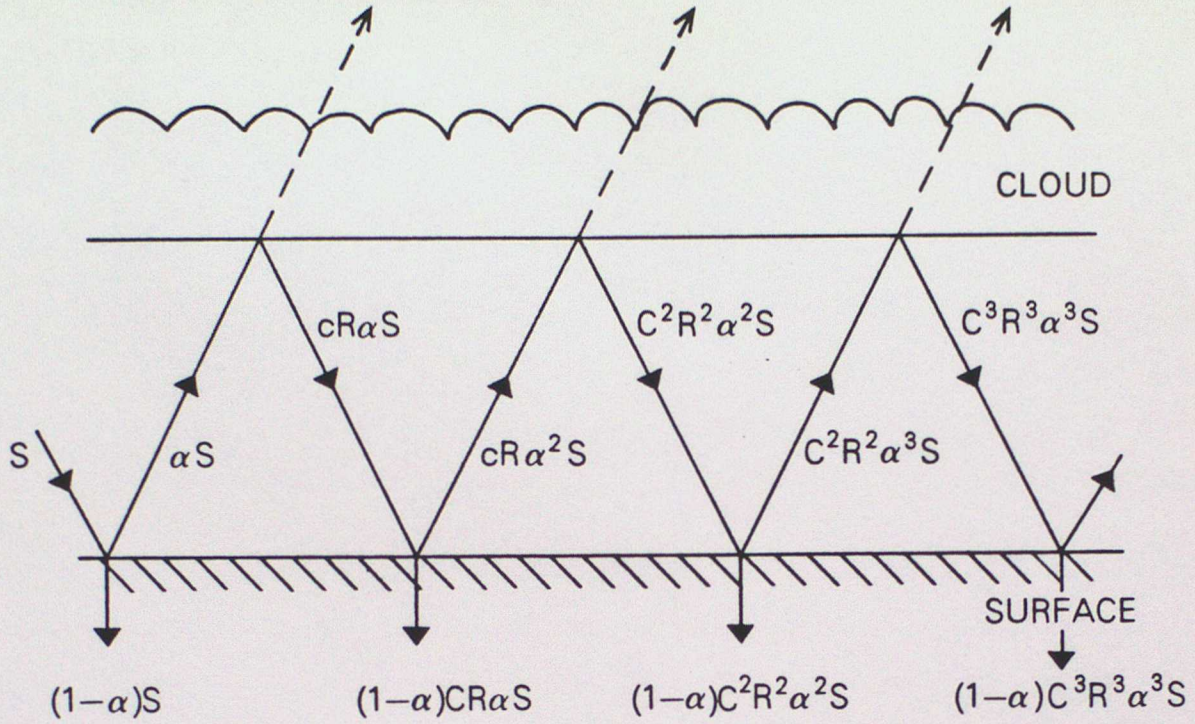

Figure 4.4 Multiple reflections between clouds and the surface.

Let S = incoming solar flux

C = cloud amount

R = cloud reflectivity

α = surface albedo

α_{eff} = effective surface albedo

Net solar flux absorbed by surface = $(1 - \alpha_{eff})S$

$= (1-\alpha)S + (1-\alpha)\,CR\alpha S + (1-\alpha)C^2R^2\alpha^2S + \ldots.$

Hence $(1-\alpha_{eff}) = (1-\alpha)\,(1 + CR\alpha + C^2R^2\alpha^2 + \ldots.)$

$$= \frac{(1-\alpha)}{(1 - CR\alpha)}$$

Thus $\alpha_{eff} = \dfrac{\alpha\,(1 - CR)}{(1 - \alpha CR)}$

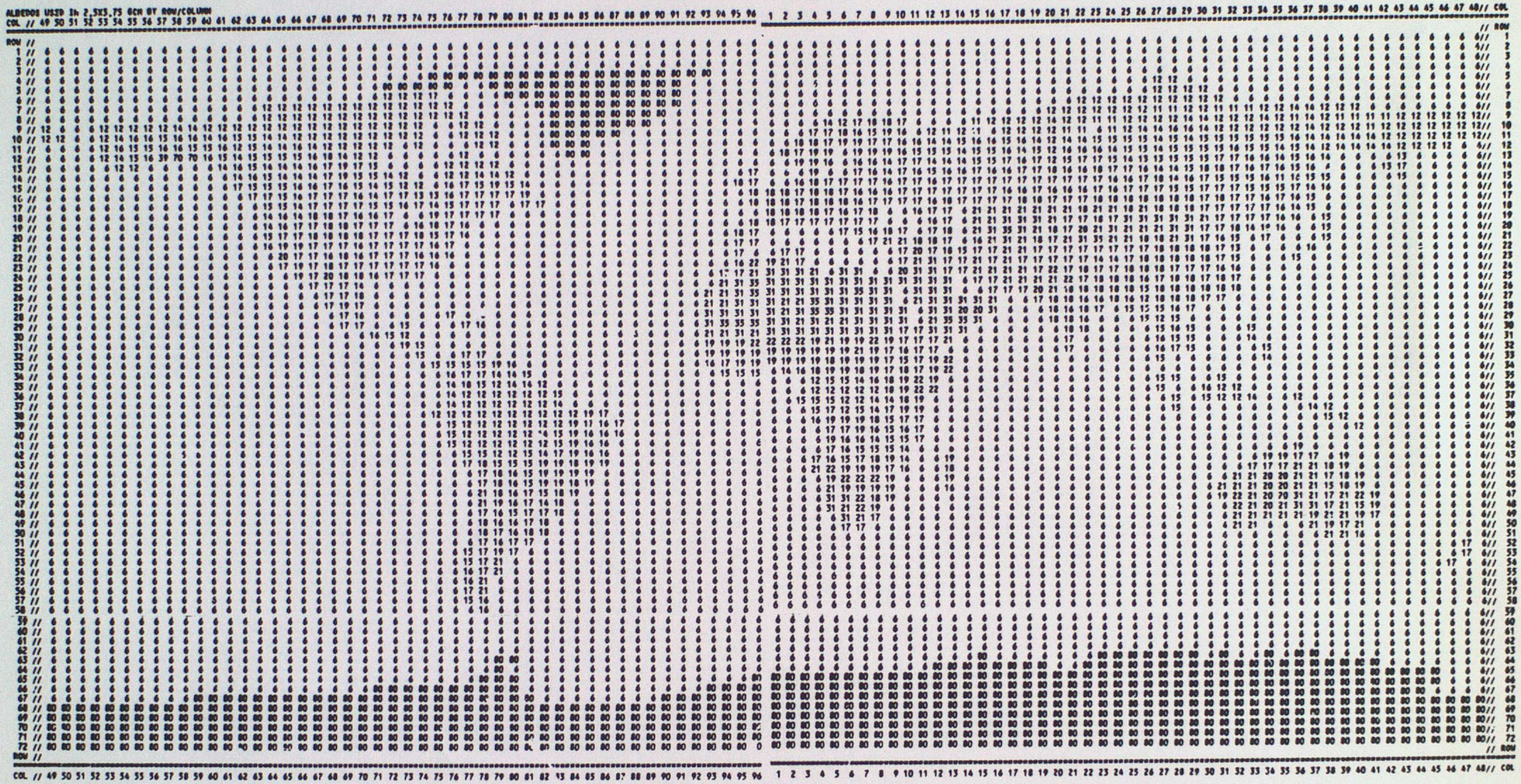

Figure 4.5 Snow-free surface shortwave albedos (%) used in the model when integrated on the 2.5 x 3.75 degree latitude-longitude grid. In this dataset sea-ice is ignored, so all sea points are allocated the value 6%.

ALBEDOS USED IN 5X7.5 GCM BY ROW/COLUMN

COL//	25	26	27	28	29	30	31	32	33	34	35	36	37	38	39	40	41	42	43	44	45	46	47	48	1	2	3	4	5	6	7	8	9	10	11	12	13	14	15	16	17	18	19	20	21	22	23	24
ROW//																																																		
1 //	6	6	6	6	6	6	6	6	6	6	6	6	6	6	6	6	6	6	6	6	6	6	6	6	6	6	6	6	6	6	6	6	6	6	6	6	6	6	6	6	6	6	6	6	6	6	6	6
2 //	6	6	6	6	6	6	6	6	6	6	6	6	6	6	80	80	80	80	80	80	80	80	6	6	6	6	6	6	6	6	6	6	6	6	6	6	6	6	6	6	6	6	6	6	6	6	6	6
3 //	6	6	6	6	6	6	6	6	6	6	6	14	80	80	6	80	80	80	80	80	80	80	6	6	6	6	6	6	6	6	6	6	6	6	6	6	6	6	6	6	6	6	6	6	6	6	6	6
4 //	6	6	6	6	6	6	6	6	12	12	12	12	12	12	6	6	6	80	80	80	80	6	6	6	6	6	6	6	6	6	6	6	6	6	6	6	12	6	6	6	6	6	6	6	6	6	6	6
5 //	6	6	12	14	14	14	14	13	12	12	12	12	12	6	12	6	6	80	80	80	6	6	6	6	6	6	6	6	6	6	6	6	6	12	12	12	11	12	11	11	6	6	6	6	6	6	6	6
6 //	6	6	13	15	35	29	14	15	15	15	12	12	6	6	12	6	6	80	80	6	6	6	6	6	6	15	16	17	6	11	10	12	12	11	10	12	13	14	12	12	12	13	11	11	12	12	12	12
7 //	6	6	6	6	6	6	15	15	14	16	17	15	6	6	12	6	6	6	6	6	6	6	6	6	6	19	6	16	15	15	15	16	16	16	16	17	15	14	16	17	16	15	15	6	6	15	6	6
8 //	6	6	6	6	6	6	6	16	15	17	16	15	13	15	16	17	6	6	6	6	6	6	6	18	18	17	17	16	16	17	17	17	16	17	16	16	17	16	16	15	15	15	6	6	6	6	6	6
9 //	6	6	6	6	6	6	6	14	15	17	17	16	16	16	17	17	6	6	6	6	6	6	6	6	18	18	17	17	17	16	17	19	19	19	18	19	19	18	17	17	17	16	15	6	6	6	6	6
10 //	6	6	6	6	6	6	6	14	17	18	18	17	17	17	16	6	6	6	6	6	6	6	6	18	17	6	17	16	6	16	6	23	32	23	18	22	26	28	25	17	16	16	6	6	6	6	6	6
11 //	6	6	6	6	6	6	6	6	19	17	17	17	17	16	6	6	6	6	6	6	6	6	6	17	6	6	6	6	20	18	17	18	23	17	21	22	18	19	21	15	6	6	15	6	6	6	6	6
12 //	6	6	6	6	6	6	6	6	18	18	17	17	17	6	6	6	6	6	6	6	6	6	6	19	25	23	6	6	6	28	17	20	20	18	17	15	18	18	17	16	6	6	6	6	6	6	6	6
13 //	6	6	6	6	6	6	6	6	6	17	16	6	6	6	6	6	6	6	6	6	6	6	21	33	31	31	31	32	31	31	31	17	19	21	19	18	17	18	18	18	6	6	6	6	6	6	6	6
14 //	6	6	6	6	6	6	6	6	6	6	17	6	5	6	6	6	6	6	6	6	6	6	26	31	26	30	32	31	31	28	28	26	6	18	17	17	14	17	17	6	6	6	6	6	6	6	6	6
15 //	6	6	6	6	6	6	6	6	6	6	6	15	6	6	6	6	6	6	6	6	6	6	27	30	31	28	26	31	27	23	33	6	6	6	17	6	6	14	6	6	6	6	6	6	6	6	6	6
16 //	6	6	6	6	6	6	6	6	6	6	6	6	16	6	6	6	6	6	6	6	6	6	19	20	20	20	19	20	17	17	6	6	6	6	17	6	6	16	6	6	14	6	6	6	6	6	6	6
17 //	6	6	6	6	6	6	6	6	6	6	6	6	6	15	16	16	6	6	6	6	6	6	16	17	17	18	19	19	17	18	22	6	6	6	6	6	6	6	6	6	6	6	6	6	6	6	6	6
18 //	6	6	6	6	6	6	6	6	6	6	6	6	6	6	14	12	12	6	6	6	6	6	6	6	6	12	13	13	18	21	6	6	6	6	6	6	6	6	6	15	6	13	6	6	6	6	6	6
19 //	6	6	6	6	6	6	6	6	6	6	6	6	6	13	12	12	12	13	6	6	6	6	6	6	6	15	14	14	17	19	6	6	6	6	6	6	6	6	6	6	12	6	6	13	6	6	6	6
20 //	6	6	6	6	6	6	6	6	6	6	6	6	6	15	12	12	12	16	16	6	6	6	6	6	6	18	18	16	6	6	6	6	6	6	6	6	6	6	6	6	6	12	6	6	13	6	6	6
21 //	6	6	6	6	6	6	6	6	6	6	6	6	6	6	13	12	13	17	16	6	6	6	6	6	6	17	15	15	6	6	6	6	6	6	6	6	6	6	6	6	6	6	12	6	6	6	6	6
22 //	6	6	6	6	6	6	6	6	6	6	6	6	6	6	17	16	17	19	19	6	6	6	6	6	6	18	18	16	6	18	6	6	6	6	6	6	6	6	6	6	18	18	19	6	6	6	6	6
23 //	6	6	6	6	6	6	6	6	6	6	6	6	6	6	17	16	18	6	6	6	6	6	6	6	6	20	20	19	6	6	6	6	6	6	6	6	6	6	6	21	20	20	18	18	6	6	6	6
24 //	6	6	6	6	6	6	6	6	6	6	6	6	6	6	16	16	18	6	6	6	6	6	6	6	6	28	20	6	6	6	6	6	6	6	6	6	6	6	6	21	20	26	21	20	6	6	6	6
25 //	6	6	6	6	6	6	6	6	6	6	6	6	6	18	16	18	6	6	6	6	6	6	6	6	6	24	18	6	6	6	6	6	6	6	6	6	6	6	6	6	21	6	20	19	6	6	6	6
26 //	6	6	6	6	6	6	6	6	6	6	6	6	6	16	17	6	6	6	6	6	6	6	6	6	6	6	6	6	6	6	6	6	6	6	6	6	6	6	6	6	6	6	18	6	6	6	6	6
27 //	6	6	6	6	6	6	6	6	6	6	6	6	6	16	6	6	6	6	6	6	6	6	6	6	6	6	6	6	6	6	6	6	6	6	6	6	6	6	6	6	6	6	6	6	6	6	6	6
28 //	6	6	6	6	6	6	6	6	6	6	6	6	6	19	6	6	6	6	6	6	6	6	6	6	6	6	6	6	6	6	6	6	6	6	6	6	6	6	6	6	6	6	6	6	6	6	6	6
29 //	6	6	6	6	6	6	6	6	6	6	6	6	6	16	6	6	6	6	6	6	6	6	6	6	6	6	6	6	6	6	6	6	6	6	6	6	6	6	6	6	6	6	6	6	6	6	6	6
30 //	6	6	6	6	6	6	6	6	6	6	6	6	6	6	6	6	6	6	6	6	6	6	6	6	6	6	6	6	6	6	6	6	6	6	6	6	6	6	6	6	6	6	6	6	6	6	6	6
31 //	6	6	6	6	6	6	6	6	6	6	6	6	6	6	6	6	6	6	6	6	6	6	6	6	6	6	6	6	6	6	6	6	6	6	6	6	6	6	6	6	6	6	6	6	6	6	6	6
32 //	6	6	6	6	6	6	6	6	6	6	6	6	6	6	6	6	6	6	6	6	6	6	6	6	6	6	6	6	6	6	6	6	6	6	6	6	6	6	6	6	6	6	6	6	6	6	6	6
33 //	6	6	6	6	6	6	6	6	6	6	6	6	6	6	6	6	6	6	6	6	6	6	6	6	6	6	6	6	6	6	80	80	80	6	6	80	80	80	80	80	80	80	6	6	6	6	6	6
34 //	6	6	6	6	80	80	80	80	80	80	80	80	80	80	80	80	6	6	6	6	6	6	6	80	80	80	80	80	80	80	80	80	80	80	80	80	80	80	80	80	80	80	80	80	6	6	6	6
35 //	80	80	80	80	80	80	80	80	80	80	80	80	80	80	80	80	6	6	6	80	80	80	80	80	80	80	80	80	80	80	80	80	80	80	80	80	80	80	80	80	80	80	80	80	80	80	6	6
36 //	80	80	80	80	80	80	80	80	80	80	80	80	80	80	80	80	80	80	80	80	80	80	80	0	80	80	80	80	80	80	80	80	80	80	80	80	80	80	80	80	80	80	80	80	80	80	80	80

Figure 4.6 Same as Figure 4.5 for the 5 x 7.5 degree grid.

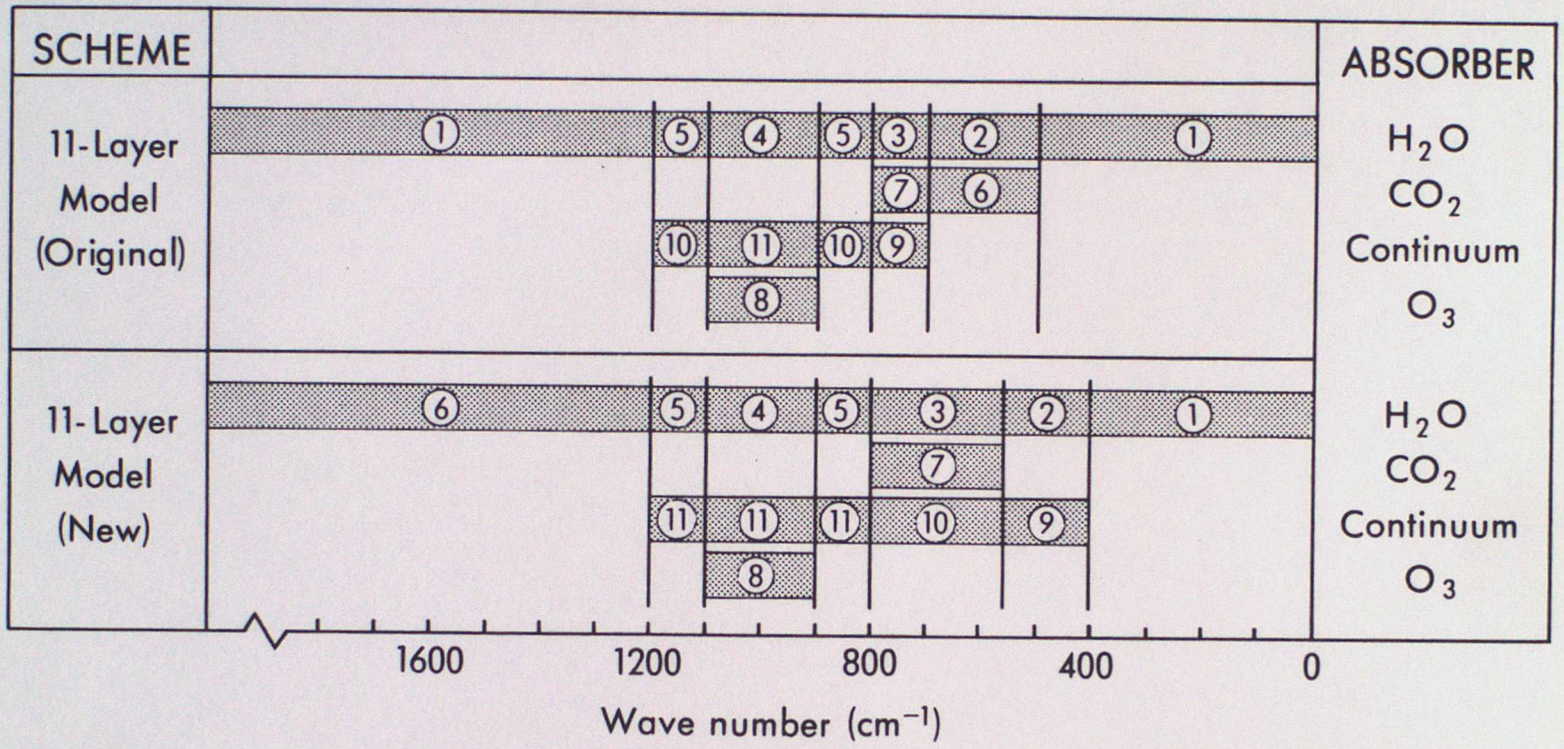

Figure 4.7 Band limits and absorbers taken into account in the original and new versions of the 11-Layer Model longwave radiation scheme. The numbers identify the separate contributions to the total flux from each of the absorbers listed on the right.

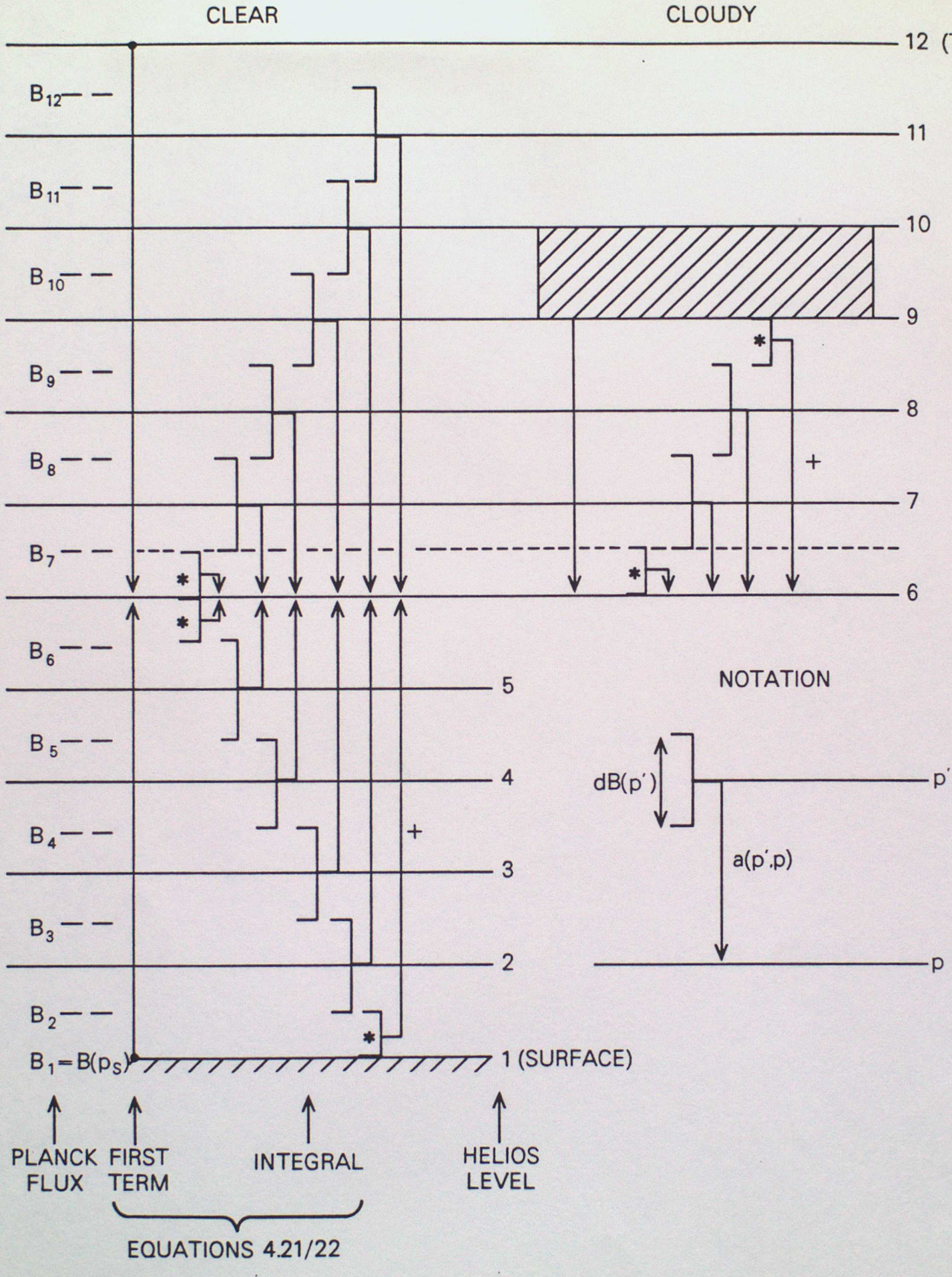

Figure 4.8 Illustration of how the contributions to equations 4.21 and 4.22 from each layer are added. See text for discussion.

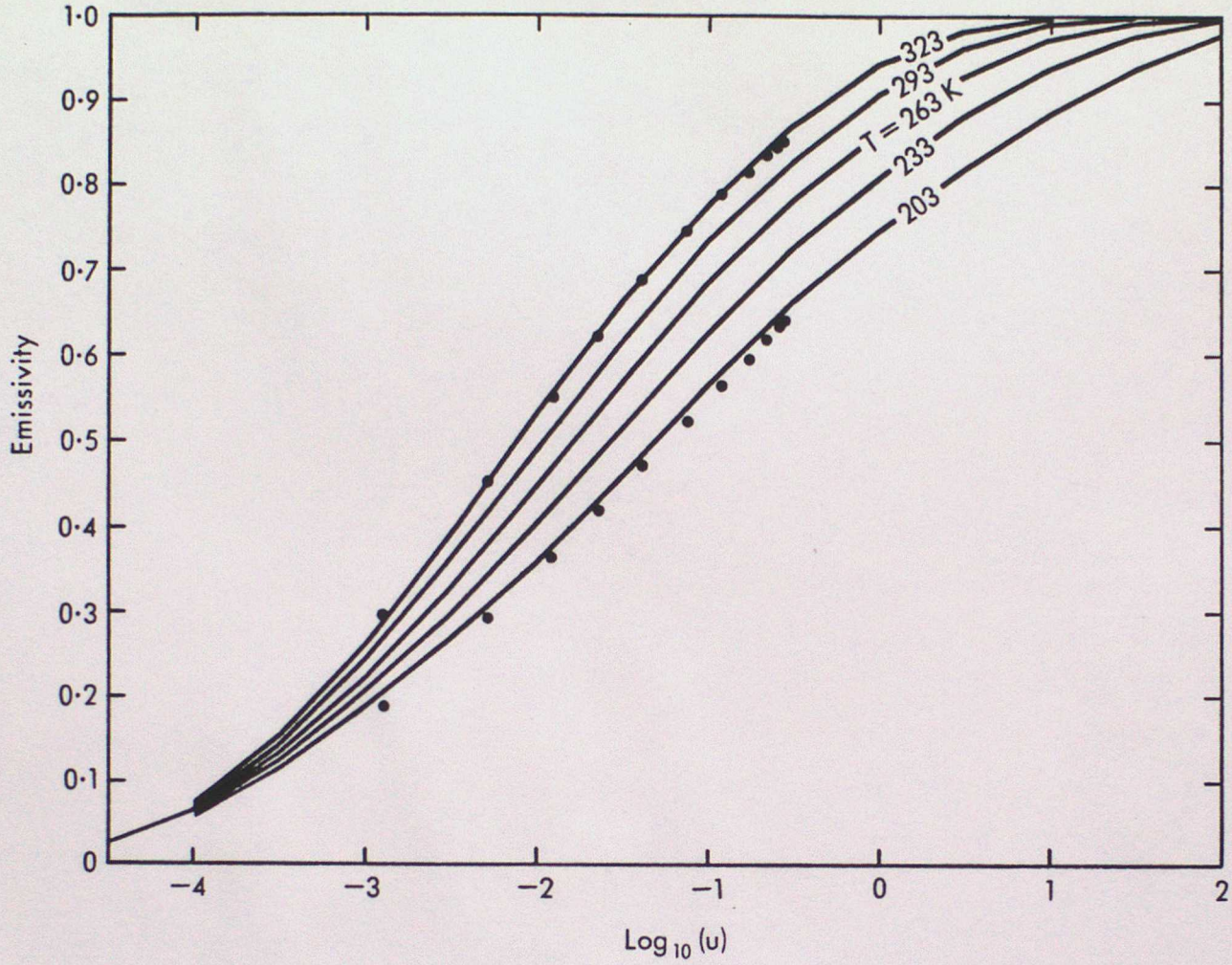

Figure 4.9 Normalized CO_2 emissivity for 560–800 cm^{-1} for various temperatures as a function of the absorber amount u (in g cm^{-2}). Emissivities at 203K and 323K obtained from the 263 K data by scaling the absorber amounts according to equation 4.29 are shown as the dots.

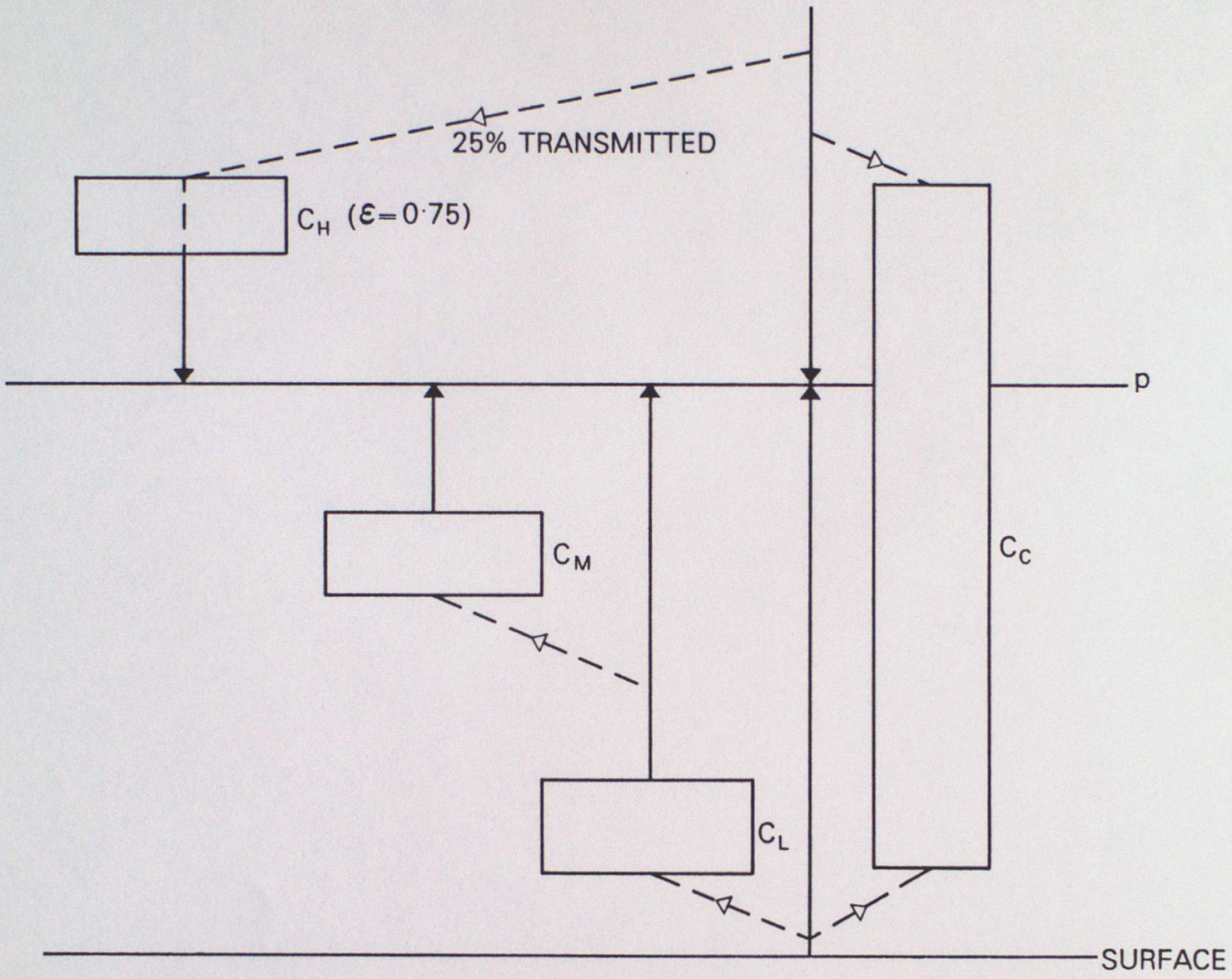

Figure 4.10 Longwave fluxes at pressure level p in a cloudy atmosphere. Unless stated otherwise, the fluxes incident on each cloud (shown dashed) are assumed to be absorbed totally by the cloud.

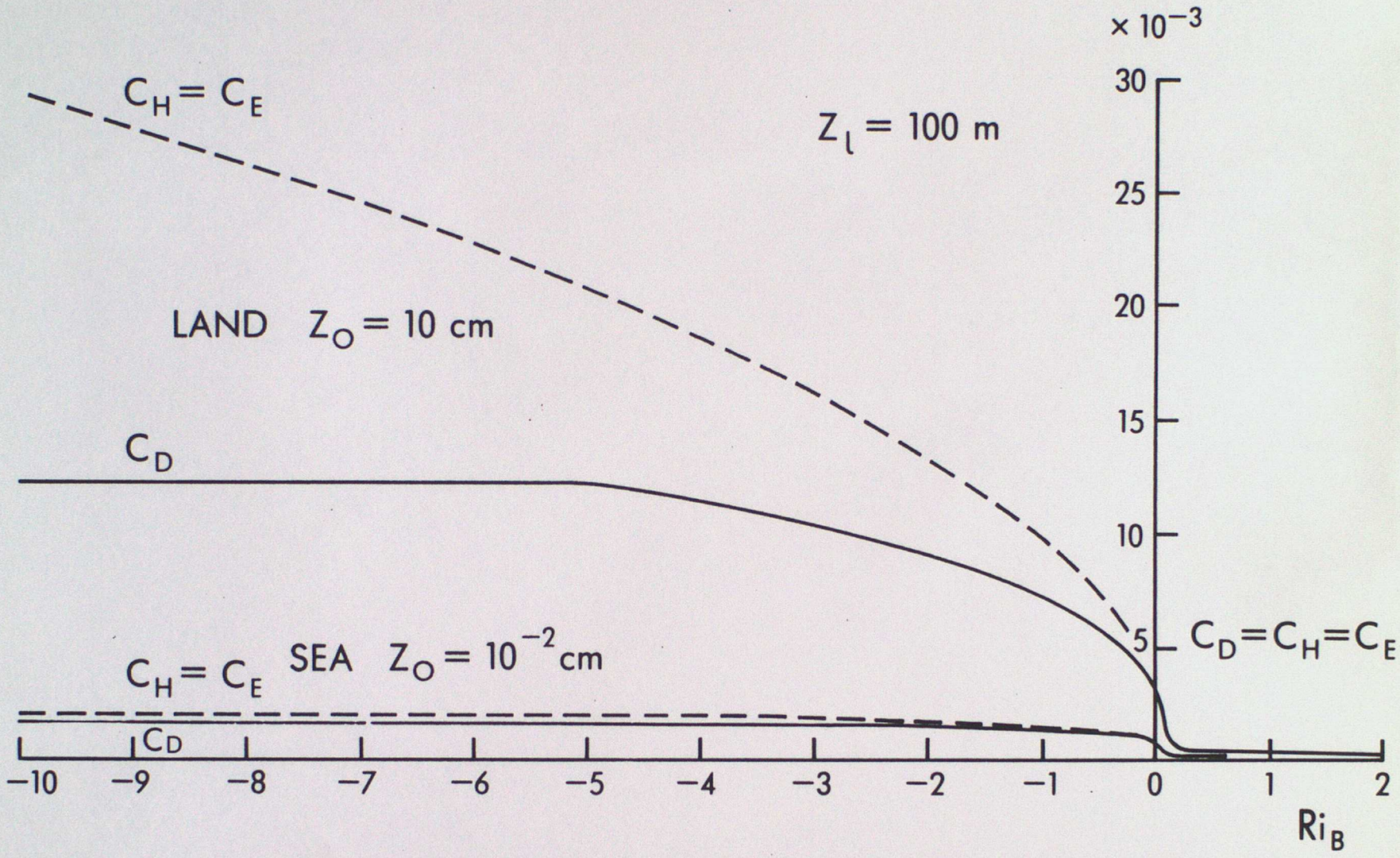

Figure 5.1 Surface layer bulk transfer coefficients derived from Monin-Obukhov similarity theory and used in the 11-Layer Model.

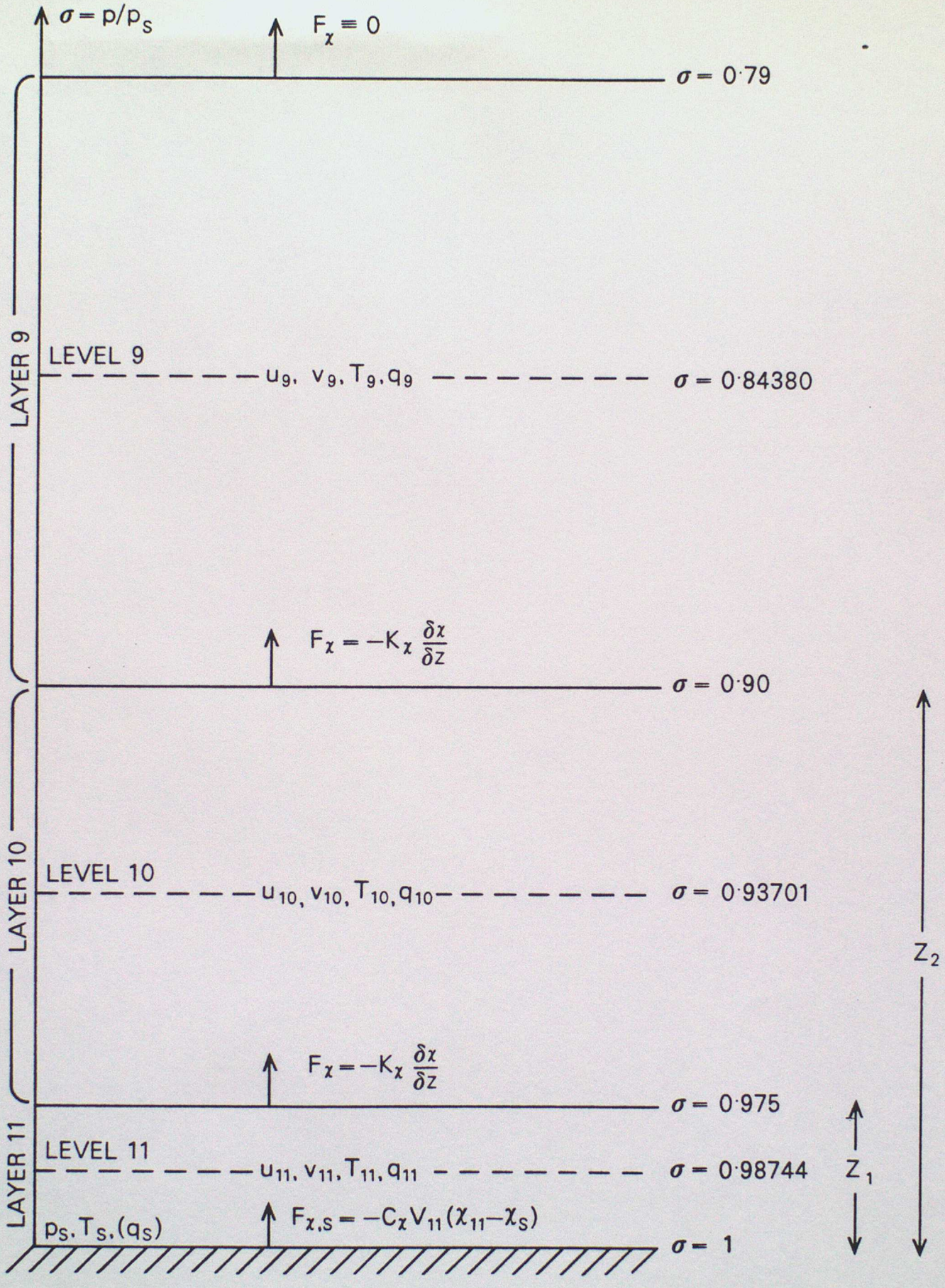

Figure 5.2 Schematic representation of the boundary layer structure in the Clarke boundary layer scheme. The Richards scheme is similar except that the boundary layer may occupy NBL layers, the flux out of the top layer being zero.

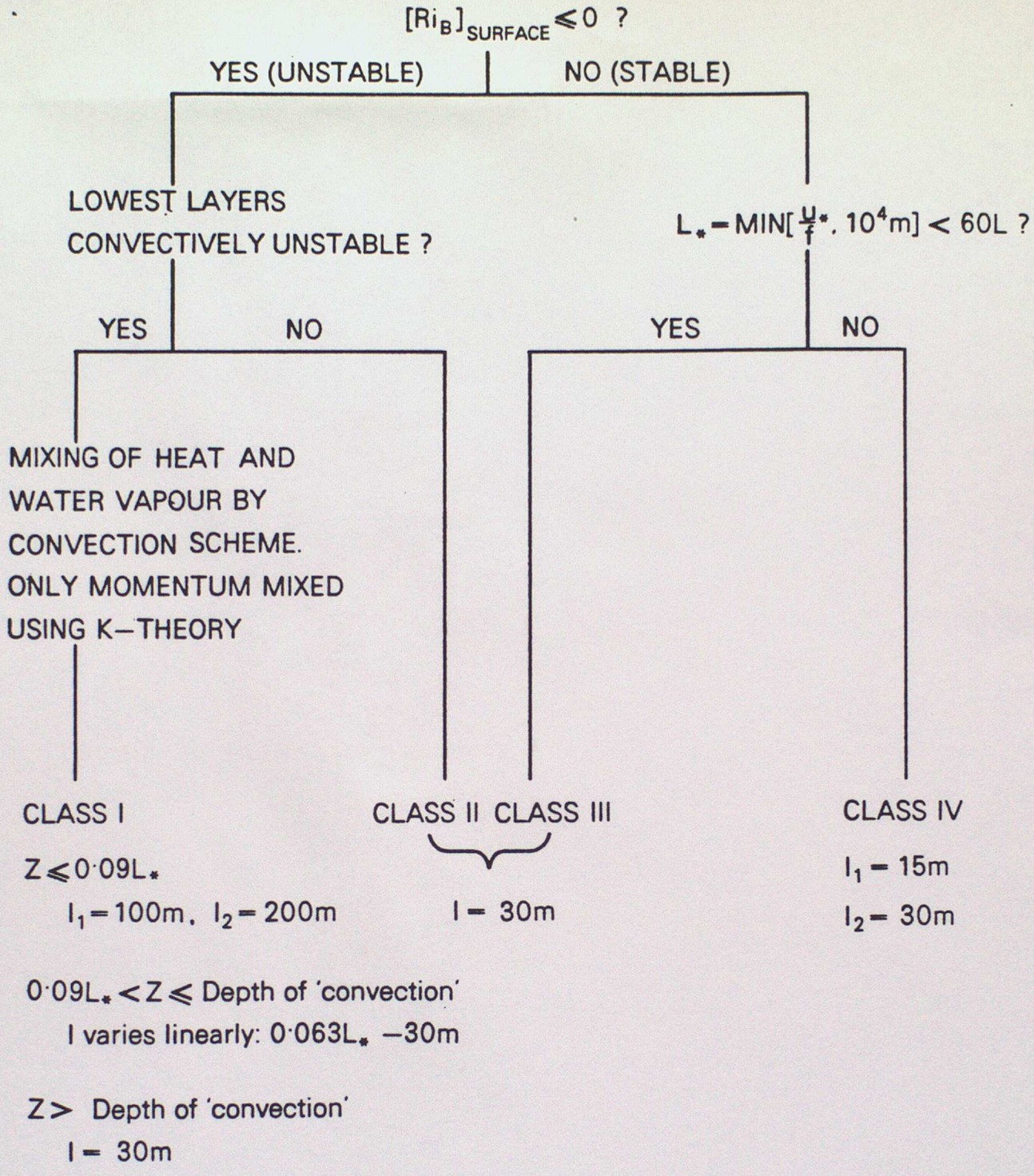

Figure 5.3 Simplified, schematic description of Method I of Clarke (1970) for estimating the Ekman-layer turbulent fluxes, as employed in the Clarke boundary layer scheme. L_* is the surface Monin-Obukhov length, u_* is the surface friction velocity and f is the Coriolis parameter. It is assumed that $\sigma = 0.975$ corresponds to $z_1 \approx 200$ m and $\sigma = 0.900$ to $z_2 = 830$ m, with corresponding mixing lengths l_1 and l_2 (see also Figure 5.2).

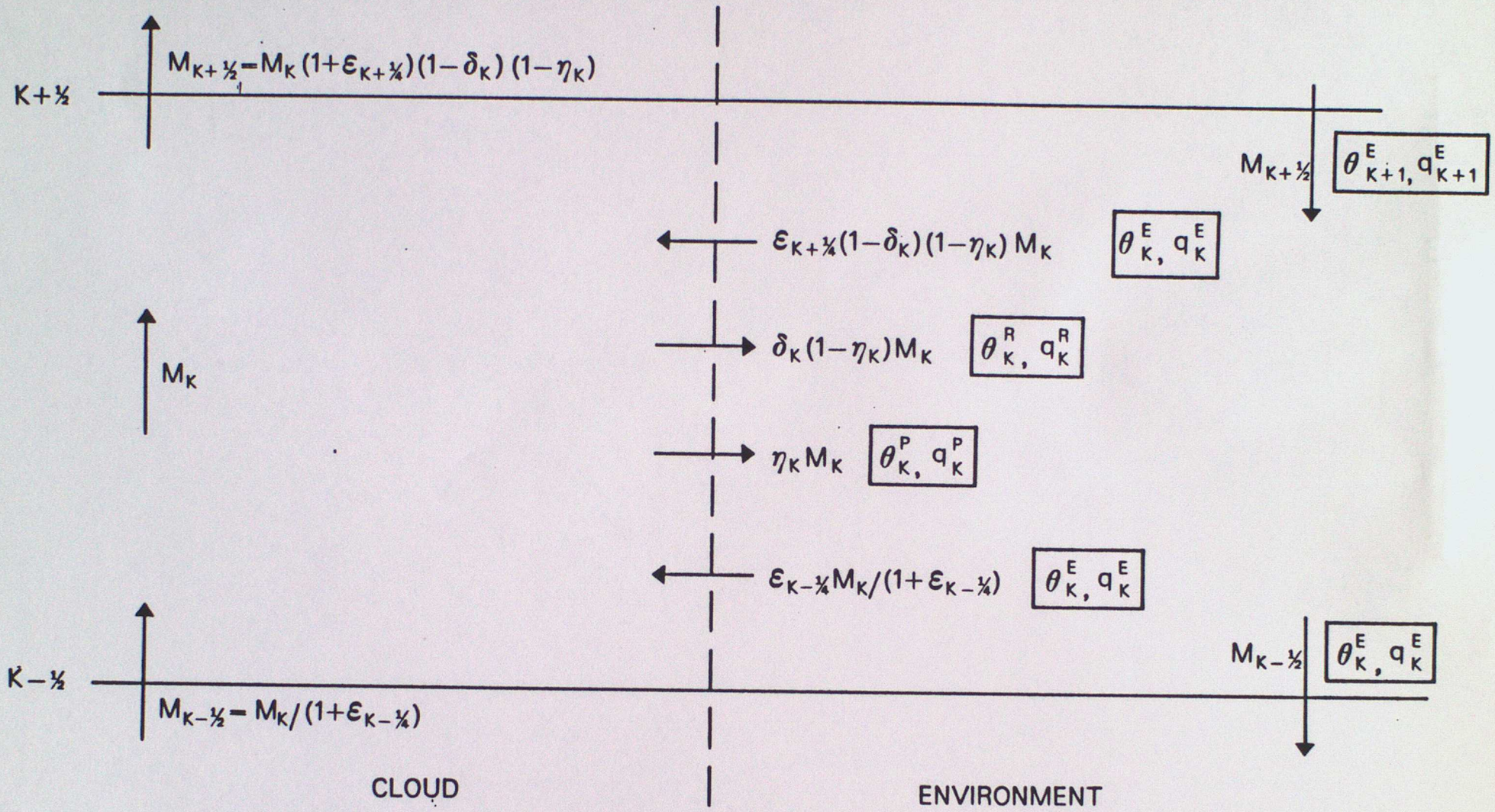

Figure 7.1 Vertical fluxes, entrainment and detrainment in the convection scheme.